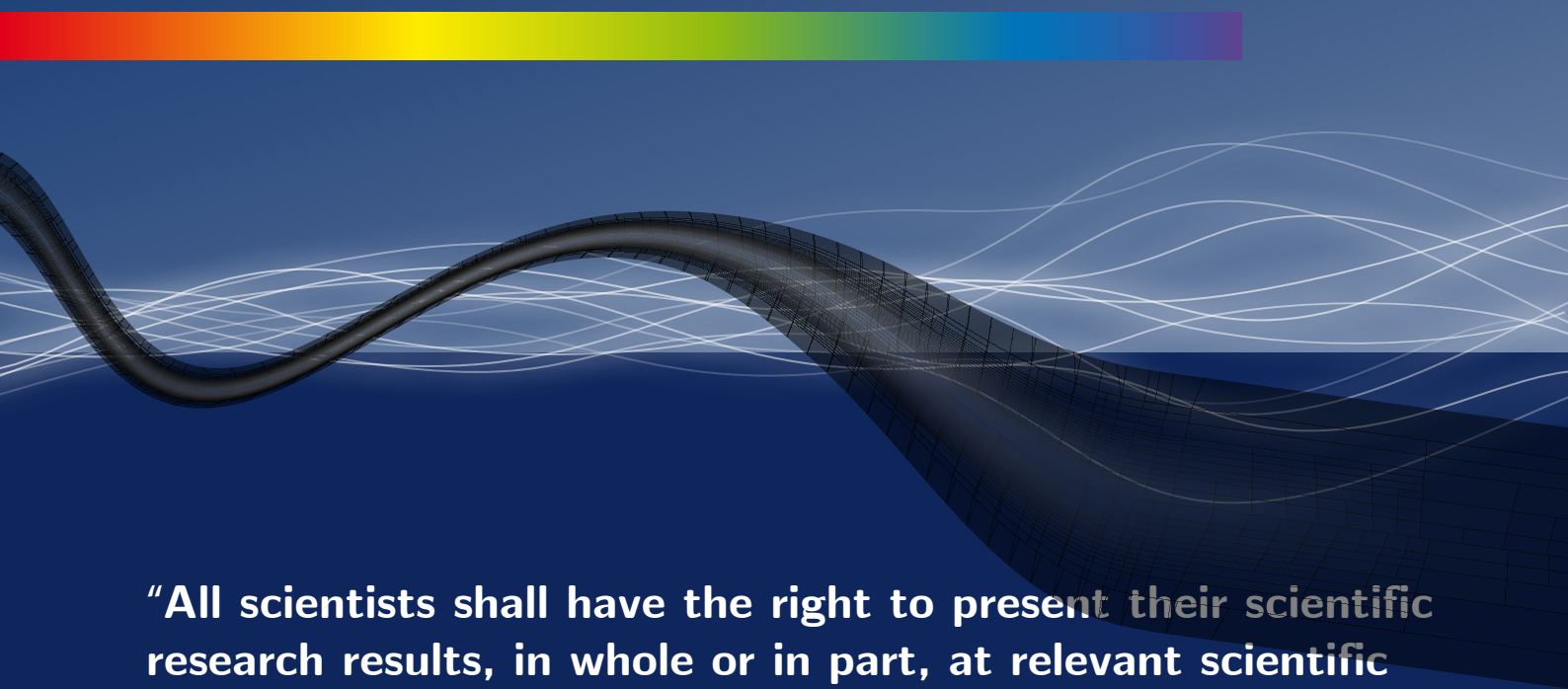


Issue 1

2024 | Volume 20

The Journal on Advanced Studies in Theoretical and Experimental Physics,
including Related Themes from Mathematics

PROGRESS IN PHYSICS



"All scientists shall have the right to present their scientific research results, in whole or in part, at relevant scientific conferences, and to publish the same in printed scientific journals, electronic archives, and any other media." — Declaration of Academic Freedom, Article 8

ISSN 1555-5534

PROGRESS IN PHYSICS

A Scientific Journal on Advanced Studies in Theoretical and Experimental Physics, including Related Themes from Mathematics. This journal is registered with the Library of Congress (DC, USA).

Electronic version of this journal:
<https://www.progress-in-physics.com>

Editorial Board

Dmitri Rabounski
rabounski@yahoo.com
Pierre Millette
pierremillette@sympatico.ca
Andreas Ries
andreasries@yahoo.com
Florentin Smarandache
fsmarandache@gmail.com
Larissa Borissova
lborissova@yahoo.com
Ebenezer Chifu
ebenechifu@yahoo.com

Postal Address

Department of Mathematics and Science,
University of New Mexico,
705 Gurley Ave., Gallup, NM 87301, USA

Copyright © Progress in Physics, 2024

All rights reserved. The authors of the articles do hereby grant *Progress in Physics* non-exclusive, worldwide, royalty-free license to publish and distribute the articles in accordance with the Budapest Open Initiative: this means that electronic copying, distribution and printing of both full-size version of the journal and the individual papers published therein for non-commercial, academic or individual use can be made by any user without permission or charge. The authors of the articles published in *Progress in Physics* retain their rights to use this journal as a whole or any part of it in any other publications and in any way they see fit. Any part of *Progress in Physics* howsoever used in other publications must include an appropriate citation of this journal.

This journal is powered by L^AT_EX

A variety of books can be downloaded free from the Digital Library of Science:
<http://fs.gallup.unm.edu/ScienceLibrary.htm>

ISSN: 1555-5534 (print)

ISSN: 1555-5615 (online)

Standard Address Number: 297-5092

Printed in the United States of America

June 2024

Vol. 20, Issue 1

CONTENTS

Smarandache F., Ries A., Millette P., Chifu E. Progress in Physics: Twentieth Year of Publication	3
Rabounski D., Borissova L. On the Lambda Term in Einstein's Equations and Its Influence on the Cosmological Redshift	4
Rabounski D., Borissova L. Cosmological Redshift: Which Cosmological Model Best Explains It?	13
Noh Y. J. Interpretation of Quantum Mechanics in Terms of Discrete Time II	21
Dvoeglazov V. V. Addendum to "The Feynman-Dyson propagators for neutral particles (locality or non-locality?)"	24
Muktibodh A. Santilli's Recovering of Einstein's Determinism	26
Smarandache F. Partial Collisions of Unmatter-Matter, Unmatter-Antimatter, and Unmatter1-Unmatter2 to Generate High Energy	33
Marquet P. The Vacuum Stress-Energy Tensor in General Relativity	36
Marquet P. Gödel Time Travel: New Highlights	41
Abbey G. F., Simfukwe J., Simpemba P. C., Phiri S. P., Srivastava A., Nyambuya G. G. Inference of Plausible Spatial Sizes of GRB Systems Using Newly Proposed FDSL-Model for GRB Time Delays	47
Potter F. Graph Theory Entropy Values for Lepton and Quark Discrete Symmetry Quantum States and Their Decay Channels	61

Information for Authors

Progress in Physics has been created for rapid publications on advanced studies in theoretical and experimental physics, including related themes from mathematics and astronomy. All submitted papers should be professional, in good English, containing a brief review of a problem and obtained results.

All submissions should be designed in L^AT_EX format using *Progress in Physics* template. This template can be downloaded from *Progress in Physics* home page <http://www.ptep-online.com>

Preliminary, authors may submit papers in PDF format. If the paper is accepted, authors can manage L^AT_EX typing. Do not send MS Word documents, please: we do not use this software, so unable to read this file format. Incorrectly formatted papers (i.e. not L^AT_EX with the template) will not be accepted for publication. Those authors who are unable to prepare their submissions in L^AT_EX format can apply to a third-party payable service for LaTeX typing. Our personnel work voluntarily. Authors must assist by conforming to this policy, to make the publication process as easy and fast as possible.

Abstract and the necessary information about author(s) should be included into the papers. To submit a paper, mail the file(s) to the Editor-in-Chief.

All submitted papers should be as brief as possible. Short articles are preferable. Large papers can also be considered. Letters related to the publications in the journal or to the events among the science community can be applied to the section *Letters to Progress in Physics*.

All that has been accepted for the online issue of *Progress in Physics* is printed in the paper version of the journal. To order printed issues, contact the Editors.

Authors retain their rights to use their papers published in *Progress in Physics* as a whole or any part of it in any other publications and in any way they see fit. This copyright agreement shall remain valid even if the authors transfer copyright of their published papers to another party.

Electronic copies of all papers published in *Progress in Physics* are available for free download, copying, and re-distribution, according to the copyright agreement printed on the titlepage of each issue of the journal. This copyright agreement follows the *Budapest Open Initiative* and the *Creative Commons Attribution-Noncommercial-No Derivative Works 2.5 License* declaring that electronic copies of such books and journals should always be accessed for reading, download, and copying for any person, and free of charge.

Consideration and review process does not require any payment from the side of the submitters. Nevertheless the authors of accepted papers are requested to pay the page charges. *Progress in Physics* is a non-profit/academic journal: money collected from the authors cover the cost of printing and distribution of the annual volumes of the journal along the major academic/university libraries of the world. (Look for the current author fee in the online version of *Progress in Physics*.)

LETTERS TO PROGRESS IN PHYSICS**Progress in Physics: Twentieth Year of Publication**Florentin Smarandache¹, Andreas Ries², Pierre Millette³, and Ebenezer Chifu⁴

Progress in Physics Editorial Team

¹fsmarandache@gmail.com, ²ries@ptep-online.com, ³millette@ptep-online.com, ⁴ebenechifu@yahoo.com

“All scientists shall have the right to present their scientific research results, in whole or in part, at relevant scientific conferences, and to publish the same in printed scientific journals, electronic archives, and any other media.”

Declaration of Academic Freedom, Article 8 [1]

With this inauguration of Volume 20 of *Progress in Physics*, the journal starts its twentieth year of publication, offering a much-needed avenue for the dissemination of truly scientific submissions that are written as proper scientific papers that are free of logical, mathematical and physical errors.

The journal *Progress in Physics* was created in January 2005 on behalf of many influential scientists with whom we were in correspondence. The main reason was that publications in other journals were allowed only if the submitter was affiliated with a scientific institution or research organization. Given this situation, many working scientists finding themselves partially employed or unemployed, such as in between research grants, find themselves unable to publish their research results. Even e-print archives such as Cornell’s arXiv required scientific affiliation and still follow this policy. This is why the Declaration of Academic Freedom was written and published in ten languages in *Progress in Physics* [1], and why the journal was started.

Since commencing in 2005, we have published 967 articles till now, which are accessed free of charge online. We have also distributed printed copies of the journal to major libraries of science throughout the world and offer open access online based on library preferences. The journal has a stable position among other scientific journals published by scientific institutions, and at the same time remains absolutely independent from any bureaucratic influence on the part of scientific organizations.

Our aim is to publish a professional journal by keeping a high professional level of operation. Therefore, we always review submitted papers accepting those that meet the requirements stated above, and rejecting those that are not written as proper scientific papers or that contain formal errors. We follow our major principle according to which we consider submissions on the basis of what has been written in the submissions, without any connection with the submitter’s affiliation, personality and other considerations.

This has allowed us to make our journal a repository for high quality scientific research over the last two decades. We still do everything to keep the high level of the journal, which is a great advantage for our authors. Our Editorial Team as-

ures our readers and authors that we will continue to adhere to this independent editorial policy in the future, thereby following the Declaration of Academic Freedom.

In conclusion, we have done, and will continue to do, everything to support the principles of open and free dissemination of scientific information in the future. We open this 20th anniversary volume of our journal with faith in the future and invite all researchers who want to publish their scientific results to submit their manuscripts to our journal.

Submitted on January 2, 2024

References

1. Rabounski D. Declaration of Academic Freedom (Scientific Human Right). *Progress in Physics*, 2006, v. 2 (1), 57–60.

LETTERS TO PROGRESS IN PHYSICS

On the Lambda Term in Einstein's Equations and Its Influence on the Cosmological Redshift

Dmitri Rabounski and Larissa Borissova

Puschino, Moscow Region, Russia

E-mail: rabounski@yahoo.com, lborissova@yahoo.com

Here we analyze our theory of the physical vacuum (λ -field filling de Sitter spaces), in which we calculated its physically observable properties (2001) and the parabolic (non-linear) cosmological redshift specific to de Sitter spaces (2013). To explain the recently discovered non-linear cosmological redshift, we consider the following options: 1) our Universe is a de Sitter world with $\lambda > 0$ and, therefore, with a parabolic cosmological redshift (because with $\lambda > 0$ the non-Newtonian gravitational forces acting in a de Sitter world are forces of repulsion, which decelerate photons), but in this case the physical vacuum has a negative density $\check{\rho} < 0$, and the observable curvature radius of space is imaginary (the space geometry is hyperbolic); 2) our Universe is a de Sitter world with $\lambda < 0$, where the physical vacuum has a positive density $\check{\rho} > 0$, and the observable curvature radius is real (the space geometry is spherical), but with a parabolic cosmological blueshift (and not a redshift) because with $\lambda < 0$ the non-Newtonian forces are forces of attraction (they accelerate photons); 3) our Universe is a de Sitter world with $\lambda > 0$ and, hence, a parabolic cosmological redshift, but the $\lambda g_{\alpha\beta}$ term in Einstein's field equations has the opposite (negative) sign. We vote for the 3rd option, because in this case a) the physical vacuum has a positive density $\check{\rho} > 0$, which satisfies the physical requirement that any kind of observable matter must have a positive mass and density, b) the observable curvature radius of space is real (and not imaginary) and, hence, the space geometry is spherical (and not hyperbolic), c) the non-Newtonian gravitational forces are forces of repulsion (they decelerate photons, thereby producing a redshift), d) the event horizon in such a universe is outlined by the gravitational radius of the de Sitter sphere. All this confirms the supposition that our Universe is a huge de Sitter gravitational collapsar with $\lambda > 0$ and a non-linear (parabolic) cosmological redshift.

In the late 1980s and 1990s, we undertook a massive theoretical research on the motion of particles in the space-time of General Relativity, which we published in 2001 in our two monographs [1, 2]. In particular, we created a theory of the physical vacuum (λ -field filling de Sitter spaces), in which we calculated its physically observable properties such as density, pressure, etc. [2, Chapter 5]. In 2010, using the mentioned theory of the physical vacuum, Larissa created a theory of the de Sitter gravitational collapsar (de Sitter bubble), which she suggested as a model of the observable Universe [3]. In our third monograph [4], published in 2013, we predicted a parabolic (non-linear) cosmological redshift in a de Sitter space [4, §6.4–§6.5]. In 2018, we also published a short paper on the mentioned parabolic redshift [5].

Meanwhile there was a serious problem with determining the cosmological shift in the frequency of photons travelling in a de Sitter world. This problem arose due to the sign of the λ -term, because it is not specified in de Sitter's metric. So, our closest colleagues drew our attention to some confusion in our sequential publications on this subject.

First, in our theory of the physical vacuum, where we did not consider the cosmological redshift, we assumed $\lambda < 0$ and,

therefore, a positive vacuum density $\check{\rho} > 0$ in our Universe [2, §5.3]. In this case, the non-Newtonian gravitational forces acting in any de Sitter space are forces of attraction, and the physically observable three-dimensional curvature is positive $C > 0$. Since $C = \frac{1}{\mathfrak{R}^2}$, the latter means that such a universe has a real observable curvature radius \mathfrak{R} , and, therefore, the space geometry is spherical (this is what the geometry of a de Sitter space should be). But a few years later, when Larissa suggested a collapsed de Sitter sphere as a model of the observable Universe [3], and then, in our monograph on the internal constitution of stars, where we considered de Sitter collapsars [4, Chapter 6], and also in our subsequent paper on the cosmological redshift [5], it was assumed that $\lambda > 0$. This is because forces of attraction ($\lambda < 0$) accelerate photons, thereby producing a photon blueshift (gain of the photon energy), and forces of repulsion ($\lambda > 0$) decelerate photons, thereby producing a photon redshift (loss of the photon energy). But in the case of $\lambda > 0$ we should expect a negative vacuum density $\check{\rho} < 0$, a negative physically observable curvature $C < 0$ and, hence, an imaginary numerical value of the observable curvature radius \mathfrak{R} of such a universe (this means that the space geometry is hyperbolic).

To resolve this contradiction, a solution was proposed in §6.5 of our book [4] (§5.1 in the 1st edition, 2013). But this solution was not well recognized by the readers, because it was “lost” among many other new results presented in that book. As a result, the above confusion has created a problem in understanding the parabolic cosmological redshift that we had predicted for a de Sitter universe.

Note that the cosmological redshift problem was never our task or field of interest. The parabolic redshift in a de Sitter universe was just one of the spin-off theoretical results that we obtained in the course of our long-term work on other, much more important mathematical and applied problems in the General Theory of Relativity.* On the other hand, we must respond to our colleagues regarding the parabolic cosmological redshift in a de Sitter universe, which we had predicted “at the tip of the pen”. It looks like it is time to dot all the i’s in this problem.

Let us begin. The λ -term was introduced in 1917 by Albert Einstein [6]. He added it multiplied by the fundamental metric tensor $g_{\alpha\beta}$ to the right-hand side of the field equations (known also as Einstein’s equations), which thus acquired their final well-known form[†]

$$R_{\alpha\beta} - \frac{1}{2} g_{\alpha\beta} R = -\kappa T_{\alpha\beta} + \lambda g_{\alpha\beta}.$$

He did this, because the metric of a static finite spherically symmetric space filled with a homogeneous and isotropic distribution of substance — Einstein’s metric, which he initially considered as the basic cosmological model of our Universe, — does not satisfy the original field equations (which do not contain the λ -term). Mathematically, this means that substituting the components of the fundamental metric tensor $g_{\alpha\beta}$, taken from Einstein’s metric, into the original field equations (without the λ -term), the left-hand side of the field equations does not equalize the right-hand side. But with the λ -term

*“As you know, our success depends on the fact that nearly all major scientific advances have been made while looking for something else, or following up curious observations.” — David Jones, Editor of *New Scientist*, May 1981. Cited from: Jones D. *The Inventions of Daedalus*. W. H. Freeman & Co., Oxford, 1982, page 3.

[†]Here $R_{\alpha\sigma} = R_{\alpha\beta\gamma\sigma}^{\dots\beta}$ [cm⁻²] is Ricci’s tensor (obtained as the contraction of the Riemann-Christoffel curvature tensor $R_{\alpha\beta\gamma\delta}$ by one index in each pair of its four indices), $R = g^{\alpha\beta} R_{\alpha\beta}$ is the scalar curvature, $\kappa = 8\pi G/c^2 = 1.862 \times 10^{-27}$ [cm/gram] is Einstein’s constant, $G = 6.672 \times 10^{-8}$ [cm³/gram sec²] is Gauss’ gravitational constant, and $T_{\alpha\beta}$ [gram/cm³] is the energy-momentum tensor of a distributed matter that fills the space.

Einstein’s field equations show how in a Riemannian space the field of its four-dimensional curvature depends on the field of a distributed matter (substance or, say, electromagnetic field) that fills this space. Note that Einstein’s field equations are not some kind of physical hypothesis. They follow mathematically from the geometric structure characteristic of any Riemannian space (as well as the Riemannian quadratic metric and its invariance throughout the entire space). For example, let us have a space determined by a metric. In order for this space to be Riemannian, it is necessary that its metric has the Riemannian quadratic form $ds^2 = g_{\alpha\beta} dx^\alpha dx^\beta$, be invariant throughout the entire space, and satisfy the field equations.

added to the right-hand side of the field equations, the fundamental metric tensor $g_{\alpha\beta}$ of a spherically symmetric static homogeneous and isotropic universe (*Einstein’s cosmological model*) makes both sides of the equations equal to each other, so the equations vanish. For detail, see Einstein’s 1917 paper [6] and the comprehensive review on this subject [7].

A year later, in 1918, Willem de Sitter [8] mathematically deduced that, in addition to Einstein’s metric (which determines a space filled with a static finite spherically homogeneous and isotropic distribution of substance), there is also another space metric satisfying the field equations containing the λ -term. De Sitter’s space metric has the form

$$ds^2 = \left(1 - \frac{\lambda r^2}{3}\right) c^2 dt^2 - \frac{dr^2}{1 - \frac{\lambda r^2}{3}} - r^2 (d\theta^2 + \sin^2\theta d\varphi^2)$$

and describes a static finite spherically symmetric space filled with a homogeneous and isotropic distribution of the λ -field (determined by the λ -term) without any islands of mass or distributed substance. The above metric then became known as *de Sitter’s cosmological model*.

Since the zero component T_{00} of the energy-momentum tensor of a distributed matter is associated with the density of the matter [6], then, according to the right-hand side of the field equations, the λ -term divided by Einstein’s constant κ should be associated with the density of the λ -field. Over the last century many astronomers tried to measure the numerical value of the λ -term, using various measurement methods; see the 2001 review on this subject [9]. However, all that they achieved does not differ from the result known in already the 1950s, according to which even the sign of the λ -term is under question, and the upper limit of its numerical value is $|\lambda| \leq 10^{-56}$ [cm⁻²]. Even now the astronomers can only say that the λ -field is an extremely rarefied medium, the density of which cannot be surely detected within the current accuracy of astronomical measurements.

There was no theory of the λ -field until the mid-1990s, when we began our own research on this subject. As a result of our research, in Chapter 5 of our monograph [2], first published in 2001, we presented a mathematical theory of the λ -field. In the framework of this theory, we theoretically determined the physically observable properties of the λ -field and much more. As always in our studies, we used the mathematical apparatus of physically observable quantities in General Relativity, known also as the Zelmanov chronometric invariants [10–12]; see the most comprehensive review of this mathematical technique in our survey [13].

In [2] we called the λ -field the *physical vacuum*, because it has vacuum-like properties. We relied on the works of Erast Gliner [14, 15], announced in 1966 by Andrew Sakharov [16]. Gliner selected and then studied a special state of distributed matter for which the energy-momentum tensor is $T_{\alpha\beta} = \mu g_{\alpha\beta}$, where μ is a constant number[‡]. He called this state of matter

[‡]Gliner used the space signature $(-+++)$, resulting in $T_{\alpha\beta} = -\mu g_{\alpha\beta}$.

the μ -vacuum, because it is related to vacuum-like states of substance ($T_{\alpha\beta} \sim g_{\alpha\beta}$, which means $R_{\alpha\beta} = k g_{\alpha\beta}$, $k = \text{const}$), but is not the vacuum (because $T_{\alpha\beta} = 0$ in the vacuum). Following this way, we introduced a new geometric classification of the states of distributed matter (and of space-time itself) according to the form of the energy-momentum tensor. We called this new classification the *T-classification of matter*:

- I. The emptiness is the state of space-time, for which the Ricci tensor is zero $R_{\alpha\beta} = 0$, which means the absence of both distributed substance ($T_{\alpha\beta} = 0$) and the physical vacuum ($\lambda = 0$).^{*} So, the emptiness is the state of a space-time without any kind of distributed matter;
- II. The physical vacuum or, simply, the vacuum is the state of distributed matter (space-time), which is determined by only the λ -field ($\lambda = \text{const} \neq 0$);
- III. The μ -vacuum is the state of distributed matter (space-time), which is determined by the energy-momentum tensor of the form $T_{\alpha\beta} = \mu g_{\alpha\beta}$ (where $\mu = \text{const}$). This is a vacuum-like state of matter, because $T_{\alpha\beta} \sim g_{\alpha\beta}$;
- IV. Substance is the state of distributed matter (space-time) for which $T_{\alpha\beta} \neq 0$, but $T_{\alpha\beta} \not\sim g_{\alpha\beta}$. This state comprises both ordinary substance and electromagnetic fields.

For the above reasons, we called the mathematical theory of the λ -term, which we presented in Chapter 5 of our monograph [2], the *theory of the physical vacuum*.

The energy-momentum tensor and physical properties of the physical vacuum (λ -field) were derived as follows. We presented the field equations in the form

$$R_{\alpha\beta} - \frac{1}{2} g_{\alpha\beta} R = -\kappa \tilde{T}_{\alpha\beta},$$

where $\tilde{T}_{\alpha\beta} = T_{\alpha\beta} + \check{T}_{\alpha\beta}$ is the joint energy-momentum tensor that describes both distributed substance and the physical vacuum, and

$$\check{T}_{\alpha\beta} = -\frac{\lambda}{\kappa} g_{\alpha\beta}$$

is the energy-momentum tensor of the physical vacuum. The physically observable properties of a medium are expressed with the projections of its energy-momentum tensor $T_{\alpha\beta}$ onto the time line and the three-dimensional spatial section of the observer [10–13]: the observable density ρ , the observable momentum density J^i and the observable stress tensor U^{ik}

$$\rho = \frac{T_{00}}{g_{00}}, \quad J^i = \frac{c T_0^i}{\sqrt{g_{00}}}, \quad U^{ik} = c^2 T^{ik},$$

Since the observable density of matter is positive, $\rho = \frac{T_{00}}{g_{00}} = -\mu > 0$, he obtained negative numerical values of μ . We always use the space signature $(+---)$, because in this case the three-dimensional observable interval is positive [10–13]. Therefore, we have $\mu > 0$ and $T_{\alpha\beta} = \mu g_{\alpha\beta}$.

^{*}In an empty space, we have the field equations $R_{\alpha\beta} - \frac{1}{2} g_{\alpha\beta} R = 0$ or, in the mixed form, $R^\beta_\alpha - \frac{1}{2} g^\beta_\alpha R = 0$. After their contraction $R^\alpha_\alpha - \frac{1}{2} g^\alpha_\alpha R = 0$, we obtain $R - \frac{1}{2} 4R = 0$. Hence, the scalar curvature of any empty space is $R = 0$, and the field equations in an empty space have the form $R_{\alpha\beta} = 0$.

which, when calculated for the energy-momentum tensor of the physical vacuum $\check{T}_{\alpha\beta} = -\frac{\lambda}{\kappa} g_{\alpha\beta}$, have the form

$$\check{\rho} = \frac{\check{T}_{00}}{g_{00}} = -\frac{\lambda}{\kappa},$$

$$\check{J}^i = \frac{c \check{T}_0^i}{\sqrt{g_{00}}} = 0,$$

$$\check{U}^{ik} = c^2 \check{T}^{ik} = \frac{\lambda}{\kappa} c^2 h^{ik} = -\check{\rho} c^2 h^{ik},$$

where h^{ik} is the upper-index form of the physically observable three-dimensional metric tensor $h_{ik} = -g_{ik} + \frac{1}{c^2} v_i v_k$.[†]

From here we see that the physical vacuum (λ -field) is a *uniformly distributed matter* (since it has a constant density $\check{\rho} = \text{const}$), and also is a *non-emitting medium* (the energy flux in the physical vacuum is zero $c^2 \check{J}^i = 0$).

The equation of state of the physical vacuum[‡] follows from the general formula of the stress tensor

$$U_{ik} = p_0 h_{ik} - \alpha_{ik} = p h_{ik} - \beta_{ik},$$

which is applicable to any medium [12]. Here p_0 is the equilibrium pressure of the medium, p is the true pressure, α_{ik} is the viscosity of the 2nd kind, and $\beta_{ik} = \alpha_{ik} - \frac{1}{3} \alpha h_{ik}$ is the anisotropic part of α_{ik} ($\alpha = \alpha^i_i$ is its trace), called the viscosity of the 1st kind and manifested in anisotropic deformations of the medium. Since the physical vacuum (λ -field) is the only filler of any de Sitter space, and de Sitter's metric means a spherically symmetrical, homogeneous, isotropic and static (non-deforming) space, then in the physical vacuum $\check{\alpha}_{ik} = 0$ and $\check{\beta}_{ik} = 0$ (it is a *non-viscous medium*). Hence, the energy-momentum tensor of the physical vacuum has the form

$$\check{U}_{ik} = \check{p} h_{ik} = -\check{\rho} c^2 h_{ik},$$

and the equation of state of the physical vacuum is

$$\check{p} = -\check{\rho} c^2,$$

which means the *state of inflation*: if the density of a medium is positive, then the pressure inside it is negative (the medium expands).

So, we have obtained that the physical vacuum has the following physical properties:

[†]The physically observable three-dimensional spatial interval is determined as $d\sigma^2 = h_{ik} dx^i dx^k$, where $h_{ik} = -g_{ik} + \frac{1}{c^2} v_i v_k$ for which $h^{ik} = -g^{ik}$ and $h^i_k = -g^i_k = \delta^i_k$. Here $v_i = -c \frac{g_{0i}}{\sqrt{g_{00}}}$ is the linear velocity with which the reference space of the observer rotates (in the case, if it rotates), for which $v^i = -c g^{0i} \sqrt{g_{00}}$, $v_i = h_{ik} v^k$, $v^2 = v_k v^k = h_{ik} v^i v^k$. See the mathematical apparatus of chronometric invariants [10–13] for detail.

[‡]The equation of state of a distributed matter is the relationship between the pressure and density in the medium. For instance, $p = 0$ is the equation of state of a dust medium, $p = \rho c^2$ is the equation of state of a matter inside atomic nuclei, $p = \frac{1}{3} \rho c^2$ is the equation of state of an ultra-relativistic gas.

The physical vacuum, i.e., the λ -field, is a homogeneous ($\check{\rho} = \text{const}$), non-viscous ($\check{\alpha}_{ik} = 0, \check{\beta}_{ik} = 0$) and non-emitting ($\check{J}^i = 0$) medium, which is in the state of inflation ($\check{p} = -\check{\rho}c^2$).

We are able to calculate the numerical value of the physically observable density of the physical vacuum $\check{\rho} = -\frac{\lambda}{\kappa}$ and, therefore, the numerical value of the λ -term, if the physically observable three-dimensional curvature of the observable space will once be somehow measured in astronomical observations. How to do this is explained below.

In constant curvature spaces such as de Sitter spaces the Riemann-Christoffel curvature tensor is [17, Chapter VII]

$$R_{\alpha\gamma\delta} = K(g_{\alpha\gamma}g_{\beta\delta} - g_{\alpha\delta}g_{\beta\gamma}), \quad K = \text{const},$$

where K is a constant number proportional to the constant scalar curvature R . Contracting it step-by-step we obtain the Ricci tensor $R_{\alpha\beta} = -3K g_{\alpha\beta}$, the scalar curvature $R = -12K$ (because $g_{\alpha\beta}g^{\alpha\beta} = 4$) and, as a result, the field equations in a constant curvature space

$$3K g_{\alpha\beta} = -\kappa T_{\alpha\beta} + \lambda g_{\alpha\beta},$$

which mean $(\lambda - 3K) g_{\alpha\beta} = \kappa T_{\alpha\beta}$. Because $T_{\alpha\beta} = 0$ in any de Sitter space (its only filler is the λ -field), then the observable density of the physical vacuum in a de Sitter space is

$$\check{\rho} = -\frac{\lambda}{\kappa} = -\frac{3K}{\kappa} = -\frac{3Kc^2}{8\pi G},$$

and, since the physically observable three-dimensional curvature C of a de Sitter space is $C = -6K$,* we obtain the physically observable density of the physical vacuum $\check{\rho}$, the λ -term and the pressure \check{p} inside the vacuum (the latter follows from the equation of state of the physical vacuum, $\check{p} = -\check{\rho}c^2$), expressed with the physically observable space curvature C

$$\check{\rho} = \frac{C}{2\kappa}, \quad \lambda = -\frac{C}{2}, \quad \check{p} = -\frac{c^2 C}{2\kappa},$$

or, since C is known to be related to the physically observable curvature radius \mathfrak{R} of a three-dimensional constant curvature space as follows $C = \frac{1}{\mathfrak{R}^2}$,

$$\check{\rho} = \frac{1}{2\kappa\mathfrak{R}^2}, \quad \lambda = -\frac{1}{2\mathfrak{R}^2}, \quad \check{p} = -\frac{c^2}{2\kappa\mathfrak{R}^2}.$$

Astronomical observations performed over the last century indicate that the physically observable event horizon in our Universe is approximately 10^{28} cm (within one order of magnitude). Therefore, if we assume that our Universe is a de Sitter sphere with the observable curvature radius 10^{28} cm,

*It was obtained by projecting the Riemann-Christoffel curvature tensor $R_{\alpha\beta\gamma\delta}$ onto the time line and the three-dimensional spatial section of the observer; see [2, §5.3] for detail.

then we should expect (all within one order of magnitude):

$$\check{\rho} \approx 3 \times 10^{-30} \text{ gram/cm}^3,$$

$$\check{p} \approx -2 \times 10^{-9} \text{ gram/cm sec}^2,$$

$$|\lambda| \approx 5 \times 10^{-57} \text{ cm}^{-2}.$$

Gravitational forces act in any de Sitter space, but they are non-Newtonian gravitational forces because they arise due to the non-Newtonian gravitational potential created by the physical vacuum (λ -field). Below explains why.

In general, gravitational forces are forces caused by the non-uniform distribution of the gravitational potential w determined by the zero component g_{00} of the fundamental metric tensor $g_{\alpha\beta}$. As is known, in a general case [18],

$$g_{00} = \left(1 - \frac{w}{c^2}\right)^2, \quad \text{hence} \quad w = c^2(1 - \sqrt{g_{00}}),$$

and the physically observable vector of the gravitational inertial force, determined in the framework of the mathematical apparatus of chronometric invariants [10–13], is

$$F_i = \frac{1}{\sqrt{g_{00}}} \left(\frac{\partial w}{\partial x^i} - \frac{\partial v_i}{\partial t} \right).$$

In a space of de Sitter's metric (see the metric in the beginning of this article) we have

$$g_{00} = 1 - \frac{\lambda r^2}{3}, \quad \text{hence} \quad w = c^2 \left(1 - \sqrt{1 - \frac{\lambda r^2}{3}} \right)$$

is the *non-Newtonian gravitational potential* specific to de Sitter metric spaces. The mixed components g_{0i} are zero in de Sitter's metric, hence $v_i = -c \frac{g_{0i}}{\sqrt{g_{00}}} = 0$ (which means that de Sitter spaces do not rotate). Using the above, we obtain that the physically observable gravitational inertial force in a de Sitter space has the following non-zero components

$$F_1 = \frac{\lambda c^2}{3} \frac{r}{1 - \frac{\lambda r^2}{3}}, \quad F^1 = \frac{\lambda c^2}{3} r,$$

or, when expressed with the physically observable density of the physical vacuum $\check{\rho}$ and the observable curvature radius of space \mathfrak{R} ,

$$F_1 = -\frac{\kappa \check{\rho} c^2}{3} \frac{r}{1 + \frac{\kappa \check{\rho} r^2}{3}} = -\frac{c^2}{6\mathfrak{R}^2} \frac{r}{1 + \frac{r^2}{6\mathfrak{R}^2}},$$

$$F^1 = -\frac{\kappa \check{\rho} c^2}{3} r = -\frac{c^2}{6\mathfrak{R}^2} r.$$

This is a *non-Newtonian gravitational force*, because it arises due to the non-Newtonian gravitational potential specific to de Sitter spaces, and also increases with the distance over which it acts (the force is proportional to r).

Based on the results presented above, we arrive at the following conclusions:

1. If the λ -term is negative $\lambda < 0$, then the density of the physical vacuum is positive $\check{\rho} > 0$, the pressure inside it is negative $\check{p} < 0$ (which means that the vacuum expands), the non-Newtonian gravitational forces acting in the space are negative $F^i < 0$ (this means that they are forces of attraction), and the three-dimensional observable curvature is positive $C > 0$;
2. On the contrary, if the λ -term is positive $\lambda > 0$, then the density of the physical vacuum is negative $\check{\rho} < 0$, the pressure inside it is positive $\check{p} > 0$ (the vacuum contracts), and the non-Newtonian gravitational forces acting in the space are positive $F^i > 0$ (therefore, they are forces of repulsion). But in this case, the physically observable three-dimensional curvature is negative $C < 0$ and, therefore, the observable curvature radius of space \mathfrak{R} has an imaginary numerical value $\mathfrak{R} = \frac{1}{\sqrt{C}} = \frac{1}{\sqrt{-2\lambda}}$, which means that the three-dimensional space geometry is hyperbolic (but not spherical, how the geometry of a de Sitter space should be).

Let us now study how the sign of the λ -term affects the frequency shift gained by a photon travelling in a de Sitter universe. It is called the *cosmological frequency shift*, because it is calculated for a photon fled a “cosmological” distance comparable to the radius of the Universe.

As we have shown and applied in our previous studies since 2009 [3–5], the physically observable cosmological frequency shift in photons is deduced by integrating the scalar equation of isotropic geodesic lines (trajectories of free light-like particles, e.g., free photons), which is the equation of the physically observable photon energy. This equation follows from the theory of chronometric invariants [10–13] (physical observables in the space-time of General Relativity), and is the chronometrically invariant (physically observable) projection of the four-dimensional equations of isotropic geodesics (the four-dimensional equations of motion of free photons) onto the time line of the observer, while the chronometrically invariant projection of the four-dimensional equations of isotropic geodesics onto the three-dimensional spatial section associated with the observer gives the three-dimensional physically observable equations of motion of free photons.

In particular, in 2011, following this calculation method applied to the equations of motion of mass-bearing particles, the cosmological mass defect of mass-bearing particles had been predicted [19]. The *cosmological mass-defect* is a new effect predicted according to General Relativity.

In short, the aforementioned calculation method applied to photons is as follows.

The four-dimensional (general covariant) equations of an isotropic geodesic line, which is the four-dimensional trajectory of a free photon*, when projected onto the time line and

the three-dimensional spatial section associated with an observer, have two physically observable (chronometrically invariant) projections, which are[†]

$$\frac{d\omega}{d\tau} - \frac{\omega}{c^2} F_i c^i + \frac{\omega}{c^2} D_{ik} c^i c^k = 0,$$

$$\frac{d(\omega c^i)}{d\tau} - \omega F^i + 2\omega (D_k^i + A_k^i) c^k + \omega \Delta_{nk}^i c^n c^k = 0,$$

where ω is the photon's frequency, c^i is the physically observable chr.inv.-vector of the light velocity ($h_{ik} c^i c^k = c^2$), and

$$d\tau = \sqrt{g_{00}} dt - \frac{1}{c^2} v_i dx^i$$

is the physically observable time interval. The factors under which photons move freely, aside of the chr.inv.-gravitational inertial force F_i (explained above), are the chr.inv.-angular velocity tensor of the space rotation A_{ik} , the chr.inv.-tensor of the space deformation D_{ik} and the chr.inv.-Christoffel symbols Δ_{jk}^i (they mean the non-uniformity of space)[‡]

$$A_{ik} = \frac{1}{2} \left(\frac{\partial v_k}{\partial x^i} - \frac{\partial v_i}{\partial x^k} \right) + \frac{1}{2c^2} (F_i v_k - F_k v_i),$$

$$D_{ik} = \frac{1}{2} \frac{\partial h_{ik}}{\partial t}, \quad D^{ik} = -\frac{1}{2} \frac{\partial h^{ik}}{\partial t},$$

$$\Delta_{jk}^i = h^{im} \Delta_{jk,m} = \frac{1}{2} h^{im} \left(\frac{\partial h_{jm}}{\partial x^k} + \frac{\partial h_{km}}{\partial x^j} - \frac{\partial h_{jk}}{\partial x^m} \right).$$

We call the time projection (first equation) the *chr.inv.-energy equation*, because it gives the physically observable energy $E = \hbar\omega$ of the photon as it travels. The spatial (second) projection represents the chr.inv.-equations of the photon's motion in the three-dimensional space.

We calculate the cosmological frequency shift of a photon by integrating the chr.inv.-energy equation. De Sitter metric spaces do not rotate or deform[§], therefore the only acting

under the action of another additional force, that force deviates it from the geodesic (shortest) path thereby making the photon's motion non-geodesic. Such a deviating non-geodesic force or forces appear in the right-hand side of the equations of motion thereby making the right-hand side of the equations nonzero and, thus, transforming them into the non-geodesic equations of motion. See our monograph [2] for detail.

[†]For details on how these projections are deduced, see our first monograph [1], in which we considered geodesic particle motion in terms of chronometric invariants (physically observable quantities in General Relativity), and also our second monograph [2] focused on non-geodesic motion.

[‡]The chr.inv.-derivation operators with respect to time and the spatial coordinates have the form: $\frac{\partial}{\partial t} = \frac{1}{\sqrt{g_{00}}} \frac{\partial}{\partial t}$ and $\frac{\partial}{\partial x^i} = \frac{\partial}{\partial x^i} + \frac{1}{c^2} v_i \frac{\partial}{\partial t}$.

[§]In de Sitter's metric (see it in the beginning of this article), we have $g_{0i} = 0$. This means that the linear rotational velocity of such a space is zero $v_i = -c \frac{g_{0i}}{\sqrt{g_{00}}} = 0$ and also the angular velocity tensor $A_{ik} = 0$. Hence, de Sitter metric spaces do not rotate. In addition, the chr.inv.-metric tensor in a de Sitter space has the form $h_{ik} = -g_{ik} + \frac{1}{c^2} v_i v_k = -g_{ik}$. It does not depend on time because the non-zero g_{ik} components of de Sitter's metric, which are $g_{11} = -(1 - \frac{\lambda r^2}{3})^{-1}$, $g_{22} = -r^2$, $g_{33} = -r^2 \sin^2 \theta$, do not depend on time. Hence, the space deformation tensor is zero $D_{ik} = 0$. This means that de Sitter metric spaces do not deform, i.e., they are a kind of static spaces.

*This is a photon, the motion of which is non-deviated by another force than the forces caused by the space itself (gravitation, rotation and deformation), so it travels along a shortest (geodesic) trajectory. If a photon is also

factor in the chr.inv.-energy equation is the non-Newtonian gravitational force F_i . Because the force and the physically observable time interval in a de Sitter space are

$$F_1 = \frac{\lambda c^2}{3} \frac{r}{1 - \frac{\lambda r^2}{3}}, \quad d\tau = \sqrt{g_{00}} dt = \sqrt{1 - \frac{\lambda r^2}{3}} dt,$$

we obtain the chr.inv.-energy equation of a photon travelling along the radial direction $x^1 = r$ in a de Sitter space

$$\frac{d\omega}{d\tau} - \frac{\omega}{c^2} F_1 c^1 = 0$$

in the form

$$d \ln \omega = \frac{\lambda r}{3} \frac{dr}{1 - \frac{\lambda r^2}{3}}$$

or, since $d \ln \left(1 - \frac{\lambda r^2}{3}\right) = -\frac{2\lambda r}{3} \frac{dr}{1 - \frac{\lambda r^2}{3}}$,

$$d \ln \omega = -\frac{1}{2} d \ln \left(1 - \frac{\lambda r^2}{3}\right),$$

integrating which we obtain the photon's frequency ω and its cosmological shift z (without specifying the sign of λ)*

$$\omega = \frac{\omega_0}{\sqrt{1 - \frac{\lambda r^2}{3}}} \simeq \omega_0 \left(1 + \frac{\lambda r^2}{6}\right),$$

$$z = \frac{\omega - \omega_0}{\omega_0} = \frac{1}{\sqrt{1 - \frac{\lambda r^2}{3}}} - 1 \simeq \frac{\lambda r^2}{6}.$$

As you can see from the above formula, we have obtained that in any de Sitter universe there is a parabolic (non-linear) cosmological shift in the frequency of photons. Two options of the cosmological frequency shift are conceivable, depending on the sign of λ :

1. In a de Sitter universe with $\lambda > 0$, we have $z > 0$ that means a *parabolic cosmological redshift* — the frequency of a photon decreases as it travels, because with $\lambda > 0$ the non-Newtonian gravitational forces acting in a de Sitter world are forces of repulsion, which decelerate photons travelling towards the observer. In this case, the physical vacuum has a negative density $\check{\rho} < 0$,

*The above z is not a kind of the Doppler frequency shift and is therefore calculated using a different formula. The Doppler redshift z is a decrease in the frequency of the signal emitted by a source moving away from the observer, and the Doppler blueshift is an increase in the signal's frequency when its source moves towards the observer. In contrast, in the case of a de Sitter space under consideration, the source of photons neither moves away nor approaches the observer (the distance r between them remains unchanged). In this case, the photon frequency shift is due only to the non-Newtonian gravitational field attributed to such a space (see the chr.inv.-energy equation that above). In the formula for z , which we have obtained, ω_0 is the frequency of the photon in the case, where its source coincides with the observer ($r = 0$), and ω is the photon's frequency in the case, where the source of the photon is located at a distance r from him.

the pressure inside it is positive $\check{p} = -\check{\rho}c^2 > 0$ (which means that the physical vacuum contracts), the three-dimensional physically observable curvature $C = \frac{1}{\Re^2}$ is negative $C < 0$ and, therefore, the observable curvature radius of space \Re has an imaginary numerical value. The latter means that the space geometry is hyperbolic (what the geometry of a de Sitter space should not be). In addition, $\check{\rho} < 0$ contradicts the physical requirement that any kind of observable matter must have a positive mass and density;

2. In a de Sitter universe with $\lambda < 0$, we have $z < 0$ that means a *parabolic cosmological blueshift* — the frequency of a photon increases as it travels, since with $\lambda < 0$ the non-Newtonian gravitational forces acting in a de Sitter world are forces of attraction (they accelerate photons travelling towards the observer). In this case, the physical vacuum has a positive density $\check{\rho} > 0$, its pressure is negative $\check{p} = -\check{\rho}c^2 < 0$ (which means that the physical vacuum is an expanding medium), the three-dimensional physically observable curvature is positive $C = \frac{1}{\Re^2} > 0$ and, therefore, the observable curvature radius of space \Re has a real numerical value (this means that the space geometry is spherical as it should be in a de Sitter space).

In other words, in a de Sitter world with $\lambda > 0$ there is a non-linear (parabolic) cosmological redshift, and this our theoretical finding corresponds to the non-linearity of the cosmological redshift in the spectra of distant galaxies, which was recently discovered by astronomers[†]. But the $\lambda > 0$ case considered above does not satisfy such obvious physical requirements as a positive density of distributed matter and the real radius of the Universe. On the other hand, despite the fact that in a de Sitter world with $\lambda < 0$ there are no violations of the above physical requirements, in such a universe we have a parabolic cosmological blueshift.

We were looking for a solution that would resolve this dilemma. As a result, we have arrived at a conclusion that the above contradiction is resolved if we take Einstein's field equations in the following form

$$R_{\alpha\beta} - \frac{1}{2} g_{\alpha\beta} R = -\kappa T_{\alpha\beta} - \lambda g_{\alpha\beta},$$

where the last term $\lambda g_{\alpha\beta}$ is taken with the opposite (negative) sign unlike Einstein's original equations, in which this term is positive. In this case,

$$R_{\alpha\beta} - \frac{1}{2} g_{\alpha\beta} R = -\kappa \left(T_{\alpha\beta} + \frac{\lambda}{\kappa} g_{\alpha\beta} \right),$$

where the right-hand side contains the sum $T_{\alpha\beta} + \frac{\lambda}{\kappa} g_{\alpha\beta}$ (as it should be according to the logic of things) and the energy-

[†]See, for example, the surveys [20–22] and the original research results referred therein.

momentum tensor of the physical vacuum is*

$$\check{T}_{\alpha\beta} = \frac{\lambda}{\kappa} g_{\alpha\beta}.$$

In this case, in a de Sitter world with $\lambda > 0$ and, therefore, with a parabolic cosmological redshift, we have

$$\check{\rho} = \frac{\lambda}{\kappa} > 0, \quad \check{p} = -\check{\rho}c^2 < 0,$$

and, therefore (following the same deduction as on page 7),

$$\check{\rho} = \frac{C}{2\kappa} = \frac{1}{2\kappa\mathfrak{R}^2}, \quad \lambda = \frac{C}{2} = \frac{1}{2\mathfrak{R}^2},$$

$$\check{p} = -\frac{c^2 C}{2\kappa} = -\frac{c^2}{2\kappa\mathfrak{R}^2},$$

from which we obtain positive numerical values of the three-dimensional physically observable curvature $C = \frac{1}{\mathfrak{R}^2}$ and the observable curvature radius of space \mathfrak{R}

$$C = 2\lambda > 0, \quad \mathfrak{R} = \frac{1}{\sqrt{C}} > 0.$$

In addition, there is one more property of de Sitter worlds with $\lambda > 0$. As follows from de Sitter's metric (see it in the beginning of this article) that the state of gravitational collapse (it is characterized by the condition $g_{00} = 0$) arises in a de Sitter space with $\lambda > 0$ under the obvious condition $\frac{\lambda r^2}{3} = 1$. As Larissa obtained in 2010 [3], "...since Schwarzschild's metric of the space inside a sphere of incompressible liquid transforms into de Sitter's metric by the collapse condition and the condition $\lambda = \frac{3}{a^2}$, we arrive at the conclusion: space inside a sphere of incompressible liquid, which is in the state of gravitational collapse, is described by de Sitter's metric, where the λ -term is $\lambda = \frac{3}{a^2}$. All these can be applied to the Universe as a whole, because it has mass, density, and radius such as those of a collapsar. Therefore, the Universe is a collapsar, whose internal space, being assumed to be a sphere of incompressible liquid, is a de Sitter space with $\lambda = \frac{3}{a^2}$ (here a is the radius of the Universe)." Larissa called this model the *de Sitter bubble*.

Let us calculate the physically observable curvature radius \mathfrak{R} of such a de Sitter space (it does not coincide with the metric radius a of the de Sitter sphere). Since the collapse condition in a de Sitter world arises under $\frac{\lambda r^2}{3} = 1$, where the radial coordinate r meets the metric radius a of the de Sitter sphere ($r = a$), we have $\lambda = \frac{3}{a^2}$. On the other hand, the λ -term expressed with the three-dimensional physically observable curvature radius $C = \frac{1}{\mathfrak{R}^2}$ has the form $\lambda = \frac{C}{2} = \frac{1}{2\mathfrak{R}^2}$ (see the deduction above). As a result, we obtain that the observable

curvature radius of a de Sitter space with $\lambda > 0$, expressed with the metric radius a of the de Sitter sphere in the state of gravitational collapse, is

$$\mathfrak{R} = \frac{a}{\sqrt{6}} \approx 0.41 a,$$

which means that from the point of view of an observer located inside such a de Sitter bubble, the curvature radius of the bubble \mathfrak{R} is less than its metric radius a (which is the greatest metric distance in the space).[†] As is seen from the above deduction, this is an observable effect of General Relativity due to the physically observable distortion of space caused by the gravitational field (λ -field, in this case).

Let us provide astronomers with a formula of physically observable cosmological distances inside a de Sitter universe with $\lambda > 0$. The theory of chronometric invariants (physical observables in the space-time of General Relativity) determines the square of the three-dimensional physically observable interval as $d\sigma^2 = h_{ik} dx^i dx^k$, where $h_{ik} = -g_{ik} + \frac{1}{c^2} v_i v_k$ is the chr.inv.-metric tensor, and $v_i = -c \frac{g_{0i}}{\sqrt{g_{00}}}$ is the linear rotational velocity of space. Since $g_{0i} = 0$ in de Sitter's metric (see the metric in the beginning of this article), de Sitter metric spaces do not rotate ($v_i = 0$). Therefore, $h_{ik} = -g_{ik}$ in any de Sitter space and, hence, $d\sigma^2 = h_{ik} dx^i dx^k = -g_{11} dr^2$ along the radial direction $x^1 = r$ in it. As a result, the three-dimensional physically observable interval along the radial direction in a de Sitter space has the form

$$d\sigma = \frac{dr}{\sqrt{1 - \frac{\lambda r^2}{3}}},$$

the integration of which together with the collapse condition $\frac{\lambda a^2}{3} = 1$ gives the formula of physically observable cosmological distances inside the de Sitter bubble

$$\sigma = a \arcsin \frac{r}{a}.$$

At small metric distances $r \ll a$ between cosmic objects and an observer (compared to the metric radius of the de Sitter sphere a , which is the metric radius of the Universe), we have $\arcsin \frac{r}{a} \approx \frac{r}{a}$. Therefore, at small metric distances $r \ll a$, the physically observable distances σ to the cosmic objects are $\sigma \approx r$. The farther a cosmic object is located from the observer, the greater the physically observed distance σ to this object is than the metric distance r to it. For the ultimately distant cosmic objects that are located at the distance equal to the metric radius of the Universe $r = a$ (the radius of the de Sitter bubble), the physically observable distance to them is

$$\sigma = a \arcsin 1 = \frac{\pi}{2} a \approx 1.57 a.$$

*And not $\check{T}_{\alpha\beta} = -\frac{\lambda}{\kappa} g_{\alpha\beta}$ as in the original version of Einstein's equations $R_{\alpha\beta} - \frac{1}{2} g_{\alpha\beta} R = -\kappa T_{\alpha\beta} + \lambda g_{\alpha\beta}$ that means $R_{\alpha\beta} - \frac{1}{2} g_{\alpha\beta} R = -\kappa (T_{\alpha\beta} - \frac{\lambda}{\kappa} g_{\alpha\beta})$, where on the right-hand side is the energy-momentum tensor of distributed matter $T_{\alpha\beta}$, from which $\frac{\lambda}{\kappa} g_{\alpha\beta}$ is subtracted.

[†]Note that the observable curvature radius is constant $\mathfrak{R} = \text{const}$ throughout a de Sitter space, because de Sitter metric spaces are a kind of constant curvature spaces by definition.

Finally, assuming the corrected version of Einstein's field equations (see above), we arrive at the third option to represent the observable Universe as a de Sitter world:

3. Our Universe is a de Sitter world with $\lambda > 0$, but the $\lambda g_{\alpha\beta}$ term in Einstein's field equations has the opposite (negative) sign unlike Einstein's original equations (in which this term is positive). In this case, the physical vacuum has a positive density $\check{\rho} > 0$, the pressure inside it is negative $\check{p} = -\check{\rho}c^2 < 0$ (the physical vacuum expands), the three-dimensional physically observable curvature is positive $C = \frac{1}{\mathfrak{R}^2} > 0$ and, therefore, the observable curvature radius of space \mathfrak{R} has a real numerical value (this means that the space geometry is spherical as it should be in a de Sitter space). Since $\lambda > 0$ the non-Newtonian gravitational forces acting in the space are forces of repulsion. They decelerate photons travelling towards the observer (the frequency of the photons decreases as they travel). As a result, the observer should register a *parabolic (non-linear) cosmological redshift* in the frequency of the photons arriving at him from the far cosmos.

We vote for the above 3rd option as a model of the observable Universe, because in this case:

- a) the physical vacuum has a positive density $\check{\rho} > 0$, which satisfies the obvious physical requirement that any kind of observable matter in the Universe must have a positive mass and density,
- b) the observable curvature radius of space \mathfrak{R} is real (and not imaginary) and, hence, the space geometry is spherical (and not hyperbolic),
- c) the forces acting in such a space are the non-Newtonian gravitational forces of repulsion: they decelerate photons travelling towards the observer, thereby causing a non-linear (parabolic) redshift in the frequency of the photons,
- d) the entire observable Universe is located inside a huge de Sitter gravitational collapsar (its gravitational radius outlines the observable event horizon).

Let us apply this model to calculate the metric distance r to the galaxy JADES-GS-z13-0 that is the highest redshift galaxy known to date. It was discovered by astronomers in 2022, and its redshift is $z = 13.2$ [23]. Therefore, applying our parabolic redshift formula for this galaxy, we have

$$z = \frac{1}{\sqrt{1 - \frac{\lambda r^2}{3}}} - 1 = 13.2,$$

which with $\lambda = \frac{3}{a^2}$ taken into account (where a is the metric radius of the collapsed de Sitter sphere, i.e., the metric radius of the Universe) gives

$$r = a \sqrt{1 - \frac{1}{(z+1)^2}} = 0.998 a,$$

i.e., this galaxy is located on the very edge of the Universe. This fact is consistent with the observed non-linearity of the cosmological redshift discovered by astronomers [20–22] in the spectra of distant galaxies.

Even if galaxies with redshifts higher than $z = 13.2$ are discovered in the future, we will find that they are not much farther away from us than the aforementioned galaxy. This is thanks to our redshift formula, according to which the parabolic redshift curve z rises very strongly upward at large distances r even for very small increments of r . For example, a galaxy, the redshift of which is $z = 25$, according to our redshift formula is located at the distance $r = 0.999a$ from us, and the distance to a galaxy with $z > 100$ is $r = 0.99(9)a$.

For more or less nearby galaxies, the redshift of which is $z \approx 0.1$, our formula that above gives $r \approx 0.4a$.

All this confirms Larissa's suggestion, made in 2010 [3], according to which the observable Universe is a huge de Sitter gravitational collapsar (de Sitter bubble) with $\lambda > 0$, the gravitational radius of which outlines the observable event horizon.

We thank Pierre A. Millette for discussion and comments.

Submitted on January 7, 2024

References

1. Rabounski D. and Borissova L. Particles Here and Beyond the Mirror. The 4th revised edition, New Scientific Frontiers, London, 2023 (the 1st edition was issued in 2001).
Rabounski D. et Larissa Borissova L. Particules de l'Univers et au delà du miroir. La 2ème édition révisée en langue française, New Scientific Frontiers, Londres, 2023 (French translation).
2. Borissova L. and Rabounski D. Fields, Vacuum, and the Mirror Universe. The 3rd revised edition, New Scientific Frontiers, London, 2023 (the 1st edition was issued in 2001).
Borissova L. et Rabounski D. Champs, Vide, et Univers miroir. La 2ème édition révisée en langue française, New Scientific Frontiers, Londres, 2023 (French translation).
3. Borissova L. De Sitter bubble as a model of the observable Universe. *The Abraham Zelmanov Journal*, 2010, v. 3, 3–24.
4. Borissova L. and Rabounski D. Inside Stars. The 3rd edition, revised and expanded, New Scientific Frontiers, London, 2023 (the 1st edition was issued in 2013).
5. Borissova L. and Rabounski D. Cosmological redshift in the de Sitter stationary Universe. *Progress in Physics*, 2018, no. 1, 27–29.
6. Einstein A. Kosmologische Betrachtungen zur allgemeinen Relativitätstheorie. *Sitzungsberichte der Königlich Preussischen Akademie der Wissenschaften*, 142–152.
7. O'Riadaigh C., O'Keeffe M., Nahm W., Mitton S. Einstein's 1917 static model of the Universe: a centennial review. *The European Physical Journal H*, 2017, v. 42, 431–474; arXiv: 1701.07261.
8. De Sitter W. On the curvature of space. *Koninklijke Nederlandsche Akad. van Wetenschappen, Proceedings*, 1918, vol. XX, part I, no. 2, 229–243.
9. Carroll S. M. The cosmological constant. *Living Reviews in Relativity*, 2001, v. 4, 1–56.
10. Zelmanov A. L. Chronometric Invariants. Translated from the 1944 PhD thesis, American Research Press, Rehoboth, New Mexico, 2006.
11. Zelmanov A. L. Chronometric invariants and accompanying frames of reference in the General Theory of Relativity. *Soviet Physics Doklady*, 1956, v. 1, 227–230 (translated from *Doklady Akademii Nauk USSR*, 1956, v. 107, issue 6, 815–818).

12. Zelmanov A. L. On the relativistic theory of an anisotropic inhomogeneous universe. *The Abraham Zelmanov Journal*, 2008, vol. 1, 33–63 (translated from the thesis of the 6th Soviet Conference on the Problems of Cosmogony, USSR Academy of Sciences Publishers, Moscow, 1957, 144–174).
13. Rabounski D. and Borissova L. Physical observables in General Relativity and the Zelmanov chronometric invariants. *Progress in Physics*, 2023, no. 1, 3–29.
14. Gliner E. B. Algebraic properties of energy-momentum tensor and vacuum-like states of matter. *Journal of Experimental and Theoretical Physics*, 1966, v. 22, no. 2, 378–382.
Translated from: *Zhurnal Eksperimental'noi i Teoreticheskoi Fiziki*, 1966, v. 49, no. 2, 543–548.
15. Gliner E. B. Vacuum-like state of medium and Friedmann's cosmology. *Soviet Physics Doklady*, 1970, v. 15, 559–562.
Translated from: *Doklady Akademii Nauk SSSR*, 1970, v. 192, no. 4, 771–774.
16. Sakharov A. D. The initial stage of an expanding Universe and the appearance of a nonuniform distribution of matter. *Journal of Experimental and Theoretical Physics*, 1966, v. 22, no. 1, 241–249.
Translated from: *Zhurnal Eksperimental'noi i Teoreticheskoi Fiziki*, 1966, v. 49, no. 1, 345–357.
17. Synge J. L. *Relativity: the General Theory*. North Holland, Amsterdam, 1960.
18. Landau L. D. and Lifshitz E. M. *The Classical Theory of Fields*. The 4th edition, Butterworth-Heinemann, 1979 (the first English edition was issued in 1951, translated from the 1939 Russian edition).
19. Rabounski D. Cosmological mass-defect — a new effect of General Relativity. *The Abraham Zelmanov Journal*, 2011, v. 4, 137–161.
20. Heavens A. F., Matarrese S., Verde L. The non-linear redshift-space power spectrum of galaxies. *Monthly Notices of the Royal Astron. Society*, 1998, v. 301, 797–808.
21. Sigad Y., Branchini E., Dekel A. Measuring the nonlinear biasing function from a galaxy redshift survey. *The Astronomical Journal*, 2000, v. 540, 62–73.
22. Gebhardt H. and Jeong D. Nonlinear redshift-space distortions in the harmonic-space galaxy power spectrum. *Physical Review D*, 2020, v. 102, 083521; arXiv: 2008.08706.
23. Curtis-Lake E., Carniani S., Cameron A. et al. Spectroscopic confirmation of four metal-poor galaxies at $z = 10.3$ – 13.2 . *Nature Astronomy*, 2023, v. 7, 622–632; arXiv: 2212.04568.

LETTERS TO PROGRESS IN PHYSICS

Cosmological Redshift: Which Cosmological Model Best Explains It?

Dmitri Rabounski and Larissa Borissova

Puschino, Moscow Region, Russia

E-mail: rabounski@yahoo.com, lborissova@yahoo.com

Here we list three options that General Relativity has proposed over the past decade to explain the non-linear cosmological redshift, observed by astronomers. 1) If the redshift law is linear for nearby galaxies, then turns into exponential for distant galaxies, and triangulation of galaxies reveals non-zero curvature of space, then our Universe is an expanding Friedmann world. 2) If the linear redshift law turns into parabolic for distant galaxies, then our Universe is a static de Sitter world with $\lambda > 0$, in which the physical vacuum has a positive density, the observable curvature of space is positive, and the non-Newtonian gravitational forces acting there are repulsive forces increasing with distance (which cause photons to lose energy as they move). 3) If for distant galaxies the linear redshift law turns into exponential, but triangulation of galaxies does not reveal even the slightest curvature of space, then our Universe has a flat space, where the redshift in the spectra of distant objects is due only to the fact that the light-like sub-space (home of photons) of any metric space-time rotates with the speed of light, thereby creating a repulsive centrifugal force (which causes photons to lose energy as they move). In this case, any particular space metric creates only an addition to the exponential redshift law, which must take place even in a flat unperturbed space.

Cosmological redshift was discovered by Vesto Slipher (Flagstaff Observatory, Arizona), who first registered it on September 17, 1912 in the spectrum of Andromeda Nebula M31 [1], then over subsequent years in the spectra of other galaxies [2, 3]. Slipher's discovery of the cosmological redshift and the key contribution of his measurements into the discovery of the redshift law are explained in detail in the comprehensive 2013 surveys [4–6].

Slipher explained this result by the Doppler effect, saying that most galaxies move away from the observer with high velocities (therefore their spectra become redshifted). A few years after the discovery in the early 1920s, a number of scientists came up with the idea of explaining the cosmological redshift in the framework of one of the cosmological models proposed by the General Theory of Relativity. They all tried to deduce the dependence of the redshift and the corresponding radial velocity of galaxies on their distance from the observer as the Doppler effect in the framework of de Sitter's cosmological model. These were researchers such as Ludwik Silberstein, Knut Lundmark, Carl Wirtz, Edwin Hubble, Willem de Sitter. Their work is discussed in detail in recent historical studies by Michael Way, Harry Nussbaumer, Cormac O'Riada and their co-authors (if any), which are referred here in context of the discovery of the redshift law (see References).

Abbé Georges Lemaître was one of the researchers. After his "Docteur en Sciences" graduation from Université catholique de Louvain à Bruxelles and being ordained as a diocesan (secular) priest, he spent 1923–1925 outside Belgium. During

1923 he was a research associate in astronomy with Arthur Eddington at the Cambridge Observatory in England, then during 1924 — with Harlow Shapley at the Harvard Observatory (Massachusetts). Eddington introduced Lemaître to the General Theory of Relativity and relativistic cosmology, and with Shapley he studied the spectra of galaxies.

Returning to Belgium in 1925, Lemaître, like his aforementioned predecessors, tried to explain the observed cosmological redshift in the framework of de Sitter's cosmological model. This is a spherical universe of constant curvature filled with the physical vacuum called the λ -field, which is given by the λ -term in de Sitter's space metrics. Such a universe is usually static ($\lambda = \text{const}$), but can also be expanding if the λ -term and the space curvature (it is proportional to λ), having the same numerical value at any point in space, are proportional to the expansion rate, i.e., they depend on time (the case considered by Lemaître and his predecessors). Galaxies in an expanding universe are scattering away from the observer, so their observed spectra must be redshifted due to the Doppler effect. But, following his predecessors, Lemaître had come to an unsatisfactory result. He had deduced the same linear redshift law as Silberstein before him. But the obtained solution becomes invalid at the coordinate origin and even at a small distance from it, and also there the light source and the observer cannot be swapped (the solution depends on the coordinates). This means that, if the λ -term and the space curvature depend on time (the universe is expanding or compressing), then they can have the same numerical values at any point in space only if the space is either inhomogeneous or

anisotropic (or both) thereby contradicting the conditions of spherical symmetry and isotropy, which are assumed in de Sitter's metric. In other words, Lemaître had proved that the studies of his predecessors, in which they tried to deduce the Doppler redshift in an expanding de Sitter universe, lead to nonsense. Lemaître explained all of the above in his 1925 paper [7], which was then reprinted in 1926 [8].

The mentioned defeat does not mean that de Sitter's metric itself is bad, but is due to the fact that this metric can only be static. Whereas the Doppler redshift, which Lemaître and his predecessors tried to deduce, is specific to such a space metric that initially depends on time.

Therefore in 1926, Lemaître immediately turned to Friedmann's cosmological model of an expanding (or compressing) universe [9, 10], since the Doppler redshift naturally accompanies the expansion of space. This model describes an approximately empty spherical universe (with no islands of mass or distributed substance), which is expanding or contracting on its own. Success awaited Lemaître on this path. He assumed that the Friedmann universe is expanding with a constant radial velocity, then easily expressed the expansion velocity from Friedmann's space metric and substituted it into the Doppler law known from classical physics. As a result, Lemaître had obtained a linear relationship between the cosmological redshift in the spectra of galaxies and the distance from them to the observer, which means a linear redshift law according to which the redshift for distant galaxies is greater than for nearby ones and increases proportionally to the distance. Then, using Slipher's measurements, he had estimated the numerical value of the constant coefficient in this linear relationship, which is now known as the *Hubble constant*. Lemaître reported these results, including the discovery of the redshift law and the estimation of the redshift law constant, in his fundamental 1927 paper published in *Annales de la Société Scientifique de Bruxelles* [11]. But this publication in the obscure French-language journal was not noticed in the scientific community.

Two years later, Edwin Hubble published his 1929 paper [12] that brought him worldwide fame. In this paper, with a number of omissions because he was never fluent in General Relativity, Hubble repeated the results obtained by Lemaître, including the linear redshift law and the redshift law constant estimated using Slipher's measurement data. Hubble did not refer to his use of Slipher's measurements and Lemaître's 1927 paper in which Lemaître reported his discovery of the redshift law. Therefore, the redshift law later became known as *Hubble's law* or the *Hubble redshift*.

When in 1931 an English translation of Lemaître's 1927 paper was submitted through Eddington to the *Monthly Notices of the Royal Astronomical Society*, the passages about his discovery of the redshift law and his estimate of the redshift law constant were removed by the editor because these results had already been attributed to Hubble. Finally, the English translation of Lemaître's 1927 paper was published [13],

but with significant censorship. In the same issue of the journal, Lemaître also published another paper [14], in which he outlined the details of his theory of the expanding Universe; a short version of the second article was then reprinted in French [15]. Lemaître did not discuss the above editorial decision: as a truly good Catholic, he always believed that "God hath commanded so" and never tried to defend his authorship of the redshift law and the redshift constant.

This story was known to a narrow circle of scientists back in the 1980s [16]. Then in the early 2000s, Hubble's authorship of the redshift law was publicly questioned in favour of Lemaître in the 2003 article [17] and the detailed 2009 book [18] on this subject. This drama was revealed in full power in 2011 by two historians of science [19, 20], which caused widespread resonance in the scientific community in the same 2011 thanks to the science news reports on this subject, which were first published in *Forbes* [21], then — in *Nature News* [22, 23] and *Nature* [24]. All this in 2011–2013 led to a revision of Hubble's rôle in this discovery and the recognition of Lemaître's authorship of the redshift law with the key contribution of Slipher's measurements; see [25–29] for example.

In the century passed since Slipher's measurements, observational astronomy techniques and observational equipment have made significant progress. Astronomers now have a vast amount of data on the redshifts and radial velocities of galaxies (instead of only a few dozens known in the 1920s). As a result, in the last two decades, astronomers claim about the possible existence of a deviation from the linear redshift law, which needs a theoretical explanation: see, for example, the surveys [30–32] on this subject and the original research results referred therein.

However, if following the same way of theoretical explanation as Lemaître and his predecessors did, we arrive at a problem. The essence of the problem is that neither Lemaître nor his predecessors deduced the cosmological redshift law directly from the specific space metric that they chose. In essence, they merely postulated that the redshift occurs in the spectra of galaxies due to their scattering away from the observer, i.e., due to the Doppler effect. They followed the "two-step path" of mathematical deduction. At the first stage of their deduction, they somehow extracted the expansion rate of the Universe from the specific space metric that they chose (as the change rate of the curvature radius of space). Then they merely substituted this speed into the Doppler effect formula known from classical physics, and thus obtained the cosmological redshift law. This is what Lemaître did, and this is what his predecessors did. It cannot be said that such a method is very consistent with theoretical physics, since the origin of the cosmological redshift is initially postulated as a result of the Doppler effect in scattering galaxies in an expanding universe, and also a "mixture" of classical physics and General Relativity is used in the derivation.

If, in solving a physics problem, we decide to solve, say, the forced oscillation equation, we are essentially postulating that the cause of this effect lies in forced oscillations, and then we obtain a solution that automatically “confirms” the initially postulated forced oscillations. In other words, if we initially postulate the origin of the cosmological redshift effect, say, as a result of the Doppler effect or something else, then no matter what mathematical operations we perform next, we get the same effect that we postulated at the beginning, but only expressed in a mathematically more extended and elegant form.

Therefore, if we like to find the truly origin of the cosmological redshift effect, we should never postulate its origin. In addition, in order to be honest, if we like to deduce the cosmological redshift law as a space-time effect, i.e., as an effect in the framework of a cosmological model provided by General Relativity, we should follow only with the equations of General Relativity, and never use the equations and laws of classical physics (such as the Doppler effect formula). In other words, the cosmological redshift law should be obtained from the equations of General Relativity, and without any preliminary assumptions about its origin. This is the solely right way how to do things in theoretical physics.

In this letter, we list the newest solutions that are most fit for explaining the observed cosmological redshift, including its non-linearity. These solutions have been obtained since 2009 using the same original derivation method that has never been used for this purpose before — solving the scalar geodesic equation (energy equation) for a photon travelling from a source to an observer in the space-time of General Relativity. These solutions were obtained using only the equations of General Relativity, and without any prior assumptions about the nature of the cosmological redshift.

The solutions are different only because of the geometric structure of space, which is different for different space metrics (cosmological models). In other words, the mathematical derivation merely follows the geometric structure of the space in which it is performed. Thus, the resulting redshift law merely shows how the frequency of a travelling photon changes according to the geometric structure of the particular space (cosmological model) in which the photon travels.

The mentioned new method used to derive the cosmological redshift law dates back to our research studies of the 1990s, which we summarized in 2001 in our two monographs [33, 34]. The first monograph focuses on the geodesic (free) motion of mass-bearing and massless (light-like) particles in the space-time of General Relativity, and the second monograph examines their non-geodesic (non-free) motion.

As always in our studies we used the mathematical apparatus of chronometric invariants, which are physically observable quantities in the space-time of General Relativity. Such quantities are obtained as the projections of four-dimensional

(general covariant) quantities onto the three-dimensional spatial section and the time line associated with a particular observer and his laboratory. Such quantities depend on the geometric and physical properties of the real physical space of the observer, as well as the laboratory standards to which he compares his measurement results. Therefore, if we have all quantities and equations of General Relativity expressed in the chronometrically invariant form, then we do not need to think about which of the obtained solutions are physically observable (that was a common problem in General Relativity in the past), since all the obtained solutions are, by definition, measurable on practice. The mathematical apparatus of chronometric invariants is also known as the Zelmanov chronometric invariants in honor of Abraham Zelmanov, who developed it in 1944; see our detailed survey of chronometric invariants [35] and references therein.

As for the mentioned new method used to derive the cosmological redshift law, it is simple.

The four-dimensional equations of motion of a particle in space-time have two physically observable projections. The projection onto the time line of the observer is a scalar equation showing how the particle’s energy changes in time, depending on the properties of the observer’s space. In other words, this is the *energy equation* of the particle. The projection onto the spatial section associated with the observer (his three-dimensional space) is the three-dimensional vector equation of motion of the particle, which also depends on the properties of the observer’s space.

Integrating the scalar equation of motion (energy equation) of mass-bearing particles, Dmitri in 2009–2011 derived that the observable masses of cosmic bodies depend on their distance from the observer. He had called this the *cosmological mass-defect* [36], which is a new effect predicted according to General Relativity. The cosmological mass-defect depends on the specific metric of space, i.e., on the geometric structure of the specific space (particular cosmological model). Dmitri had calculated the cosmological mass-defect in the space of the most commonly used space metrics (cosmological models), such as Schwarzschild’s mass-point metric, Reissner-Nordström’s metric of the space of an electrically charged mass-point, Gödel’s metric of the rotating space with self-closed time-like geodesics, Schwarzschild’s metric inside a sphere filled with an incompressible liquid, de Sitter’s metric inside a sphere filled with the physical vacuum, Einstein’s metric inside a sphere filled with an ideal liquid and the physical vacuum, and also Friedmann’s metric of a deforming (expanding or compressing) space.

Accordingly, by integrating the scalar equation of motion (energy equation) of a massless light-like particle, such as a photon, we obtain its physically observable frequency as a function of the travelled distance. This is the way to derive the cosmological redshift law in the space of any specific metric (particular cosmological model), without any prior assumptions about the nature of the cosmological redshift. This is

how Dmitri in 2011 derived the cosmological redshift law in the space of each of the aforementioned cosmological models [37] (see also his 2012 short paper [38]), by analogy with the cosmological mass-defect.

The above work [37] has its own background and continuation. A year earlier, in 2010, Larissa considered a Sitter sphere in the state of gravitational collapse (its radius coincides with its gravitational radius). She showed that a de Sitter collapsar (*de Sitter bubble*) is fit to the observed Universe [39]. Integrating the scalar equation of motion (energy equation) of photons, based on her *de Sitter bubble model*, showed a parabolic redshift law [37, §6], which remains valid outside the state of gravitational collapse. Then in 2013, in our monograph on astrophysics [40, §6.4–6.5] (§5.1 in the 1st edition), we proved that the parabolic redshift law takes place a de Sitter space, in which $\lambda > 0$, the physical vacuum has a positive density, and the observable curvature radius of space is positive (otherwise it is a blueshift). Our redshift studies in a de Sitter universe were summarized in a short paper in 2018 [41] and then in an extended paper in 2023 [42].

The same method as above for deriving the cosmological redshift law was used in the 2009 papers [43–45], in which Dmitri had derived an exponential cosmological redshift due to the global non-holonomy of space.

The term *holonomy* dates back to Schouten's theory of non-holonomic manifolds and was first used in General Relativity in 1944 by Zelmanov [35]. If the time lines that “pierce” a three-dimensional spatial section are everywhere orthogonal to it, then the space (space-time) is *holonomic*. Otherwise it is *non-holonomic*. Zelmanov had proved that $g_{0i} \neq 0$ in non-holonomic spaces, which manifests itself in the form of a rotation of the spatial section (three-dimensional space) with a speed depending on g_{0i} , and this rotation cannot be removed by coordinate transformations. See [35] for detail.

Dmitri had showed in the third paper [45] that although each particular space (space-time) has its own specific metric and does not necessarily have a three-dimensional rotation, its light-like sub-space (home of photons) always rotates with the speed of light (varying depending on the gravitational potential). The light-speed rotation of the light-like space cannot be removed by coordinate transformations and is due to the sign-alternating structure of any space-time metric (which distinguishes the time axis from the spatial coordinate axes). In other words, the light-like space (in which photons travel) is always strictly non-holonomic. This rotation creates a centrifugal force that affects only particles in the light-like space (such as photons). By assuming the mentioned rotation when integrating the scalar equation of motion (energy equation) of photons, Dmitri had derived the exponential redshift law. This law should take place even in a flat unperturbed space (space-time), while each particular space metric creates only an addition to the exponent.

As for the origin of the cosmological redshift and the cosmological mass-defect, it can be understood from the scalar

equation of motion (energy equation), which for photons and mass-bearing particles has the form, respectively,

$$\frac{d\omega}{d\tau} - \frac{\omega}{c^2} F_i c^i + \frac{\omega}{c^2} D_{ik} c^i c^k = 0,$$

$$\frac{dm}{d\tau} - \frac{m}{c^2} F_i v^i + \frac{m}{c^2} D_{ik} v^i v^k = 0,$$

in which m is the relativistic mass of a mass-bearing particle, travelling with the velocity $v^i = \frac{dx^i}{d\tau}$, and ω is the frequency of a photon (photons travel with the velocity of light $c^i = \frac{dx^i}{d\tau}$, for which $c_i c^i = c^2 = \text{const}$).

If the space is static (the tensor of the space deformation rate is $D_{ik} = 0$), then $d\tau$ is reduced in the equations, which then are integrated with respect to the radial coordinate $x^1 = r$. As a result, we obtain the mass-bearing particle's mass m and the photon's frequency ω as a function of the distance r from the observer (for whom $r = r_0 = 0$).

If the gravitational inertial force is $F_i = 0$ (there is no gravitational field and rotation of space), but the space is deforming (expanding or compressing), then when multiplying the equations by the metric tensor h_{ik} , the multiplier $h_{ik} c^i c^k = c^2$ is reduced and the equations are integrated with respect to the travel time τ . In this case, we obtain the mass-bearing particle's mass m and the photon's frequency ω as a function of the time t travelled from the source (where $t = t_0 = 0$) to the observer (which is the reverse path of integration, changing the sign of the integration result).

Therefore, the origin of the cosmological redshift and the cosmological mass-defect is clearly seen from the equations. If the gravitational inertial force, consisting of a term given by the gravitational potential and a term given by the centrifugal force, is a force of repulsion ($F_1 > 0$) or the space is expanding ($D_{11} > 0$), then the repulsive force decelerates photons travelling to the observer, thereby producing a loss of the photon energy $E = \hbar\omega$ (*photon redshift*). In the case of mass-bearing particles such as cosmic bodies, their masses (and energies $E = mc^2$) registered by the observer are less than their actual masses (and energies) at their distant locations.

Otherwise, if the gravitational inertial force is a force of attraction ($F_1 < 0$) or the space is compressing ($D_{11} < 0$), then the force accelerates photons travelling to the observer, thereby producing a gain of their energy (*photon blueshift*), and the masses of distant cosmic bodies registered by the observer are greater than their actual masses at their distant locations.

This means that both the cosmological mass-defect and the cosmological redshift arise from the specific geometric structure of each particular space.

Below we list three different solutions for the cosmological redshift law, which can be considered to fit to the observed Universe. The first two were derived in 2011 [37], while the third solution — in 2009 [43–45], all using the above method of integrating the scalar equation of motion (energy equation) for photons.

Cosmological redshift in an expanding Friedmann universe. In such a universe, the frequency ω of a photon registered by an observer away from the emitted photon is

$$\omega = \omega_0 e^{-\frac{\dot{R}}{R} t},$$

where R is the curvature radius of space (the Universe's radius in this case), and \dot{R} is the rate of its expansion. This exponential law transforms into the linear

$$\omega \simeq \omega_0 \left(1 - \frac{\dot{R}}{R} t\right)$$

at short duration of the photon's travel (and, respectively, at small distances from the photon's emitter to the observer).

We see from the above formulae that the photon's frequency ω registered by the observer is lower than its frequency ω_0 at the initial moment of time $t = t_0 = 0$, when it was emitted by a source in the far cosmos. The farther the photon's emitter is located from the observer, the lower the photon's frequency ω registered by him: the photon's frequency is redshifted upon arrival at the observer.

The above formulae for the photon's frequency result in the *exponential redshift law*

$$z = \frac{\omega_0 - \omega}{\omega} = e^{\frac{\dot{R}}{R} t} - 1, \quad z > 0,$$

which transforms into the *linear redshift law* at short duration (and small distances) of the photon's travel

$$z \simeq \frac{\dot{R}}{R} t.$$

As was shown in [37], the above formulae for the photon's frequency and redshift are the same in both a constant-speed expanding Friedmann universe ($\dot{R} = \text{const}$) and a constant-deformation Friedmann universe (where $\frac{\dot{R}}{R} = \text{const}$).

So, the cosmological redshift in an expanding Friedmann universe increases with distance to cosmic bodies according to the *exponential redshift law*, which transforms into the *linear redshift law* at short duration (and small distances) of photons' travel.

Here we should make a short remark about Lemaître's linear redshift law. With all our respect to Georges Lemaître, he did not solve any equations. His 1927 paper focused on how to find the expansion rate of the Universe from Friedmann's metric. Then he substituted this rate into the Doppler redshift formula taken from classical physics. In fact, he merely renamed the emitter's velocity in Doppler's formula as the expansion rate of the Universe (and justified this renaming by showing how the expansion rate is found from Friedmann's metric). But by doing this, Lemaître could not obtain anything other than the linear redshift law, because it initially follows from Doppler's formula at the velocity of the emitter, much lower than the velocity of light.

In contrast to what Lemaître did, the exponential redshift law formula that above is a mathematical solution obtained directly by solving the scalar equation of motion (energy equation) for photons travelling in an expanding Friedmann universe. It was derived without any prior assumptions about the form of the redshift law. This is the solely right way how to do things in theoretical physics.

The said does not affect the memory about Abbé Lemaître as an outstanding scientist and good Catholic, an exemplar of human decency and honesty, and does not diminish his fundamental contribution to relativistic cosmology.

Cosmological redshift in a static de Sitter universe. In a de Sitter universe, the frequency ω_0 of a photon registered by an observer (for whom $r = r_0 = 0$) upon its arrival is also lower than its frequency ω at the location of its distant source, from which it was emitted. This dependence is expressed with the parabolic (square) law

$$\omega = \frac{\omega_0}{\sqrt{1 - \frac{\lambda r^2}{3}}},$$

which at small distances r between the photon's source and the observer transforms into the simplified law

$$\omega \simeq \omega_0 \left(1 + \frac{\lambda r^2}{6}\right).$$

The farther the emitter is located from the observer, the lower the photon's frequency ω_0 registered by him. Thus, the photon's frequency is redshifted upon arrival at the observer in a de Sitter universe.

These formulae for the photon's frequency result in the *parabolic (square) redshift law*

$$z = \frac{\omega - \omega_0}{\omega_0} = \frac{1}{\sqrt{1 - \frac{\lambda r^2}{3}}} - 1, \quad z > 0,$$

which at small distances r takes the simplified form

$$z \simeq \frac{\lambda r^2}{6}.$$

At the ultimately large distance in space (event horizon, where $r = a$), which is determined in a de Sitter universe by the condition $\frac{\lambda r^2}{3} = \frac{\lambda a^2}{3} = 1$, the photon's frequency and redshift are maximum: $\omega_{\max} = \infty$ and $z_{\max} = \infty$.

So, the cosmological redshift in a static de Sitter universe increases with distance to cosmic bodies according to the *parabolic (square) redshift law*.

This redshift law depends on the sign of the λ -term and, accordingly, the sign of the density of the physical vacuum (which is the filler of de Sitter space) and the sign of the physically observable curvature of space (since these quantities are connected with λ). It was proved in [40, §6.4–6.5] (§5.1 in the 2013 edition) and then summarized in [41, 42] that the

cosmological redshift ($z > 0$) takes place in a de Sitter universe, where $\lambda > 0$, the physical vacuum has a positive density (like substance, and not a negative density like field), the curvature radius of space is positive (the geometry of space is spherical, and not hyperbolic), and the non-Newtonian gravitational forces that act in any de Sitter space and increase with distance from the observer are repulsive forces. These repulsive forces cause photons to lose energy as they travel to the observer, thereby producing a redshift in the frequency of the photons. Otherwise (if $\lambda < 0$), there is not a cosmological redshift, but a blueshift ($z < 0$) and the curvature radius of space takes an imaginary numerical value (the geometry of space is hyperbolic).

Cosmological redshift due to the global non-holonomy of the light-like space. The term *non-holonomy* dates back to Schouten's theory of non-holonomic manifolds and was first used in General Relativity in 1944 by Zelmanov. If the time lines that "pierce" a three-dimensional spatial section are everywhere orthogonal to it, then the space (space-time) is *holonomic*. Otherwise it is *non-holonomic*. Zelmanov had proved that $g_{0i} = 0$ in holonomic spaces and $g_{0i} \neq 0$ in non-holonomic spaces. The latter manifests itself as a rotation of the spatial section (three-dimensional space) with a speed depending on g_{0i} , which cannot be removed by coordinate transformations. For detail, see our survey [35] and references therein.

It was proved [45] that the light-like sub-space of any space-time metric rotates with the speed of light, thereby creating a repulsive centrifugal force. This repulsive force only acts on particles in the light-like space (i.e., photons) in the direction away from the observer (coordinate origin), thereby causing photons to lose energy and frequency as they travel to him

$$\omega = \omega_0 e^{-\Omega t}, \quad \Omega \equiv H_0,$$

resulting in the *exponential redshift law*

$$z = \frac{\omega_0 - \omega}{\omega} = e^{\Omega t} - 1, \quad z > 0,$$

where ω_0 is the photon's frequency at the initial moment of time $t = t_0 = 0$, when it was emitted by a distant source in the cosmos, ω is its frequency upon arrival at the observer, and Ω is the angular rotational velocity of the light-like space due to its global non-holonomy (light-speed rotation), which is equal to the Lemaître-Hubble constant $H_0 = 2.3 \pm 0.3 \times 10^{-18} \text{ sec}^{-1}$ (as measured in the framework of the Hubble Space Telescope Key Project for 2001 [46]).

We see that the repulsive centrifugal force, which is always present in the light-like space (home of photons) due to its light-speed rotation, causes a redshift (loss of energy) in the frequency of a photon arrived from a distant source at the observer. The farther the photon's emitter (and longer is its travel time t), the lower the photon's frequency ω registered by the observer upon its arrival.

At short duration (and small distances) of the photon's travel we have the linear approximation for the photon's frequency

$$\omega \simeq \omega_0 (1 - H_0 t)$$

and the *linear redshift law*

$$z \simeq H_0 t.$$

So, the cosmological redshift due to the light-speed rotation of the light-like space (its global non-holonomy) increases with distance to cosmic bodies according to the *exponential redshift law*, which at short duration (and small distances) of photons' travel transforms into the *linear redshift law*.

Since the light-like space rotates with the speed of light due to only the sign-alternating structure of any space-time metric (which distinguishes the time axis from the spatial coordinate axes), and this rotation cannot be removed by coordinate transformations, the above exponential redshift law and its linear approximation at small distances should take place even in a flat unperturbed space. Any particular space metric should create only an addition to the above exponential redshift law, straightening this exponential curve or making it more curved.

Thus, the following three versions have been proposed according to General Relativity to explain the observed non-linear cosmological redshift law.

1. If the redshift in the spectra of nearby galaxies increases linearly with distance to them, then it turns into exponential for distant galaxies, and triangulation of galaxies reveals non-zero curvature of space, then our Universe is an expanding Friedmann world. In this case, photons lose energy as they travel to the observer due to the fact that they are decelerated by the expansion of space.

2. If the linear redshift law turns into parabolic for distant galaxies, then our Universe is a static de Sitter world with $\lambda > 0$, in which the physical vacuum has a positive density, the observable curvature is positive, and the non-Newtonian gravitational forces acting there are repulsive forces increasing with distance from the observer (which cause photons to lose energy as they travel to the observer).

3. If for distant galaxies the linear redshift law turns into exponential, but triangulation of galaxies does not reveal even the slightest curvature of space, then our Universe has a flat space, where the redshift in the spectra of distant objects is due only to the light-speed rotation of the light-like sub-space (home of photons) in any metric space-time, which creates a repulsive centrifugal force causing photons to lose energy as they travel to the observer. But in this case we should assume that the device with which the observer measures the redshift is connected with a light-like reference frame, which creates a problem for an ordinary observer, since he and his laboratory reference frame are related to ordinary substance.

Which of the above three options best explains the cosmological redshift in our Universe will be decided in accordance with astronomical observations.

Submitted on February 5, 2024

References

- Slipher V. M. The radial velocity of the Andromeda Nebula. *Lowell Observatory Bulletin*, 1913, v. 2, no. 8, 56–57.
- Slipher V. M. Spectrographic observations of nebulae (Reports of the 17th Meeting of the American Astron. Society). *Popular Astronomy*, 1915, v. 23, 21–24.
- Slipher V. M. Radial velocity observations of spiral nebulae. *The Observatory*, 1917, v. 40, 304–306.
- Peacock J. A. Slipher, galaxies, and cosmological velocity fields. *Astronomical Society of the Pacific Conference Series*, 2013, v. 471 “Origins of the Expanding Universe 1912–1923”, 3–23; arXiv: 1301.7286 (2013).
- Nussbaumer H. Slipher’s redshifts as support for de Sitter’s model and the discovery of the dynamic Universe. *Astronomical Society of the Pacific Conference Series*, 2013, v. 471 “Origins of the Expanding Universe 1912–1923”, 25–38; arXiv: 1303.1814 (2013).
- O’Raifeartaigh C. The contribution of V. M. Slipher to the discovery of the expanding Universe. *Astronomical Society of the Pacific Conference Series*, 2013, v. 471 “Origins of the Expanding Universe 1912–1923”, 49–61; arXiv: 1212.5499 (2013).
- Lemaître G. Note on de Sitter’s universe. *Journal of Mathematical Physics*, 1925, v. 4, no. 3, 188–192.
- Lemaître G. Note on de Sitter’s universe. *Publications du Laboratoire d’astronomie et de géodésie de l’Université de Louvain*, 1926, v. 2, 37–41 (reprinted from *Journal of Math. Physics*, see above).
- Friedmann A. Über die Krümmung des Raumes. *Zeitschrift für Physik*, 1922, Band 10, No. 1, 377–386 (published in English as: Friedman A. On the curvature of space. *General Relativity and Gravitation*, 1999, vol. 31, no. 12, 1991–2000).
- Friedmann A. Über die Möglichkeit einer Welt mit konstanter negativer Krümmung des Raumes. *Zeitschrift für Physik*, 1924, Band 21, No. 1, 326–332 (published in English as: Friedmann A. On the possibility of a world with constant negative curvature of space. *General Relativity and Gravitation*, 1999, vol. 31, no. 12, 2001–2008).
- Lemaître G. Un Univers homogène de masse constante et de rayon croissant rendant compte de la vitesse radiale des nébuleuses extragalactiques. *Annales de la Société Scientifique de Bruxelles*, ser. A, 1927, tome 47, 49–59.
- Hubble E. A relation between distance and radial velocity among extragalactic nebulae. *Proceedings of the National Academy of Sciences*, 1929, v. 15, 168–173.
- Lemaître G. A homogeneous universe of constant mass and increasing radius accounting for the radial velocity of extra-galactic nebulae. *Monthly Notices of the Royal Astronomical Society*, 1931, v. 91, no. 5, 483–490 (this is a substantially shortened English translation of the 1927 paper).
- Lemaître G. The expanding universe. *Monthly Notices of the Royal Astronomical Society*, 1931, v. 91, no. 5, 490–501.
- Lemaître G. L’expansion de l’espace. *Publications du Laboratoire d’astronomie et de géodésie de l’Université de Louvain*, 1931, v. 8, 101–120.
- Peebles P. J. E. Impact of Lemaître’s ideas on modern cosmology. In: “The Big Bang and Georges Lemaître”, Proceedings of the Symposium (Louvain-la-Neuve, Belgium, October 10–13, 1983), D. Reidel Publishing Co., Dordrecht, 1984, 23–30.
- Kragh H. and Smith R. W. Who discovered the expanding universe? *History of Science*, 2003, v. 41, 141–162.
- Nussbaumer H. and Bieri L. Discovering the Expanding Universe. Cambridge University Press, Cambridge, 2009.
- Van den Bergh S. The curious case of Lemaître’s equation no. 24. *Journal of the Royal Astronomical Society of Canada*, 2011, v. 105, 151; arXiv: 1106.1195 (2011).
- Block D. L. Georges Lemaître and Stigler’s law of eponymy. In the paper collection: “Georges Lemaître: Life, Science and Legacy”, *Astrophysics and Space Science Library*, 2012, v. 395, 89–96; Initially posted under the title “A Hubble eclipse: Lemaître and censorship”, arXiv: 1106.3928 (2011).
- Farrell J. Why Hubble’s law... wasn’t really Hubble’s. *Forbes*, June 15, 2011.
- Reich E. S. Edwin Hubble in translation trouble. Amateur historians say famed astronomer may have censored a foreign rival. *Nature News*, 27 June 2011.
- Reich E. S. Letter sheds light on alleged censorship by Hubble. *Nature News*, 11 July 2011.
- Livio M. Lost in translation: Mystery of the missing text solved. *Nature*, v. 479, 10 November 2011, 171–173.
- Shaviv G. Did Edwin Hubble plagiarize? arXiv: 1107.0442 (2011).
- Way M. J. and Nussbaumer H. Lemaître’s Hubble relationship. arXiv: 1104.3031 (2011).
- Nussbaumer H. and Bieri L. Who discovered the expanding universe? arXiv: 1107.2281 (2011).
- Way M. J. Dismantling Hubble’s legacy? *Astronomical Society of the Pacific Conference Series*, 2013, v. 471 “Origins of the Expanding Universe 1912–1923”, 97–132; arXiv: 1301.7294 (2013).
- Luminet J.-P. Editorial note to: Georges Lemaître, A homogeneous universe of constant mass and increasing radius accounting for the radial velocity of extra-galactic nebulae. *General Relativity and Gravitation*, 13 June 2013, v. 45, 1619–1633; arXiv: 1305.6470 (2013).
- Heavens A. F., Matarrese S., Verde L. The non-linear redshift-space power spectrum of galaxies. *Monthly Notices of the Royal Astronomical Society*, 1998, v. 301, 797–808.
- Sigad Y., Branchini E., Dekel A. Measuring the nonlinear biasing function from a galaxy redshift survey. *The Astronomical Journal*, 2000, v. 540, 62–73.
- Gebhardt H. and Jeong D. Nonlinear redshift-space distortions in the harmonic-space galaxy power spectrum. *Physical Review D*, 2020, v. 102, 083521; arXiv: 2008.08706.
- Rabounski D. and Borissova L. Particles Here and Beyond the Mirror. The 4th revised edition, New Scientific Frontiers, London, 2023 (the 1st edition was issued in 2001).
- Rabounski D. et Larissa Borissova L. Particules de l’Univers et au delà du miroir. La 2ème édition révisée en langue française, New Scientific Frontiers, Londres, 2023 (French translation).
- Borissova L. and Rabounski D. Fields, Vacuum, and the Mirror Universe. The 3rd revised edition, New Scientific Frontiers, London, 2023 (the 1st edition was issued in 2001).
- Borissova L. et Rabounski D. Champs, Vide, et Univers miroir. La 2ème édition révisée en langue française, New Scientific Frontiers, Londres, 2023 (French translation).
- Rabounski D. and Borissova L. Physical observables in General Relativity and the Zelmanov chronometric invariants. *Progress in Physics*, 2023, no. 1, 3–29.
- Rabounski D. Cosmological mass-defect — a new effect of General Relativity. *The Abraham Zelmanov Journal*, 2011, v. 4, 137–161.
- Rabounski D. Non-linear cosmological redshift: The exact theory according to General Relativity. *The Abraham Zelmanov Journal*, 2012, v. 5, 3–30.
- Rabounski D. On the exact solution explaining the accelerate expanding Universe according to General Relativity. *Progress in Physics*, 2012, no. 2, L1–L6.

39. Borissova L. De Sitter bubble as a model of the observable Universe. *The Abraham Zelmanov Journal*, 2010, v. 3, 3–24.
 40. Borissova L. and Rabounski D. Inside Stars. The 3rd edition, revised and expanded, New Scientific Frontiers, London, 2023 (the 1st edition was issued in 2013).
 41. Borissova L. and Rabounski D. Cosmological redshift in the de Sitter stationary Universe. *Progress in Physics*, 2018, no. 1, 27–29.
 42. Rabounski D. and Borissova L. On the lambda term in Einstein's equations and its influence on the cosmological redshift. *Progress in Physics*, 2023, no. 2, 4–12.
 43. Rabounski D. An explanation of Hubble redshift due to the global non-holonomy of space. *Progress in Physics*, 2009, no. 1, L1–L2.
 44. Rabounski D. Hubble redshift due to the global non-holonomy of space. *The Abraham Zelmanov Journal*, 2009, v. 2, 11–28.
 45. Rabounski D. On the speed of rotation of the isotropic space: Insight into the redshift problem. *The Abraham Zelmanov Journal*, 2009, v. 2, 208–223.
 46. Freedman W. L., Madore B. F., Gibson B. K., et al. Final results from the Hubble Space Telescope Key Project to measure the Hubble constant. *Astrophysical Journal*, 2001, v. 553, no. 1, 47–72.
-

Interpretation of Quantum Mechanics in Terms of Discrete Time II

Young Joo Noh

E-mail : yjnoh777@gmail.com, Seongnam, Korea.

From the perspective of discrete time, the macroscopic world and the microscopic world are divided using the Planck mass as a reference point. The microscopic world is a world where the nature of time is discrete and non-locality dominates, and the macroscopic world is a world where the nature of time is continuous and locality dominates. The macroscopic world is not reduced to the result of the order of the microscopic world, and the physical laws of both worlds are real. The differences between the two worlds lead to limitations in applying physical intuition formed in the macroscopic world to the microscopic world. As an alternative to this, a new model of the physical reality of matter in the microscopic world was proposed.

1 Boundary between the macroscopic world and the microscopic world

From a discrete time perspective, quantum waves are formed by the contributions of Δt future and past spinors, and can be expressed as follows [1]:

$$(x^\mu + \Delta x^\mu) \Psi(x^\mu) - x^\mu \Psi(x^\mu + \Delta x^\mu) = \Delta x^\mu \exp\left(-\frac{i}{\hbar} \Delta x^\alpha P_\alpha\right) \Psi(x^\mu). \quad (1)$$

In (1), the time component of Δx^μ is $c\Delta t$.

In order for (1) to be established, the following two assumptions are necessary:

1. $\Psi(x^\mu)$ is an analytic function.
2. $[x^\mu, P_\nu] = -i\hbar\delta_\nu^\mu$, where $P_\nu = i\hbar\frac{\partial}{\partial x^\nu}$.

Mathematically, there is no limit to the lower limit of Δx^μ , or Δt , in the Taylor expansion of $\Psi(x^\mu + \Delta x^\mu)$. However, there is a physical constraint on the lower limit of Δt . Δt is defined as the time taken for light to pass through the reduced Compton wavelength λ_c [2]:

$$\Delta t = \frac{\lambda_c}{c} = \frac{\hbar}{mc^2}. \quad (2)$$

As mass increases, λ_c decreases. However, physically, this process cannot proceed without limitations, because a black hole is formed when λ_c becomes the Schwarzschild radius r_s . Therefore, λ_c must satisfy the following conditions:

$$\left(\lambda_c = \frac{\hbar}{mc}\right) > \left(r_s = \frac{2Gm}{c^2}\right). \quad (3)$$

Since the mass at $\lambda_{c,p}$, the lower limit of λ_c , is the Planck mass m_p , the lower limit of Δt is the Planck time t_p .

$$\begin{aligned} \lambda_{c,p} &= \frac{\hbar}{m_p c} = \frac{2Gm_p}{c^2} \\ \Delta t_{\text{lower limit}} &= \frac{\hbar}{m_p c^2} = \sqrt{\frac{2\hbar G}{c^5}} = t_p. \end{aligned} \quad (4)$$

If $\Delta t \leq t_p$, the analytic expansion of $\Psi(x^\mu + \Delta x^\mu)$ is mathematically possible, but physically not possible. This means that (1) is not possible, so it can be said that plane waves as harmonic oscillations are not formed. In other words, $\Delta t = t_p$ becomes the boundary point of whether a quantum wave is formed or not. Since Δt is inversely proportional to mass, this boundary is determined only by mass. That is, the Planck mass. Using this as a reference point, the quantum world and the non-quantum world are divided.

The Planck mass is the boundary, but there is one more thing to consider. Eq. (1) is for a plane wave of a single wavelength. If the mass is close to the Planck mass (1.5×10^{-8} kg), it is of course not an elementary particle but a composite. In this case as well, for (1) to hold, the waves of all components must be in a coherent state. Therefore, the Planck mass is theoretically the maximum value of a quantum system where quantum waves can be formed. However, for actual composites in thermal equilibrium, even if the mass is less than the Planck mass, quantum waves may be canceled out and quantum phenomena may not appear. This tendency will be greater as the mass of the system or the number of components increases.

In fact, it can be inferred from existing quantum mechanics that the Planck mass is the boundary between the quantum world and the non-quantum world. The Compton wavelength of matter is defined as the wavelength of a photon with energy equal to its rest energy. However, when the wavelength of the photon becomes the Schwarzschild radius, the photon is confined by its own gravitational field. Therefore, the Compton wavelength is limited by the Planck length, and the mass at this point is the Planck mass. This means that the Planck mass represents the limit to which the Compton wavelength, which refers to the quantum characteristics of matters, can be achieved.

Now, I will discuss the properties of time when $m \geq m_p$. In (1) and the physical constraints of Δt , it was discussed that if $m < m_p$ ($\Delta t > t_p$), a quantum wave is formed, and if $m \geq m_p$ ($\Delta t \leq t_p$), a quantum wave is not formed. In the latter

case, Δt is not defined by physical constraints. In other words, the concept of discrete time does not apply to the physical system. If the concept of discrete time is not applied, there is only one possibility. That is continuous time. This means that if the mass of a physical system is greater than the Planck mass, the time applied to the system must be continuous. As a result of this discussion, the following conclusions can be drawn. With the Planck mass as the reference point, elementary particles in the microscopic world have their own discrete time, while the macroscopic world has continuous time. Since the characteristics of continuous time are independent of the mass of the object, all macroscopic objects have the same continuous time in their stationary inertial frames. This is why the time we experience feels as if it is universal.

The above contents are summarized and shown in the figure below. In Fig. 1, $\Delta t = 0$ in the $m \geq m_p$ range does not mean that (1) is applied, but simply represents continuous time.

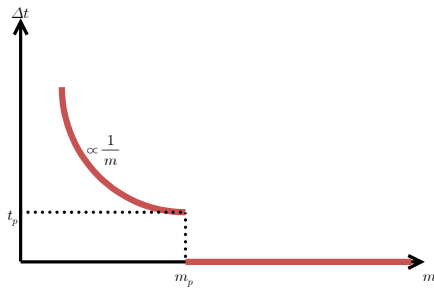


Fig. 1: $\Delta t - m$ graph

As you can see from Fig. 1, the macroscopic world is not on a continuous line with the microscopic world. In other words, the limit of any variable in the microscopic world cannot become the macroscopic world. Since the properties of time are completely different in the two worlds, the dynamical principles based on them are also bound to be different. Both the macroscopic world and the microscopic world are real worlds with their own unique characteristics. This perspective is very different from existing quantum mechanical interpretations. Most existing quantum mechanical interpretations (Copenhagen, many worlds, decoherence, etc.) view the macroscopic world as the limit of the continuum of the microscopic world.

In the microscopic world, the nature of time is discrete, and as discussed in the previous paper [4], matter in this discrete time repeats the process of wave collapse and propagation as a non-local wave. Thus, the characteristic of the microscopic world is non-locality. Meanwhile, in the macroscopic world, the nature of time is continuous. Since local principles naturally apply to fields defined in continuous time, the characteristic of the macroscopic world is locality. Naturally, the physical intuition of the world where locality ap-

plies and the world where non-locality applies is bound to be different. The physical intuition of the macroscopic world dominated by classical mechanics is clear. Things like particles, waves, and determined trajectories are concepts based on local principles. However, according to the discussion so far, the microscopic world is non-local, so intuition with concepts based on local principles is bound to have limitations. In the next section, I will present a model for a new physical intuition based on the non-locality of the microscopic world.

2 The new quantum mechanical reality of matter

As mentioned in the previous section, concepts such as particles, waves, and trajectories are concepts established in the macroscopic world where local principles are applied. They are concepts of physical reality that humans, as beings in the macroscopic world, infer from their experiences. However, there are bound to be limitations in describing the microscopic world with these concepts. One solution to this difficulty is Heisenberg's method as follows [5]:

We can no longer speak of the behaviour of the particle independently of the process of observation. As a final consequence, the natural laws formulated mathematically in quantum theory no longer deal with the elementary particles themselves but with our knowledge of them.

But I think more can be said about reality. We may think of the microscopic world as something that cannot be directly experienced. However, in reality, all parts of our body act according to the order of the microscopic world, and the basic parts of living things experience quantum phenomena. I think that what can be experienced can be drawn.

As can be seen in Fig. 2, the quantum mechanical reality presented here is composed of Compton sphere, spinor, and matter wave (i.e. de Broglie wave). The Compton sphere is a sphere with the reduced Compton wavelength as its radius, and as presented in the previous paper [4], it is a sphere formed by points contributing to the past and future of Δt at the center point. All points on the hemisphere are simultaneous events in discrete time Δt . Spinors contributing from the future hemisphere and spinors contributing from the past hemisphere combine at the center to form spinors at the central point. The spinors at this central point have phases according to (1), and a collection of identical phases forms a matter wave.

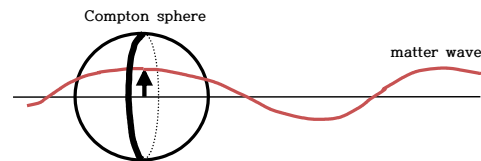


Fig. 2: The new quantum mechanical reality of matter

The wavefront of the same phase as a matter wave has the characteristics of a non-local wave. Due to their inherent characteristics, these non-local waves cause simultaneous wave collapse when they interact. (Please refer to the previous paper [4] for the process of non-local wave formation and propagation from the Compton sphere.) The start of wave propagation is the Compton sphere. While the wave is propagating, the Compton sphere no longer exists, but only a matter wave as a non-local wave. The interaction (inelastic scattering) causes an instantaneous collapse of the matter wave, and the resulting collapsed state is assumed to become a Compton sphere again. This is because the Compton sphere is the beginning of a non-local wave and can be viewed as an indecomposable elementary particle. Absorption of energy through interaction increases the frequency of the spinor phase within the Compton sphere. As a result, a matter wave as a new non-local wave with a shorter wavelength is formed and propagated. Meanwhile, electromagnetic waves are also non-local waves, but since they have no rest mass, the Compton sphere does not exist. It is assumed that the contraction of the wave due to interaction will result in only a localized electromagnetic field, the size of which will be determined by the size of the interacting matter. If there is a change in energy after interaction, it propagates as a wave with a new wavelength.

3 Conclusions

The distinction between the macroscopic world and the microscopic world has been interpreted from various perspectives since the beginning of quantum mechanics, and most perspectives have attempted to understand the macroscopic world as a continuation of the microscopic world. However, from the perspective of discrete time, the two worlds are not on a continuous line and take on completely different appearances with the Planck mass as the reference point. In the macroscopic world, the nature of time is continuous, and the principle of locality governs. In the microscopic world, the nature of time is discrete, and non-locality becomes the basic principle of existence. The macroscopic world cannot be reduced to the result of the order of the microscopic world, and the two worlds form a kind of hierarchical relationship of existence.

From the above perspective, it can be said that it is natural that concepts such as particles, waves, and trajectories, which are concepts of physical reality in the macroscopic world, that is, classical mechanics, will be difficult to apply to the microscopic world. The concept of physical reality in the microscopic world, inferred from a discrete time perspective, is quite different from that in the macroscopic world. As presented in the previous paper [4], the wave concept of the microscopic world is not a wave concept based on local principles of the macroscopic world, but a non-local wave. There are also many differences in the concept of particles. The

concept of a particle in the macroscopic world is a particle without an internal structure of finite size or a point particle with no size. These particle concepts are abstracted on the basis of continuous space and time. The concept of a particle of a finite size without an internal structure still has the meaning of an internal area, and a point particle without size is premised on the meaning of an infinite division of continuous space. From a discrete time perspective, an elementary particle in the microscopic world, in the case of matter, is a Compton sphere. The size of the Compton sphere is determined by the rest mass, and although it is an elementary particle that cannot be resolved, it has an internal structure. The internal structure mentioned here does not mean a composite such as an atom. The Compton sphere consists of two hemispheres with time differences, and has an internal structure in the sense that a spinor field is formed at the center. Since the spinor formed at the center has a phase, the Compton sphere as a particle is not maintained and propagates as a matter wave over time. Due to interaction (this corresponds to the case of inelastic scattering; during elastic scattering, it maintains its wave properties without wave collapse), the matter wave collapses into a Compton sphere again. And this process repeats. This is a new physical intuition from a discrete time perspective on the microscopic world.

Received on January 26, 2024

References

1. Noh Y.J. Propagation of a Particle in Discrete Time. *Progress in Physics*, 2020, v. 16, 116–122.
2. Noh Y.J. Anomalous Magnetic Moment in Discrete Time. *Progress in Physics*, 2021, v. 17, 207–209.
3. Noh Y.J. Lamb Shift in Discrete Time. *Progress in Physics*, 2022, v. 18, 126–130.
4. Noh Y.J. Interpretation of Quantum Mechanics in Terms of Discrete Time I. *Progress in Physics*, 2023, v. 19, 109–114.
5. Heisenberg W. The Physicist's Conception of Nature. Hutchinson, 1958, p. 15.

Addendum to “The Feynman-Dyson propagators for neutral particles (locality or non-locality?)”

Valeriy V. Dvoeglazov

UAF, Universidad de Zacatecas, Apartado Postal 636, Suc. 3, Zacatecas 98061, Zac., México. E-mail: valeri@fisica.uaz.edu.mx

We answer several questions of the referees and readers that arose after publication of the commented article [1]. Moreover, we see that it is impossible to consider correct relativistic quantum mechanics without negative energies, tachyons, and without appropriate forms of discrete symmetries.

Why did we consider four field functions in the propagator for spin-1 in [1, 2]?* Let us make some observations for spin-1/2 and spin 1.

We have 4 solutions in the original Dirac equation for u – and 4 solutions for $v = \gamma^5 u$ (remember we have $p_0 = \pm E_p = \pm \sqrt{\mathbf{p}^2 + m^2}$). See, for example, [3]. In the $S = 1$ Weinberg equation [4], we have 12 solutions†. Apart from $p_0 = \pm E_p$, we have tachyonic solutions $p_0 = \pm E'_p = \pm \sqrt{\mathbf{p}^2 - m^2}$, i.e. $m \rightarrow im$. This is easily checked on using the algebraic equations and solving them with respect to p_0 :

$$\text{Det}[\gamma^\mu p_\mu \pm m] = 0, \quad (1)$$

and

$$\text{Det}[\gamma^{\mu\nu} p_\mu p_\nu \pm m^2] = 0. \quad (2)$$

In the construction of the field operator [3], we generally need $u(-p) = u(-p_0, -\mathbf{p}, m)$ which should be transformed to $v(p) = \gamma^5 u(p) = \gamma^5 u(+p_0, +\mathbf{p}, m)$. On the other hand, when we calculate the parity properties we need $\mathbf{p} \rightarrow -\mathbf{p}$. The $u(p_0, -\mathbf{p}, m)$ satisfies

$$[\tilde{\gamma}^{\mu\nu} p_\mu p_\nu + m^2] u(p_0, -\mathbf{p}, m) = 0. \quad (3)$$

The $u(-p_0, \mathbf{p}, m)$ “spinor” satisfies:

$$[\tilde{\gamma}^{\mu\nu} p_\mu p_\nu + m^2] u(-p_0, +\mathbf{p}, m) = 0, \quad (4)$$

that is the same as above. The tilde signifies $\tilde{\gamma}^{\mu\nu} = \gamma_{00} \gamma^{\mu\nu} \gamma_{00}$ that is analogous to the $S = 1/2$ case $\tilde{\gamma}^\mu = \gamma_0 \gamma^\mu \gamma_0$. The $u(-p_0, -\mathbf{p}, m)$ satisfies:

$$[\gamma^{\mu\nu} p_\mu p_\nu + m^2] u(-p_0, -\mathbf{p}, m) = 0. \quad (5)$$

This case is opposite to the spin-1/2 case where the spinor $u(-p_0, \mathbf{p}, m)$ satisfies

$$[\gamma^\mu p_\mu + m] u(-p_0, +\mathbf{p}, m) = 0, \quad (6)$$

and $u(p_0, -\mathbf{p}, m)$,

$$[\tilde{\gamma}^\mu p_\mu - m] u(p_0, -\mathbf{p}, m) = 0, \quad (7)$$

*See also references therein.

†In [5], we have causal solutions only for the $S=1$ Tucker-Hammer equation.

and

$$[\gamma^\mu p_\mu + m] u(-p_0, -\mathbf{p}, m) = 0. \quad (8)$$

In general, we can use $u(-p_0, +\mathbf{p}, m)$ or $u(p_0, -\mathbf{p}, m)$ to construct the causal propagator in the spin-1/2 case. However, we need not use both because a) $u(-p_0, +\mathbf{p}, m)$ satisfies a similar equation as $u(+p_0, -\mathbf{p}, m)$ and b) we have the integration over \mathbf{p} . This integration is invariant with respect $\mathbf{p} \rightarrow -\mathbf{p}$:

$$S_F(x_2, x_1) = \sum_\sigma \int \frac{d^3\mathbf{p}}{(2\pi)^3} \frac{m}{E_p} \times \\ [\theta(t_2 - t_1) a u^\sigma(p) \bar{u}^\sigma(p) e^{-i\mathbf{p} \cdot (\mathbf{x}_2 - \mathbf{x}_1)} + \\ + \theta(t_1 - t_2) b v^\sigma(p) \bar{v}^\sigma(p) e^{+i\mathbf{p} \cdot (\mathbf{x}_2 - \mathbf{x}_1)}]. \quad (9)$$

So the result for the causal propagator

$$S_F(x) = \int \frac{d^4p}{(2\pi)^4} e^{-ip \cdot x} \frac{\hat{p} + m}{p^2 - m^2 + i\epsilon} \quad (10)$$

seems to not change.

The situation is different for spin 1. The tachyonic solutions of the original Weinberg equation

$$[\gamma^{\mu\nu} p_\mu p_\nu + m^2] u(p_0, +\mathbf{p}, m) = 0 \quad (11)$$

are just the solutions of the equation with the opposite square of mass ($m \rightarrow im$):

$$[\gamma^{\mu\nu} p_\mu p_\nu - m^2] u(p_0, \mathbf{p}, im) = 0. \quad (12)$$

We cannot transform the propagator of the original equation (11) to that of (12) just by the change of the variables \mathbf{p} as in the spin-1/2 case. The mass square changed the sign, just as in the case of v – “spinors”. When we construct the propagator we have to take into account this solution and, possibly, the superposition $u(p, m)$ and $u(p, im)$, and corresponding equations.

The conclusion is paradoxical: in order to construct the causal propagator for the spin 1 we have to take acausal (tachyonic) solutions of homogeneous equations into account. It is not surprising that the propagator is not causal for the Tucker-Hammer equation because the latter does not contain the tachyonic solutions. Probably, this statement is valid for all higher spins.

Received on February 20, 2024

References

1. Dvoeglazov V. V. *Rev. Mex. Fis.*, 2017, v. 65, 612.
 2. Dvoeglazov V. V. *Int. J. Theor. Phys.*, 1998, v. 37, 1915.
 3. Cázares J. A. and Dvoeglazov V. V. *Rev. Mex. Fis.*, 2023, v. 69, 050703, 1–9.
 4. Weinberg S. *Phys. Rev. B*, 1964, v. 133, 1318.
 5. Tucker R. H. and Hammer C. L. *Phys. Rev. D*, 1971, v. 3, 2448.
-

Santilli's Recovering of Einstein's Determinism

Arun Muktibodh

Department of Mathematics, Mohota College of Science, Nagpur, India. E-mail: amukti2000@yahoo.com

We study the recent series of papers by the Italian-American physicist, Ruggero Maria Santilli based on the Lie-isotopic branch of hadronic mechanics, which imply that a system of extended protons and neutrons in conditions of partial mutual penetration in a nuclear structure verifies the following properties: 1) Admits, for the first time, explicit and concrete realizations of Bohm's hidden variables. 2) Violates Bell's inequalities by therefore admitting classical counterparts. 3) Verifies the broadening of Heisenberg's indeterminacy principle for electromagnetic interactions of point-like particles in vacuum into the *isouncertainty principle* of hadronic mechanics, also called *Einstein's isodeterminism*, for extended hadrons in conditions of partial mutual penetration, which new principle allows a progressive recovering of Einstein's determinism in the transition from hadrons to nuclei and stars and its full recovering at the limit of Schwarzschild's horizon. We then indicate some of the far reaching advances that are possible for hadronic mechanics and Einstein's isodeterminism but impossible for quantum mechanics and Heisenberg's indeterminacy principle.

1 Hadronic mechanism

Experimental foundations. This paper is based on the experimental evidence that protons [1] and neutrons [2] (collectively called nucleons) have an *extended* charge distribution with the radius $R_N = 0.87$ fm in conditions of partial mutual penetration when they are members of a nuclear structure [3–5] (e.g., the charge radius of the Helium [4] $R_{He} = 1.67$ fm is 0.07 fm smaller than the nucleon diameter $D_N = 1.74$ fm), resulting in the expectation that strong nuclear interactions have a conventional potential, thus Hamiltonian component and a new, contact, thus zero-range and non-Hamiltonian component.

Origination of hadronic mechanics. The Italian-American physicist, R. M. Santilli initiated his studies on extended particles under potential/Hamiltonian and contact/non-Hamiltonian interactions during his graduate studies at the University of Torino, Italy. By recalling that quantum mechanics is reversible over time while nuclear fusions are known to be irreversible and inspired by the 1935 Einstein-Podolsky-Rosen (EPR) argument that *Quantum mechanics is not a complete theory*, [6] (see the recent studies [7–9]), Santilli dedicated his 1965 Ph.D. thesis to the EPR irreversible “completion” of quantum mechanics via the *Lie-admissible generalization of Lie's theory and Heisenberg's equation* [10–12]).

After joining Harvard University under DOE support in September 1977 for the study of irreversible processes, Santilli resumed his research on the Lie-admissible formulation of irreversibility as one can see from his 1978 papers [13, 14], his Springer-Verlag monographs [15, 16] and his axiomatic formulation of irreversibility in the 1981 paper [17] released under his affiliation at Harvard's Department of Mathematics and proposed the continuation of the studies under the name of *hadronic mechanics* which is intended to denote a mechanics for strong interactions (see p. 112 of [16] for the first ap-

pearance of the name “hadronic mechanics”).

Hamiltonian interactions, which are collectively referred to interactions that are linear, local and derivable from a potential, thus being fully representable by the conventional Hamiltonian of quantum mechanics.

Non-Hamiltonian interactions, which are collectively referred to interactions that are: *Nonlinear* (in the wave function) as pioneering by Werner Heisenberg [18]; *Nonlocal* (distributed in a volume not reducible to points) as pioneered by Louis de Broglie and David Bohm [19]; *Nonpotential* (of contact zero-range type) as pioneered by R. M. Santilli in the 1978 monograph [15] via the *conditions of variational self-adjointness* according to which Hamiltonian interactions are variationally selfadjoint (SA), while non-Hamiltonian interactions are variationally nonselfadjoint (NSA).

Lie-isotopic branch of hadronic mechanics. In this paper, we use the axiom-preserving, time reversible *Lie-isotopic branch of hadronic mechanics* introduced in Charts 5.2, 5.3 and 5.4, p.165 on of [16] for the representation of *stable* (thus, time-reversal invariant) systems of *extended* collections of particles at short mutual distances under Hamiltonian/SA and non-Hamiltonian/NSA interactions.

Santilli's Lie-isotopic methods are based on the generalization of the conventional universal enveloping associative algebra ξ with generic product $AB = A \times B$ and related unit 1 , $1 \times A = A \times 1 \equiv A$ into the associativity-preserving isoenveloping algebra $\hat{\xi}$ with isoproduct and related isounit (first presented in Eq. (5), p. 71 of [16] and Chart. 5.2 p. 154 for treatment)

$$\begin{aligned} A \hat{\times} B &= A \hat{S} B, \quad \hat{S} > 0, \\ \hat{1} &= 1/\hat{S}, \quad \hat{1} \times A = A \times \hat{1} \equiv A, \end{aligned} \quad (1)$$

where S , called the isotopic element (or the Santillian) is positive-definite but possesses otherwise an unrestricted func-

tional dependence on all needed local variables.

The lifting $\xi \rightarrow \hat{\xi}$ was proposed for the consequential generalization of all branches of Lie's theory into the axiom-preserving *Lie-Santilli isothory* (presented in Charts 5.3, 5.4 from p.114 on of [16]) (see also [20, 21]) with particular reference to the lifting of n -dimensional Lie algebras with (Hermitian) generators $X_k, k = 1, 2, \dots, n$ and conventional brackets into the form

$$\begin{aligned} [X_i, X_j] &= X_i \hat{\times} X_j - X_j \hat{\times} X_i = \\ &= X_i \hat{S} X_j - X_j \hat{S} X_i = C_{ij}^k X_k. \end{aligned} \quad (2)$$

The fundamental dynamical equation of the isotopic methods are given by the *Lie-isotopic generalization of Heisenberg equation* (Eq. (18a), p. 153 of [16])

$$idA/dt = A \hat{\times} H - H \hat{\times} A = A \hat{S} H - H \hat{S} A, \quad (3)$$

where the Hamiltonian H represents all SA interactions while the Santillian \hat{S} represents the extended character of particles and their *new* class of NSA interactions.

Subsequent studies. For advances on hadronic mechanics that occurred in the decades following the 1978 proposal [13–16], the interested reader can inspect: the overview [8] with applications in various fields; the classification of hadronic mechanics [22] (including, in addition to the *Lie-isotopic branch*, the *Lie-admissible branch* for the representation of irreversible processes; *hyperstructural branch* for biological structures and the *isodual branch* for antiparticles); the introductory reviews [23–25]; the AO collection of recent papers [26]; the list of early workshops and conferences [27]; independent monographs [28–36]; and the general presentation [37–39].

Realization of the isotopic element. To render this paper minimally self-sufficient, let us recall the generally used realization of the Santillian [8]

$$\begin{aligned} \hat{S} &= \hat{S}_{4 \times 4} = \Pi_{\alpha=1,2,3,4} \text{Diag} \left(\frac{1}{n_{1,\alpha}^2}, \frac{1}{n_{2,\alpha}^2}, \frac{1}{n_{3,\alpha}^2}, \frac{1}{n_{4,\alpha}^2} \right) \times \\ &\times e^{-\Gamma(r,p,a,E,d,\tau,\pi,\psi,\dots)} > 0, \\ n_{\mu,\alpha} &> 0, \quad \Gamma > 0, \end{aligned} \quad (4)$$

where:

- 1) The representation of the dimension and shape of the individual nucleons is done via semi-axes $n_{k,\alpha}^2, k = 1, 2, 3$ (with n_3 parallel to the spin) and normalization for the vacuum $n_{k,\alpha}^2 = 1$.
- 2) The representation of the density is done via the characteristic quantity $n_{4,\alpha}^2$ per individual nucleons with normalization for the vacuum $n_{4,\alpha}^2 = 1$.
- 3) The representation of the nonlinear, nonlocal and non-potential interactions between extended nucleons is done via the positive-definite exponential term Γ with

an arbitrary dependence on relative coordinates r , momenta p , accelerations a , energy E , density d , temperature τ , pressure, π , wave functions ψ or any needed local variable.

When representing nucleons and their NSA interactions, the space dimension of the isotopic element is restricted not to surpass the range of strong interactions $R = 1 \text{ fm} = 10^{-13} \text{ cm}$. However, the space dimension of the isotopic element can be, in general, infinite.

Elementary construction of hadronic mechanics. Despite their apparent mathematical complexity, all isotopic formulations can be constructed via the following simple *quantum mechanical nonunitary transformation* unit $1 = \hbar$, and therefore, of all related formulations according to the simple rules [40]

$$\begin{aligned} 1 &\rightarrow U1U^\dagger = \hat{1} \neq 1, \\ AB &\rightarrow U(AB)U^\dagger = \\ &= (UAU^\dagger)(UU^\dagger)^{-1}(UBU^\dagger) = \hat{A}\hat{B}, \\ [X_i, X_j] &\rightarrow U[X_i, X_j]U^\dagger = [\hat{X}_i, \hat{X}_j], \end{aligned} \quad (5)$$

which transformations essentially complete a quantum mechanical model for point-like particles into a hadronic model for extended particles under new interactions.

Invariance of isotopic formulations. All quantum mechanical nonunitary models, thus including models (5), are affected by serious inconsistency problems, such as the general lack of conservation of Hermiticity/observability, causality, etc. These problems were resolved by Santilli in the 1998 Ref. [40] via the completion of unitary law (4) into the *isounitary law*

$$\hat{W} \hat{\times} \hat{W}^\dagger = \hat{W}^\dagger \hat{\times} \hat{W} = \hat{1}, \quad (6)$$

completed by the identical reformulation of transformations (5) into the isounitary form

$$\begin{aligned} U &= \hat{W} \hat{S}^{1/2}, \\ UU^\dagger &= \hat{1} \rightarrow \hat{W} \hat{\times} \hat{W}^\dagger = \hat{W}^\dagger \hat{\times} \hat{W} = \hat{1}, \\ \hat{1} &\rightarrow \hat{W} \hat{\times} \hat{1} \hat{\times} \hat{W}^\dagger = \hat{1}' \equiv \hat{1}, \\ \hat{A} \hat{\times} \hat{B} &\rightarrow \hat{W} \hat{\times} (\hat{A} \hat{\times} \hat{B}) \hat{\times} \hat{W}^\dagger = \hat{A}' \hat{\times}' \hat{B}' = \hat{A}' \hat{S}' \hat{B}', \\ \hat{S}' &\equiv \hat{S} = (\hat{W}^\dagger \hat{\times} \hat{W})^{-1}, \end{aligned} \quad (7)$$

with consequential resolution of the problematic aspects of quantum nonunitary models (5), as well as the prediction by isotopic formulations, in view of properties (7), of the same numerical values under the same conditions at different times.

Experimental verifications. Santilli hadronic mechanics has been verified in virtually all physics fields by the exact and invariant representation of experimental data generally not representable via quantum mechanics, such as: direct experimental verifications of the EPR argument [41–43]; electrodynamics [44–47]; large ion physics [48]; particle physics

[49, 50]; Bose-Einstein correlation [51, 52]; propagation of light within physical media [53]; cosmology [54, 55]; neutron synthesis from the Hydrogen [56]; Deuteron magnetic moment [57]; Deuteron spin and rest energy [58]; and other fields.

2 Einstein's isodeterminism

EPR entanglement. Experimental evidence well known since Einstein's times establishes that particles, which are initially bounded together and then separated, can influence each other continuously and instantaneously at arbitrary distances [59]. Albert Einstein strongly objected against the very terms "quantum entanglement" on grounds that the sole possible representation of particle entanglements via the Copenhagen interpretation of quantum mechanics would require superluminal communications that violate special relativity.

For the intent of honoring the generally forgotten Einstein's view, Santilli [62] proved that the sole possible representation of particle entanglement by the Copenhagen interpretation of quantum mechanics is that for which *the particles are free*, evidently because the sole possible interactions admitted by said interpretation are those derivable from a potential which is identically null for particles at large mutual distances.

By recalling that the wave packet of particles is identically null solely at infinite distance, Ref. [62] then pointed out that the sole interactions that are continuous, instantaneous and at arbitrary distances are given by the mutual penetration of wave packets of particles which, being nonlinear, nonlocal and nonpotential, thus NSA [15], are beyond any hope of treatment via quantum mechanics.

Thanks to the prior development of isomathematics for the representation of NSA interactions [33, 36, 37], Santilli [62] proposed the axiom-preserving completion of quantum into hadronic entanglement under the suggested name of *EPR entanglements* which does indeed represent particle entanglements with non-zero, yet non-Hamiltonian-NSA interactions.

Note that the EPR entanglement of particles requires a conceptual and technical revision of the notion of interactions, e.g., because nuclear constituents admit nontrivial NSA interactions even when they are at a mutual distance bigger than that of strong interactions.

More recently, the EPR entanglement has been experimentally proved to hold at arbitrary *classical* distances [60]. This important feature appears to support Santilli's suggestion [15] that contact forces dating back to Newton, when turned into an operator form, are plausible candidates for the *fifth interactions* intended as *nonlinear, nonlocal, continuous and instantaneous interactions at arbitrary distances* due to the overlapping of the wave packets of particles (see Sect. 1.5.C of [80]). Their lack of identification to date is easily explained by their lack of existence in quantum mechanics. Therefore, in the event such a view is accepted, Santilli's

1978 monograph [15] can be considered the birth of the fifth interactions.

Note also that paper [62] confirms Einstein's additional view that "*The wave function of quantum mechanics does not provide a complete description of the entire physical reality*" [6].

Bohm's hidden variables. As it is well known, in an attempt of reconciling Einstein's determinism with quantum mechanics, D. Bohm [63, 64] submitted in 1952 the hypothesis that quantum mechanics admits *hidden variables* λ , that is, variables which are hidden in its formalism. Following half a century of failure to achieve explicit realizations, a rather general consensus (confirmed by Bell's inequalities outlined next) is that *Bohm's hidden variables do not exist within the formalism of quantum mechanics*.

In 1995, R. M. Santilli [38] proved that *hidden variables do exist within the context of hadronic mechanics, they are hidden in the axiom of associativity of quantum mechanics and are quantitatively represented by the isotopic element* (Sect. 4.C.3, p. 170 on and Sect. 6.8, p. 254 on of [38], e.g.,

$$\lambda = \hat{S}, \quad (8)$$

$$A \hat{\times} B = A \lambda B, \quad A \hat{\times} (B \hat{\times} C) = (A \hat{\times} B) \hat{\times} C.$$

It should be noted that, despite its apparent elementary character of the isotopic product (1), the quantitative study of the indicated realization of Bohm's hidden variables required collegial efforts in the nonlocal lifting of the entire 20th century applied mathematics, including the Newton-Leibnitz differential calculus [65] (see also studies [36]). Nowadays, there exists a number of explicit and concrete realization of hidden variables, among which we mention the realization used for the first numerically exact and time invariant representation of the Deuteron magnetic moment [66, 67] which achievement resulted to be impossible for quantum mechanics in one century.

Bell's inequalities. In the 1964, J. S. Bell [68] proved a number of quantum mechanical inequalities, the first one of which essentially states that systems of point like particles with spin $1/2$ represented via quantum mechanics do not admit classical counterparts. This view was assumed by mainstream physicists for over half a century to be the final disproof of the EPR argument and of Bohm's hidden variables.

Again thanks to the prior development of isomathematics as well as of explicit and concrete realizations of hidden variables, Santilli [71] proved in 1998 a number of hadronic inequalities essentially stating that *systems of extended particles with spin $1/2$ represented via the Lie-isotopic branch of hadronic mechanics do indeed admit classical counterparts*, while providing explicit examples.

Santilli's hadronic inequalities are confirmed by the direct experimental verifications of the EPR-argument [41–43] establishing the existence in nature of particle conditions which violate Bell's inequalities.

Note that the above theoretical and experimental works imply the expectation that Heisenberg's uncertainties principle is correspondingly violated by strong interactions between extended nucleons in conditions of mutual penetration.

Einstein's isodeterminism. Soon after joining Harvard University in late 1977, R. M. Santilli expressed doubts on the exact validity for strong interactions of Heisenberg's uncertainty principle (also called indeterminacy principle) and other quantum mechanical laws, as one can see from the *titles* of the 1978 memoir [14] (see also the subsequent papers [69, 70]). Santilli's argument underlying such a conviction is that Heisenberg's standard deviations for coordinates Δr , momenta Δp and their product are certainly valid for the conditions of their original conception, i.e., for point-like charged particles under electromagnetic interactions, because a point-like particle can move within a star by solely sensing action-at-a-distance interactions due to its dimensionless character.

The situation is conceptually, mathematically, theoretically and experimentally different when considering extended nucleons in conditions of mutual penetration because, in view of their "strength", strong interactions imply the creation of a *pressure* on a given nucleon by its surrounding nucleons, according to a view pioneered by L. de Broglie and D. Bohm with their nonlocal theory [19]. It is then evident that the standard deviations for the indicated nucleon Δr and Δp *cannot* be the same as the corresponding deviations for an electron in vacuum, thus implying the need for a suitable completion of Heisenberg's uncertainty principle for strong interactions.

Thanks to the original works [14, 69, 70] and the recent works [62, 71], Santilli [72] finally achieved in 2019 the axiom-preserving EPR completion of Heisenberg's uncertainty principle into the *isouncertainty principle of hadronic mechanics*, also called *Einstein's isouncertainies*, for extended nucleons under electromagnetic, weak and strong interactions whose derivation can be outlined as follows.

Let \mathcal{H} be the Hilbert-Myung-Santilli isospace [73] of isomechanics with *isostates* $|\hat{\psi}\rangle$ and isoinner product $\langle\hat{\psi}|\hat{\times}|\hat{\psi}\rangle$ (for a review, see Sect. 4 of [23]). Assume the isonormalization which is necessary for a constant Santillian

$$\langle\hat{\psi}|\hat{\times}|\hat{\psi}\rangle = \langle\hat{\psi}|\hat{S}|\hat{\psi}\rangle = \hat{S}, \quad (9)$$

the Schrödinger-Santilli isoequation [16, 38]

$$\begin{aligned} \hat{H}\hat{\times}|\hat{\psi}\rangle &= \\ &= [\Sigma_{k=1,2,\dots,n} \frac{1}{2m_k} \hat{p}_k\hat{\times}\hat{p}_k + \hat{V}(r)] \hat{S}(r, p, \psi, \dots) |\hat{\psi}\rangle = \\ &E \times |\hat{\psi}\rangle, \end{aligned} \quad (10)$$

the isolinear momentum [65]

$$\hat{p}\hat{\times}|\hat{\psi}\rangle = -i\hat{1}\partial_{\hat{r}}\hat{\psi}, \quad (11)$$

and the isocommutation rules

$$\begin{aligned} [\hat{r}_i, \hat{p}_j]\hat{\times}|\hat{\psi}\rangle &= -i\hat{1}\delta_{i,j}|\hat{\psi}\rangle, \\ [\hat{r}_i, \hat{r}_j]\hat{\times}|\hat{\psi}\rangle &= [\hat{p}_i, \hat{p}_j]\hat{\times}|\hat{\psi}\rangle = 0. \end{aligned} \quad (12)$$

Then the isounitary transformation (7) of Heisenberg's uncertainty principle

$$\Delta r \Delta p = \frac{1}{2} |\langle\hat{\psi}|\hat{r}|\hat{\psi}\rangle| |\langle\hat{\psi}|\hat{p}|\hat{\psi}\rangle| \geq \frac{1}{2} \hbar, \quad (13)$$

uniquely and unambiguously yields the *isouncertainty principle of hadronic mechanics*, also called *Einstein's isodeterminism*, whose projection on our spacetime (as needed for experiments) is given by [72] (see [23] for an extended derivation)

$$\begin{aligned} \hat{\Delta r} \hat{\Delta p} &= \frac{1}{2} |\langle\hat{\psi}|\hat{\times}[\hat{r}, \hat{p}]\hat{\times}|\hat{\psi}\rangle| = \\ &= \frac{1}{2} |\langle\hat{\psi}|\hat{S}[\hat{r}, \hat{p}]\hat{S}|\hat{\psi}\rangle| \approx \frac{1}{2} \hbar \hat{S} = \frac{1}{2} \hbar e^{-\Gamma(r, p, a, E, d, \tau, \pi, \psi, \dots)} \approx \\ &\approx \frac{1}{2} \hbar [1 - \Gamma(r, p, a, E, d, \tau, \pi, \psi, \dots) + \dots] \ll \frac{1}{2} \hbar, \end{aligned} \quad (14)$$

where the Santillian \hat{S} is given by Eq. (4) and we assumed, in first approximation, that all nucleons are perfectly spherical.

It should be mentioned that completion (14) of Heisenberg's uncertainty principle includes as particular cases most of the existing generalized uncertainty relations known to this author (see, e.g., [74–76] and papers quoted therein).

In particular, the standard isodeviations $\hat{\Delta r}$ and $\hat{\Delta p}$ progressively and individually tend to zero with the increase of the density of the hadronic medium, thus in the transition from hadrons to nuclei and stars.

Note that the completion of the value $\geq \frac{1}{2} \hbar$ into the form $\approx \frac{1}{2} \hbar \hat{S}$ is due to the nonlocality of hadronic mechanics which requires a redefinition of the very notion of standard deviations due to the very big pressure exercised on a nucleon by the surrounding nucleons under "strong" interactions [24, 72].

To achieve the full validity of Einstein's determinism, Santilli [77, 78] decomposes the Riemannian metric $g(x)$ in four dimensions into then product of the Minkowskian metric $\eta = -\text{Diag}, (1, 1, 1, -1)$ and the gravitational isotopic element \hat{S}

$$g(x) = \hat{S}_{4 \times 4} \eta_{4 \times 4}, \quad (15)$$

with particular values for the Schwartzschild metric

$$\hat{S}_{kk} = \frac{1}{1 - 2M/r}, \quad \hat{S}_{44} = 1 - 2M/r. \quad (16)$$

It is then easy to see that Einstein's determinism [6] is fully recovered at the limit of the Schwartzschild horizon.

3 Concluding remarks

Despite one century of studies under large public funds, nuclear physics has been unable to achieve the controlled nuclear fusion; the recycling of radioactive nuclear waste; the

exact representations of nuclear data; the synthesis of the neutron from the Hydrogen atom in the core of stars; the nuclear stability despite the natural instability of the neutron and extremely repulsive protonic Coulomb forces; and other open problems.

A main point which is attempted to convey in this paper is that the indicated open nuclear problems appear to be due to the *theoretical assumption* that Heisenberg's uncertainty principle for point-like particles under electromagnetic interactions is also valid for extended nucleons under strong interactions.

As an illustration, Heisenberg's uncertainty principle prohibits a structural representation of the synthesis of the neutron from the electron and the proton in the core of stars, because the standard deviation Δr_e for the coordinate of the electron is much bigger than the size of the neutron and the standard deviation Δp_e of the momentum implies a kinetic energy of the electron bigger than the rest energy of the neutron,

$$\begin{aligned}\Delta r_e &> R_n = 0.87 \times 10^{-13} \text{ cm}, \\ \Delta v_e &> \frac{\hbar}{\Delta r_e \times m_e} > 10^{10} \text{ m/s}, \\ \Delta K_e &= \frac{1}{2m_e} \times (\Delta p_e)^2 > m_n = 939.56 \text{ MeV}/c^2.\end{aligned}\quad (17)$$

By comparison, the study of the neutron synthesis via hadronic mechanics under isouncertainty principle (14), implies standard isodeviations for which Eqs. (17) become

$$\begin{aligned}\hat{\Delta} r_e &= \hat{S} \Delta r_e \leq R_n = 0.87 \times 10^{-13} \text{ cm}, \\ \hat{\Delta} v &= \hat{S} \Delta v_e \ll 10^{10} \text{ m/s}, \\ \hat{\Delta} K_e &= \hat{S} \Delta K_e \ll m_n = 939.56 \text{ MeV}/c^2,\end{aligned}\quad (18)$$

thus allowing a quantitative representation of the neutron synthesis from the Hydrogen [79] with far reaching advances that cannot be formulated in quantum mechanics, let alone treated, such as [80–82]: 1) The prediction of means for recycling radioactive nuclear waste by nuclear power plants via *new* stimulated decays; 2) The possible return to the continuous creation of matter in the universe to explain the 0.782 MeV missing in the neutron synthesis; 3) The apparent reduction of all matter in the universe to protons and electrons.

Acknowledgments

The author would like to express sincere thanks to Dr. R. Anderson of the R. M. Santilli Foundation for continuous help in the preparation of this paper, particularly for historical aspects on hadronic mechanics and related documentation. Additional thanks are due to Prof. R. M. Santilli for continuous technical assistance on hadronic mechanics, including consultations and technical controls. The author is solely respon-

sible of the content of the paper due to numerous final revisions.

Received on March 4, 2024

References

1. Pohl R., Antognini A. and Kottmann F. The size of the proton. *Nature*, 2010, v. 466, 213–216. www.nature.com/articles/nature09250
2. Wietfeldt F.E. Measurements of the Neutron Lifetime. *Atoms*, 2018, v. 6, 1–19. www.mdpi.com/2218-2004/6/4/70
3. IAEA, Nuclear data. www.iaea.org/about/organizational-structure/department-of-nuclear-sciences-and-applications/division-of-physical-and-chemical-sciences/nuclear-data-section
4. ScienceDirect, Helium nucleus. www.sciencedirect.com/topics/mathematics/helium-nucleus
5. Rau S. et al. Penning trap measurements of the deuteron and the HD^+ molecular ion. *Nature*, 2020, v. 585, 43–47. doi.org/10.1038/s41586-020-2628-7
6. Einstein A., Podolsky B. and Rosen N. Can quantum-mechanical description of physical reality be considered complete? *Phys. Rev.*, 1935, v. 47, 777–780. www.eprdebates.org/docs/epr-argument.pdf
7. Beghella-Bartoli S. and Santilli R. M., Ed. Proceedings of the 2020 Teleconference on the Einstein-Podolsky-Rosen argument that “Quantum mechanics is not a complete theory”. Curran Associates, New York, NY, 2021. Printed version: www.proceedings.com/59404.html
8. Santilli R. M. Overview of historical and recent verifications of the Einstein-Podolsky-Rosen argument and their applications to physics, chemistry and biology. APAP - Accademia Piceno Aprutina dei Velati, Pescara, Italy, 2021. www.santilli-foundation.org/epr-overview-2021.pdf
9. Dunning-Davies J. A. Present Day Perspective on Einstein-Podolsky-Rosen and its Consequences. *Journal of Modern Physics*, 2021, v. 12, 887–936. www.scirp.org/journal/paperinformation.aspx?paperid=109219
10. Santilli R. M. Embedding of Lie-algebras into Lie-admissible algebras. *Nuovo Cimento*, 1967, v. 51, 570–585. [//www.santilli-foundation.org/docs/Santilli-54.pdf](http://www.santilli-foundation.org/docs/Santilli-54.pdf)
11. Santilli R. M. Dissipativity and Lie-admissible algebras. *Meccanica*, 1969, v. 1, 3–12.
12. Santilli R. M. An introduction to Lie-admissible algebras. *Suppl. Nuovo Cimento*, 1968, v. 6, 1225.
13. Santilli R. M. On a possible Lie-admissible covering of Galilei's relativity in Newtonian mechanics for nonconservative and Galilei form-non-invariant systems. *Hadronic Journal*, 1978, v. 1, 223–423. www.santilli-foundation.org/docs/Santilli-58.pdf
14. Santilli R. M. Need of subjecting to an experimental verification the validity within a hadron of Einstein special relativity and Pauli exclusion principle. *Hadronic Journal* 1978, v. 1, 574–901. www.santilli-foundation.org/docs/santilli-73.pdf
15. Santilli R. M. Foundation of Theoretical Mechanics, Vol. I, The Inverse Problem in Newtonian Mechanics. *Springer-Verlag*, Heidelberg, Germany, 1978. www.santilli-foundation.org/docs/Santilli-209.pdf
16. Santilli R. M. Foundation of Theoretical Mechanics. Vol. II, Birkhoffian Generalization of Hamiltonian Mechanics. *Springer-Verlag*, Heidelberg, Germany, 1983. www.santilli-foundation.org/docs/santilli-69.pdf
17. Santilli R. M. Initiation of the representation theory of Lie-admissible algebras of operators on bimodular Hilbert spaces. *Hadronic J.*, 1979, v. 3, 440–467. www.santilli-foundation.org/docs/santilli-1978-paper.pdf
18. Heisenberg W. *Nachr. Akad. Wiss. Gottingen*, 1953, v. IIa, 111–133. www.link.springer.com/chapter/10.1007/978-3-642-70079-8_23

19. Stanford Encyclopedia of Philosophy, Bohmian (de Broglie-Bohm) Mechanics. 2021. plato.stanford.edu/entries/qm-bohm
20. Sourlas D.S and Tsagas Gr. T. Mathematical Foundation of the Lie-Santilli Theory. Ukraine Academy of Sciences, 1993. www.santilli-foundation.org/docs/santilli-70.pdf
21. Kadeisvili J. V. An introduction to the Lie-Santilli isotopic theory. *Mathematical Methods in Applied Sciences*, 1996, v. 19, 134–172. www.santilli-foundation.org/docs/Santilli-30.pdf
22. Anderson R. Outline of Hadronic Mathematics, Mechanics and Chemistry as Conceived by Santilli R.M. *American Journal of Modern Physics*, 2016, v. 6, 1–16. www.santilli-foundation.org/docs/HMMC-2017.pdf
23. Santilli R. M. Studies on A. Einstein, B. Podolsky and N. Rosen prediction that quantum mechanics is not a complete theory, I: Basic methods. *Ratio Mathematica*, 2020, v. 38, 5–69. eprdebates.org/docs/epr-review-i.pdf
24. Santilli R. M. Studies on A. Einstein, B. Podolsky and N. Rosen prediction that quantum mechanics is not a complete theory, II: Apparent proof of the EPR argument. *Ratio Mathematica*, 2020, v. 38, 71–138. eprdebates.org/docs/epr-review-ii.pdf
25. Santilli R. M. Studies on A. Einstein, B. Podolsky and N. Rosen prediction that quantum mechanics is not a complete theory, III: Illustrative examples and applications. *Ratio Mathematica*, 2020, v. 38, 139–222. eprdebates.org/docs/epr-review-iii.pdf
26. Anderson A. Collected OA Papers on Hadronic Mathematics, Mechanics and Chemistry. www.santilli-foundation.org/docs/HMMC.pdf
27. Anderson R. List of early OA international workshops and conferences in hadronic mechanics. www.santilli-foundation.org/docs/workshops-conf-hm.pdf
28. Aringazin A. K., Jannussis A., Lopez F., Nishioka M. and Veljanosky B. Santilli's Lie-Isotopic Generalization of Galilei and Einstein Relativities. Kostakaris Publishers, Athens, Greece, 1991. www.santilli-foundation.org/docs/Santilli-108.pdf
29. Sourlas D.S. and Tsagas Gr. T. Mathematical Foundation of the Lie-Santilli Theory. Ukraine Academy of Sciences, 1993. www.santilli-foundation.org/docs/santilli-70.pdf
30. Lohmus J., Paal E. and Sorgsepp L. Nonassociative Algebras in Physics. Hadronic Press, Palm Harbor, 1994. www.santilli-foundation.org/docs/Lohmus.pdf
31. Kadeisvili J. V. Santilli's Isotopies of Contemporary Algebras, Geometries and Relativities. Ukraine Academy of Sciences, Second edition, 1997. www.santilli-foundation.org/docs/Santilli-60.pdf
32. Jiang C-X. Foundations of Santilli Isonumber Theory. International Academic Press, 2001. www.i-b-r.org/docs/jiang.pdf
33. Ganfornina R. M. F. and Valdes J. N. Fundamentos de la Isotopia de Santilli. International Academic Press, 2001. www.i-b-r.org/docs/spanish.pdf
English translation: *Algebras, Groups and Geometries*, 2015, v. 32, 135–308. www.i-b-r.org/docs/Aversa-translation.pdf
34. Davvaz B. and Vougiouklis Th. A Walk Through Weak Hyperstructures and H_p -Structures. World Scientific, 2018.
35. Gandzha I. and Kadeisvili J. V. New Sciences for a New Era: Mathematical, Physical and Chemical Discoveries by Ruggero Maria Santilli. Sankata Printing Press, Nepal, 2011. www.santilli-foundation.org/docs/RMS.pdf
36. Georgiev S. Foundations of IsoDifferential Calculus. Nova Publishers, New York:
Vol. 1: Iso-Differential and Iso-Integral Calculus for Iso-Functions in One Variable. 2014;
Vol. 2: Iso-Differential and Iso-Integral Calculus for Iso-Functions in Several Variables. 2014;
Vol. 3: Iso-Ordinary Iso-Differential Equations. 2014;
Vol. 4: Iso-Difference Equations. 2015;
Vol. 5: Iso-Stochastic Iso-Differential Equations. 2015;
Vol. 6: Theory of Iso-Measurable Iso-Functions. 2016.
New Edition of Vol. 1: Iso-Differential and Iso-Integral Calculus for Iso-Functions in One Variable. 2022. Iso-Mathematics. Lambert Academic Publishing, 2022.
37. Santilli R. M. Elements of Hadronic Mechanics. Vol. I, Mathematical Foundations. Ukraine Academy of Sciences, Kiev, 1995. www.santilli-foundation.org/docs/Santilli-300.pdf
38. Santilli R. M. Elements of Hadronic Mechanics. Vol. II, Theoretical Foundations. Ukraine Academy of Sciences, Kiev, 1995. www.santilli-foundation.org/docs/Santilli-301.pdf
39. Santilli R. M. Elements of Hadronic Mechanics. Vol. III, Experimental verifications. Ukraine Academy of Sciences, Kiev, 2016. www.santilli-foundation.org/docs/elements-hadronic-mechanics-iii.compressed.pdf
40. Santilli R. M. Invariant Lie-isotopic and Lie-admissible formulation of quantum deformations. *Found. Phys.*, 1997, v. 27, 1159–1177. www.santilli-foundation.org/docs/Santilli-06.pdf
41. Fadel M. et al. Spatial entanglement patterns and Einstein-Podolsky-Rosen steering in Bose-Einstein condensates. *Science*, 2018, v. 360, 409–415. www.santilli-foundation.org/Basel-paper.pdf
42. Colciaghi P. et al. Einstein-Podolsky-Rosen Experiment with Two Bose-Einstein Condensates. *Phys. Rev. X*, 2023, v. 13, 021031, 10 pp. journals.aps.org/prx/pdf/10.1103/PhysRevX.13.021031
43. Aspect A. et al. Experimental Realization of Einstein-Podolsky-Rosen-Bohm Gedankenexperiment: A New Violation of Bell's Inequalities. *Phys. Rev. Lett.*, 1982, v. 49, 91–94. ui.adsabs.harvard.edu/abs/1982PhRvL..49...91A
44. Miller J. P. et al. Muon ($g-2$): experiment and theory. *Rep. Prog. Phys.*, 2007, v. 70, 795–881. news.fnal.gov/2021/04/first-results-from-fermilabs-muon-g-2-experiment-strengthen-evidence-of-new-physics
45. Santilli R. M. Apparent Unsettled Value of the Recently Measured Muon Magnetic Moment. *Progress in Physics*, 2022, v. 18, 15–18. www.santilli-foundation.org/docs/muon-meanlife-2022.pdf
46. Santilli R. M. Representation of the anomalous magnetic moment of the muons via the Einstein-Podolsky-Rosen completion of quantum into hadronic mechanics. *Progress in Physics*, 2021, v. 17, 210–215. www.progress-in-physics.com/2021/PP-62-13.PDF
47. Santilli R. M. Representation of the anomalous magnetic moment of the muons via the novel Einstein-Podolsky-Rosen entanglement in: Garcia H. M. C., Guzman J. J. C., Kauffman L. H. and Makaruk H., Eds. Scientific Legacy of Professor Zbigniew Oziewicz. World Scientific, 2024. [www.santilli-foundation.org/docs/santilli-546-\(1\).pdf](http://www.santilli-foundation.org/docs/santilli-546-(1).pdf)
48. Schukraft K. Heavy-ion physics with the ALICE experiment at the CERN Large Hadron Collider. *Trans. Royal Soc.*, 2012, v. A370, 917–932. royalsocietypublishing.org/doi/10.1098/rsta.2011.0469
49. Cardone F., Mignani R. and Santilli R. M. On a possible energy-dependence of the K^0 lifetime. Part I. *J. Phys. G: Part. Phys.*, 1992, v. 18, L141–L144. www.santilli-foundation.org/docs/Santilli-32.pdf
50. Cardone F., Mignani R. and Santilli R. M. On a possible energy-dependence of the K^0 lifetime. Part II. *J. Phys. G: Part. Phys.*, 1992, v. 18, L61–L65. www.santilli-foundation.org/docs/Santilli-32.pdf
51. Santilli R. M. Nonlocal formulation of the Bose-Einstein correlation within the context of hadronic mechanics. *Hadronic J.*, 1992, v. 5, 1–50 and v. 15, 81–133. www.santilli-foundation.org/docs/Santilli-116.pdf
52. Cardone F. and Mignani R. Nonlocal approach to the Bose-Einstein correlation. *JETP*, 1996, v. 83, 435. www.santilli-foundation.org/docs/Santilli-130.pdf
53. Ahmar H. et al. Additional experimental confirmations of Santilli's IsoRedShift and the consequential lack of expansion of the universe. *Journal of Computational Methods in Sciences and Engineering*, 2013, v. 13, 321–375. www.santilli-foundation.org/docs/IRS-confirmations-212.pdf

54. Mignani R. Quasars redshift in isominkowski space. *Physics Essay*, 1992, v. 5, 531. www.santilli-foundation.org/docs/Santilli-31.pdf
55. Santilli R. M. Experimental Verifications of IsoRedShift with Possible Absence of Universe Expansion, Big Bang, Dark Matter and Dark Energy. *The Open Astronomy Journal*, 2010, v. 3, 124–132. www.santilli-foundation.org/docs/IsoRedshift-Letter.pdf
56. Norman R., Beghella Bartoli S., Buckley B., Dunning-Davies J., Rak J. and Santilli R. M. Experimental Confirmation of the Synthesis of Neutrons and Neutroids from a Hydrogen Gas. *American Journal of Modern Physics*, 2017, v. 6, 85–104. www.santilli-foundation.org/docs/confirmation-neutron-synthesis-2017.pdf
57. Santilli R. M. A quantitative isotopic representation of the Deuteron magnetic moment. In: Proceedings of the International Symposium “Dubna Deuteron-3e”. Joint Institute for Nuclear Research, Dubna, Russia, 1994. www.santilli-foundation.org/docs/Santilli-134.pdf
58. Santilli R. M. The Physics of New Clean Energies and Fuels According to Hadronic Mechanics. Special issue of the Journal of New Energy, 1998. www.santilli-foundation.org/docs/Santilli-114.pdf
59. Bengtsson I. and Życzkowski K. An Introduction to Quantum Entanglement, second, revised edition. Cambridge University Press, 2006. chaos.if.uj.edu.pl/~karol/geometry.htm
60. Berkowitz R. Macroscopic systems can be controllably entangled and limitlessly measured. *Physics Today*, July 2021, 16–18. www.santilli-foundation.org/docs/particle-entanglement.pdf
61. Santilli R. M. Elements of nuclear physics according to hadronic mechanics. I: Exact Lie-isotopic representation of nuclear data. submitted for publication.
62. Santilli R. M. A quantitative representation of particle entanglements via Bohm’s hidden variables according to hadronic mechanics. *Progress in Physics*, 2022, v. 18, 131–137. www.santilli-foundation.org/docs/pip-entanglement-2022.pdf
63. Bohm D. A Suggested Interpretation of the Quantum Theory in Terms of “Hidden Variables”. *Phys. Rev.*, 1952, v. 85, 166–182. journals.aps.org/pr/abstract/10.1103/PhysRev.85.166
64. Bohm D. Quantum Theory. Prentice-Hall, New York, 1951.
65. Santilli R. M. Nonlocal-Integral Isotopies of Differential Calculus, Mechanics and Geometries. *Rendiconti Circolo Matematico Palermo, Suppl.*, 1996, v. 42, 7–82. www.santilli-foundation.org/docs/Santilli-37.pdf
66. Santilli R. M. Iso-Representation of the Deuteron Spin and Magnetic Moment via Bohm’s Hidden Variables. *Progress in Physics*, 2022, v. 18, 74–81. www.progress-in-physics.com/2022/PP-63-12.PDF
67. Santilli R. M. and Sobczyk G. Representation of nuclear magnetic moments via a Clifford algebra formulation of Bohm’s hidden variables. *Scientific Reports*, 2022, v. 12, 1–10. www.santilli-foundation.org/docs/Santilli-Sobczyk.pdf
68. Bell J. S. On the Einstein Podolsky Rosen paradox. *Physics*, 1964, v. 1, 195. cds.cern.ch/record/111654/files/vol1p195-200.001.pdf
69. Santilli R. M. Generalization of Heisenberg’s uncertainty principle for strong interactions. *Hadronic Journal*, 1981, v. 4, 642. www.santilli-foundation.org/docs/generalized-uncertainties-1981.pdf
70. Santilli R. M. Isotopic lifting of Heisenberg’s uncertainties for gravitational singularities. *Communications in Theoretical Physics*, 1994, v. 3, 47–66. www.santilli-foundation.org/docs/santilli-511.pdf
71. Santilli R. M. Isorepresentation of the Lie-isotopic $SU(2)$ Algebra with Application to Nuclear Physics and Local Realism. *Acta Applicandae Mathematicae*, 1998, v. 50, 177–190. www.santilli-foundation.org/docs/Santilli-27.pdf
72. Santilli R. M. Studies on the classical determinism predicted by A. Einstein, B. Podolsky and N. Rosen. *Ratio Mathematica*, 2019, v. 37, 5–23. www.eprdebates.org/docs/epr-paper-ii.pdf
73. Myung H. C. and Santilli R. M. Modular-isotopic Hilbert space formulation of the exterior strong problem. *Hadronic Journal*, 1982, v. 5, 1277. www.santilli-foundation.org/docs/myung-santilli-1982.pdf
74. Liang S.-D., Lake M. J. and Harko T., Eds. Generalized uncertainty relations: Existing paradigms and new approaches. Special Issue of *Frontiers in Astronomy and Space Sciences*, 2023. www.frontiersin.org/research-topics/25805/generalized-uncertainty-relations-existing-paradigms-and-new-approaches
75. Li J.-L., and Qiao C.-F. The Generalized Uncertainty Principle. *Annalen der Physik*, 2021, v. 533, 2000335. ui.adsabs.harvard.edu/abs/2021AnP...53300335L/abstract
76. Herdegen A. and Ziobro P. Generalized uncertainty relations. *Letters in Mathematical Physics*, 2017, v. 107, 659–671. link.springer.com/article/10.1007/s11005-016-0916-9
77. Santilli R. M. Isotopic quantization of gravity and its universal isopoincaré symmetry, in the Proceedings of The Seventh Marcel Grossmann Meeting on Gravitation. SLAC, 1992, Jantzen R. T., Keiser G. M. and Ruffini R., Editors, *World Scientific Publishers*, p. 500–505, 1994. www.santilli-foundation.org/docs/Santilli-120.pdf
78. Santilli R. M. Unification of gravitation and electroweak interactions, in the Proceedings of the Eight Marcel Grossmann Meeting on Gravitation. Israel, 1997, Piran T. and Ruffini R. Editors, *World Scientific*, p. 473–475, 1999. www.santilli-foundation.org/docs/Santilli-137.pdf
79. Santilli, R. M. Reduction of Matter in the Universe to Protons and Electrons via the Lie-isotopic Branch of Hadronic Mechanics. *Progress in Physics*, 2023, v. 19, 73–99. www.progress-in-physics.com/2023/PP-65-09.PDF
80. Santilli R. M. Elements of nuclear physics according to hadronic mechanics. I: Apparent insufficiencies of quantum mechanics in nuclear physics. *Acta Mathematica*, 2024, v. 52, in press. www.santilli-foundation.org/docs/RM-santilli-paper-1.pdf
81. Santilli R. M. Elements of nuclear physics according to hadronic mechanics. II: Exact Lie-isotopic representation of Deuteron data. *Acta Mathematica*, 2024, v. 52, in press. www.santilli-foundation.org/docs/RM-santilli-paper-2.pdf
82. Santilli R. M. Elements of nuclear physics according to hadronic mechanics. III: Exact Lie-isotopic representation of nuclear stability. *Acta Mathematica*, 2024, v. 52, in press. www.santilli-foundation.org/docs/RM-santilli-paper-3.pdf

Partial Collisions of Unmater-Matter, Unmatter-Antimatter, and Unmatter1-Unmatter2 to Generate High Energy

Florentin Smarandache

Mathematics, Physics, and Natural Science Division, University of New Mexico, Gallup, NM 87301, USA
E-mail: smarand@unm.edu

In this paper we present the possibility of partial collisions between unmater with matter, and unmater with antimatter, and two or more different types of unmaters colliding between themselves to create high energy. In general, the collisions between unmater with matter, or with antimatter, or with other type of unmater, because being partial, they release less energy than the matter-unmater collision which is a total collision. But the unmater may be easier to produce in laboratory than antimatter.

1 Introduction

According to the CERN website [1], the universe is composed from 5% matter, 26.8% dark matter, and 68.2% dark energy.

The antimatter (also called dark matter) is composed from antiparticles.

The matter-antimatter asymmetry is enormous, contrary to the Big Bang Theory, which sustains that it should have been created equal amounts of matter and antimatter.

The unmater-matter and unmater-antimatter asymmetries should also be studied. At the Big Bang, if any, not only matter and antimatter would have been generated, but unmater as well. Similarly, Unmater Plasma [8, 9, 10] is a novel form of plasma, exclusively made of matter and its antimatter counterpart. It was first generated in the 2015 experiment.

The Big Bang Theory would have occurred 13.7 billion years ago, and the accelerated expansion of the universe would be due to dark matter — which contradicts the hypothesis of the initial explosion, according to which the universe should slow down. . .

The antimatter is considered a doppelganger of the matter. According to [2], “a gram of antimatter colliding with a gram of matter would produce as much energy as a nuclear bomb”.

2 Elementary Particles

The smallest units of matter (i.e., not made up by other smaller units of matter) are called elementary particles. A particle has: charge, mass, and angular momentum (spin).

The building blocks of matter, or most elementary particles known today are:

6 quarks and 6 leptons

with their corresponding antiparticles

6 antiquarks and 6 antileptons

(see Table 1 and Table 2 on top of the next Page).

The quarks are bonded together by *gluons*, and the study of strong interactions between quarks is called Quantum Chromodynamics (QCD).

In an atom, the electrons are leptons, while the protons, neutrons, and pions are made up of quarks.

A *baryon* is made up of an odd number of quarks (usually three); while a *meson* is made up of an even number of quarks (usually a quark and an antiquark, therefore such a meson is the most elementary form of unmater, let us call it *unmater-meson*.

A *pion* (or *pi-meson*) is an unstable subatomic particle of one of the following three forms: and each one is composed from a quark and an antiquark (as such, they are mesons, and therefore elementary forms of unmater, let us call them *unmater-pions*.

The *hadron* is a particle made up of two or more quarks that, through a strong interaction, are hold together.

Antimatter is matter composed of antiparticles.

While the *antiparticle*, as partner of a particle, is matter with reversed charge, parity, and time of its corresponding particle.

The *photon particle* is its own photon antiparticle, but this is an exception. All other particles have different corresponding antiparticles.

In collision, particle and antiparticle annihilate each other and produce gamma photons, neutrinos, and other particles.

3 Standard Model

According to the Standard Model, there are 17 distinct subatomic particles:

12 fermions and 5 bosons.

The fermion is a particle that only in combination with its antiparticle can be created or destroyed. Like the electron.

While the boson is a particle that can be created and destroyed in arbitrary numbers. Like photon.

Boson is in general a force carrier particle.

The fundamental forces that act in the nature are: gravity, electromagnetism, strong force, and weak force.

4 Defining Unmater

In short, unmater is formed by matter and antimatter that bind together and it was introduced by Smarandache in 2004 on the CERN website [4], and developed later [5–17].

Quarks	up (u)	down (d)	charm (c)	strange (s)	top (t)	bottom (b)
Antiquarks	up	down	charm	strange	top	bottom

Table 1: Quarks and antiquarks.

Leptons	charged	antielelectron	antimuon	antitau
Antileptons	neutrals	anti-electron-neutrino	anti-muon-neutrino	anti-tau-neutrino

Table 2: Leptons and antileptons.

The building blocks of matter and antimatter (most elementary particles known today) are 6 quarks and 6 leptons; their 12 antiparticles also exist.

Then *unmatter* will be formed by at least a building block and at least an antibuilding block which can bind together.

Let us start from neutrosophy [3], which is a generalization of dialectics, i.e., not only the opposites are combined but also the neutralities. Why? Because when an idea is launched, a category of people will accept it, others will reject it, and a third one will ignore it (don't care). But the dynamics between these three categories changes, so somebody accepting it might later reject or ignore it, or an ignorant will accept it or reject it, and so on. Similarly the dynamicity of $\langle A \rangle$, $\langle \text{anti}A \rangle$, $\langle \text{neut}A \rangle$, where $\langle \text{neut}A \rangle$ means neither $\langle A \rangle$ nor $\langle \text{anti}A \rangle$, but in between (neutral). Neutrosophy considers a kind not of di-alectics but tri-alectics (based on three components: $\langle A \rangle$, $\langle \text{anti}A \rangle$, $\langle \text{neut}A \rangle$).

Hence unmatter is a kind of intermediary (not referring to the charge) between matter and antimatter, i.e. neither one, nor the other.

Neutrosophic Logic (NL) is a generalization of fuzzy logic (especially of intuitionistic fuzzy logic) in which a proposition has a degree of truth, a degree of falsity, and a degree of neutrality (neither true nor false); in the normalized NL the sum of these degrees is 1.

5 Unmatter Atom

It is possible to define the unmatter in a more general way, using the exotic atom. The exotic atom is an atom obtained after substituting one or more particles by other particles of the same charge (constituents).

The classical unmatter atoms were formed by particles like (a) electrons, protons, and antineutrons, or (b) antielectrons, antiprotons, and neutrons.

In a more general definition, an unmatter atom is a system of particles as above, or such that one or more particles are replaced by other particles of the same charge.

Other categories would be (c) a matter atom with where one or more (but not all) of the electrons and/or protons are replaced by antimatter particles of the same corresponding charges, and (d) an antimatter atom such that one or more (but not all) of the antielectrons and/or antiprotons are replaced by matter particles of the same corresponding charges.

In a more composed system we can substitute a particle by an unmatter particle and form an unmatter atom.

Of course, not all of these combinations are stable, semi-stable, or quasi-stable, especially when their time to bind together might be longer than their lifespan.

6 Unmatter Charge

The charge of unmatter may be positive as in the pentaquark Theta-plus, 0 (as in the atom of positronium), or negative as in anti-Rho meson, i.e. $u\bar{d}$, (M. Jordan).

7 Containment

The unmatter could be store as the antimatter atom “by atomic traps (based on electric or magnetic dipoles) and by lasers (magneto-optical traps and optical tweezers)” [18].

8 Matter and Antimatter

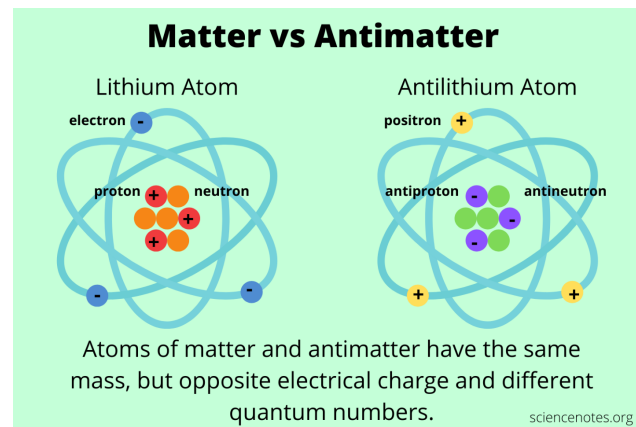


Fig. 1: Matter vs Antimatter. Courtesy of Anne Helmenstine, “What Is Antimatter? Definition and Examples” [18].

Lithium Atom:

electron1 (−), electron2 (−), electron3 (−);
proton1 (+), proton2 (+), proton3 (+);
neutron1 (0), neutron2 (0), neutron3 (0), neutron4 (0).

Lithium Antiatom:

positon1 (+), positon2 (+), positon3 (+);
antiproton1 (−), antiproton2 (−), antiproton3 (−);
antineutron1 (0), antineutron2 (0), antineutron3 (0), antineutron4 (0).

9 Proton and AntiProton

The Proton is made up of: up-quark, up-quark, down-quark; and AntiProton is made up of: anti-up-quark, anti-up-quark, anti-down-quark.

10 Real Examples of Unmatter

- (i) Meson, which in general is made up of: quark and anti-quark, and as particular cases of mesons one has:
Pion1 = anti-up-quark, down-quark;
Pion2 = up-quark, anti-down-quark. Pion2 is the Anti-Pion1.
- (ii) **Pentaquark**, which is made up of:
up-quark, up-quark, down-quark, down-quark, anti-strange-quark.

11 Partial Collisions of Unmatter-Unmatter

- (i) Pion1 vs. Pentaquark: anti-up-quark vs. up-quark (only), since between down-quark and down-quark there is no collision.
- (ii) Pion2 vs. Pentaquark: anti-down-quark vs. down-quark (only), since between up-quark and up-quark there is no collision.

12 Total Collision of Unmatter-Unmatter

Pion1 vs. Pion2: anti-up-quark vs. up-quark; and down-quark vs. anti-down-quark.

13 Partial Collisions of Unmatter-Matter

- (i) Pion1 vs. Proton: anti-up-quark vs. up-quark (only), since between down-quark and down-quark there is no collision.
- (ii) Pion2 vs. Proton: anti-down-quark vs. down-quark (only), since between up-quark and up-quark there is no collision.

14 Partial Collisions of Unmatter-Antimatter

- (i) Pion1 vs. Antiproton: down-quark vs. anti-down-quark (only), since between anti-up-quark and anti-up-quark there is no collision.
- (ii) Pion2 vs. Antiproton: up-quark vs. anti-up-quark (only), since between anti-down-quark and anti-down-quark there is no collision.

Submitted on May 5, 2024

References

1. ALPHA collaboration at CERN reports first measurements of certain quantum effects in antimatter. The measurements are consistent with predictions for "normal" matter and pave the way for future precision studies. 19 February 2020; <https://home.cern/news/news/physics/alpha-collaboration-cern-reports-first-measurements-certain-quantum-effects>
2. Levana Z. Ce mai face lumea de eclipsa (II): CERN si semnele Minunatei Lumi Noi, Active News, 07 aprilie 2024; <https://www.activenews.ro/opinii/Ce-mai-face-lumea-de-eclipsa-II-CERN-si-semnele-Minunatei-Lumi-Noi-188590>
3. Smarandache F. A unifying field in logics, neutrosophic logic. Neutrosophy, neutrosophic set, neutrosophic probability. Am. Res. Press, 1998; <https://fs.unm.edu/eBook-Neutrosophics6.pdf>
4. Smarandache F. Matter, antimatter, and unmatter. CDS-CERN, EXT-2005-142, 2004; *Bulletin of Pure and Applied Sciences*, 2004, v. 23D, no. 2, 173–177; <http://cdsweb.cern.ch/record/798551>
5. Goldfain E. and Smarandache F. On emergent physics, "unparticles" and exotic "unmatter" states. *Progress in Physics*, 2008, no. 4, 10–15.
6. Smarandache F. Verifying unmatter by experiments, more types of unmatter, and a quantum chromodynamics formula. *Progress in Physics*, 2005, no. 2, 113–116; *Infinite Energy*, 2006, v. 12, no. 67, 36–39.
7. Smarandache F., Rabounski D. Discovered "Angel Particle", which is both matter and antimatter, as a new experimental proof of unmatter. 2017 APS Annual Meeting of the Far West Section, Merced, California, Nov. 3–4, 2017; <http://meetings.aps.org/Meeting/FWS17/Session/E1.16>
8. Smarandache F. Unmatter plasma revisited. 59th Annual Meeting of the APS Division of Plasma Physics, Milwaukee, Wisconsin, Oct. 23–27, 2017; <http://meetings.aps.org/Meeting/DPP17/Session/YP11.35>
9. Smarandache F., Ali M. Neutrosophic triplet as extension of matter plasma, unmatter plasma, and antimatter plasma. 69th Annual Gaseous Electronics Conference, Bochum, Germany, v. 61, no. 9, Oct. 10–14, 2016; <http://meetings.aps.org/Meeting/GEC16/Session/HT6.111>
10. Smarandache F. Unmatter plasma. 57th Annual Meeting of the APS Division of Plasma Physics, Savannah, Georgia, Nov. 16–20, 2015; <http://meetings.aps.org/Meeting/DPP15/Session/UP12.46>
11. Smarandache F. Unmatter as a consequence of the law of included multiple-middles. Annual Meeting of the APS Four Corners Section, Tempe, Arizona, Oct. 16–17, 2015; <http://meetings.aps.org/Meeting/4CF15/Session/F1.66>
12. Smarandache F. Unparticle, a special case of unmatter. 53rd Annual Meeting of the APS Division of Plasma Physics, Salt Lake City, Utah, Nov. 14–18, 2011; <http://meetings.aps.org/Meeting/DPP11/Event/153509>
13. Rabounski D., Smarandache F. The Brightsen nucleon cluster model predicts unmatter entities inside nuclei. 2008 Annual Meeting of the Division of Nuclear Physics, Oakland, California, Oct. 23–26, 2008; <http://meetings.aps.org/Meeting/DNP08/Event/87738>
14. Goldfain E., Smarandache F. On emergent physics, unparticles and exotic unmatter states. 2009 Joint Spring Meeting of the New England Section of APS and AAPT, Boston, Massachusetts, May 8–9, 2009; <http://meetings.aps.org/link/BAPS.2009.NES.APS2>
15. Smarandache F. Verifying unmatter by experiments, more types of unmatter, and a quantum chromodynamics formula. 62nd Annual Gaseous Electronics Conference, Saratoga Springs, New York, Oct. 20–23, 2009; <http://meetings.aps.org/link/BAPS.2009.GEC.KTP.110>
16. Smarandache F. A new form of matter — Unmatter, composed of particles and anti-particles. 40th Annual Meeting of the APS Division of Atomic, Molecular and Optical Physics, Charlottesville, Virginia, May 19–23, 2009; <http://meetings.aps.org/link/BAPS.2009.DAMOP.E1.97>
17. Smarandache F. Unparticle, a special case of unmatter. 53rd Annual Meeting of the APS Division of Plasma Physics, Salt Lake City, Utah, Nov. 14–18, 2011; <http://meetings.aps.org/Meeting/DPP11/Session/Index3/?SessionEventID=158034>
18. Helmenstine A. What Is Antimatter? Definition and Examples. <https://sciencenotes.org/what-is-antimatter-definition-and-examples>

The Vacuum Stress-Energy Tensor in General Relativity

Patrick Marquet

Calais, France. E-mail: patrick.marquet6@wanadoo.fr

In General Relativity, the Einstein field equations with a massive term source are plagued with the non conservation of this energy-momentum tensor. To remedy this problem, a pseudo-tensor of the gravitational field is classically added so that the global right hand side is conserved. Using Cartan's calculus, we derive here the differential form of the Einstein field equations which provides the Landau-Lifshitz symmetric (pseudo) 3-form of the gravitational field. Assuming a slightly variable cosmological term, we then infer a vacuum energy-momentum (real) 3-form so that the global r.h.s. of the field equations eventually exhibits a full real 3-form that satisfies the conserved property. In the early phase of the universe's expansion it is suggested that the cosmological term was huge and constant, before becoming variable to yield the estimated value predicted to-day.

Notations

Space-time Greek indices α, β, \dots are 0, 1, 2, 3 for local coordinates.
Space-time Latin indices a, b, \dots are 0, 1, 2, 3 for a general basis.
The space-time signature is -2 .
Einstein's constant is denoted by κ .
The velocity of light is $c = 1$.

1 Differential calculus

1.1 The classical field equations in GR (short overview)

In General Relativity (GR), any line element on the 4-pseudo-Riemannian manifold (M, g) is given by $ds^2 = g_{ab} dx^a dx^b$. By varying the action $\mathcal{S} = \mathcal{L}_E d^4x$ with respect to the g_{ab} where the lagrangian density is given by

$$\mathcal{L}_E = g^{ab} \sqrt{-g} \left[\{^e_{ab}\} \{^d_{de}\} - \{^d_{ae}\} \{^e_{bd}\} \right] \quad (1)$$

one infers the symmetric Einstein tensor

$$G_{ab} = R_{ab} - \frac{1}{2} g_{ab} R, \quad (2)$$

where

$$R_{bc} = \partial_a \{^a_{bc}\} - \partial_c \{^a_{ba}\} + \{^d_{bc}\} \{^a_{da}\} - \{^d_{ba}\} \{^a_{dc}\} \quad (3)$$

is the (symmetric) Ricci tensor whose contraction gives the curvature scalar R . (Here $\{^e_{ab}\}$ denote the Christoffel symbols of the second kind.)

The source free field equations are

$$G_{ab} = R_{ab} - \frac{1}{2} g_{ab} R + \Lambda g_{ab} = 0, \quad (4)$$

where Λ is the Einstein cosmological constant.

The second rank tensor G_{ab} is symmetric and is only function of the metric tensor components g_{ab} and their first and second order derivatives. Due to Bianchi's identities the Einstein tensor is conceptually conserved

$$\nabla_a G^a_b = 0, \quad (5)$$

where ∇_a is the Riemann covariant derivative.

When a massive source is present, the field equations become

$$G_{ab} = R_{ab} - \frac{1}{2} g_{ab} (R - 2\Lambda) = \kappa T_{ab}. \quad (6)$$

If ρ is the matter density, then T_{ab} is here the tensor describing a pressure free fluid

$$T_{ab} = \rho u_a u_b. \quad (7)$$

1.2 The Cartan structure equations

Let us now consider a 4-manifold M referred to a vector basis e_α . The dual basis θ^β of one-forms (pfaffian forms) are related to the local coordinates x^α by

$$\theta^\beta = a^\beta_a dx^a. \quad (8)$$

These are called *vierbein* or *tetrad fields* [1].

In a dual basis θ^a , to any parallel transported vector along a closed path, can be then associated the following 2-forms:

— A rotation curvature form

$$\Omega^\alpha_\beta = \frac{1}{2} R^\alpha_{\beta\gamma\delta} \theta^\gamma \wedge \theta^\delta; \quad (9)$$

— A torsion form

$$\Omega^\alpha = \frac{1}{2} T^\alpha_{\gamma\delta} \theta^\gamma \wedge \theta^\delta. \quad (10)$$

Introducing the Cartan procedure one first defines the connection forms

$$\Gamma^\alpha_\beta = \{^\alpha_{\gamma\beta}\} \theta^\gamma. \quad (11)$$

The first Cartan structure equation is related to the torsion by [2, p.40]

$$\Omega^\alpha = \frac{1}{2} T^\alpha_{\gamma\delta} \theta^\gamma \wedge \theta^\delta = d\theta^\alpha + \Gamma^\alpha_\gamma \wedge \theta^\gamma. \quad (12)$$

The second Cartan structure equation is defined as follows [2, p.42] so that

$$\Omega_{\beta}^{\alpha} = \frac{1}{2} R_{\beta\gamma\delta}^{\alpha} \theta^{\gamma} \wedge \theta^{\delta} = d\Gamma_{\beta}^{\alpha} + \Gamma_{\gamma}^{\alpha} \wedge \Gamma_{\beta}^{\gamma}, \quad (13)$$

where $R_{\beta\gamma\delta}^{\alpha}$ are the components of the curvature tensor in the most general sense.

Within the Riemannian framework alone (torsion free), $R_{\beta\gamma\delta}^{\alpha}$ reduce to the Riemann curvature tensor components and the first structure equation (12) becomes:

$$d\theta^{\alpha} = -\Gamma_{\gamma}^{\alpha} \wedge \theta^{\gamma}. \quad (14)$$

2 Differential equations of General Relativity

2.1 The Einstein field equations

We first recall the Hodge star operator definition for an oriented 4-dimensional pseudo-Riemannian manifold (M, g) with volume element determined by g

$$\eta = \sqrt{-g} \theta^0 \wedge \theta^1 \wedge \theta^2 \wedge \theta^3. \quad (15)$$

Let $\Lambda_k(\mathbf{E})$ be the subspace of completely antisymmetric multilinear forms on the real vector space \mathbf{E} .

The Hodge star operator $*$ is a linear isomorphism, i.e., $L_k(M) \rightarrow L_{n-k}(M)$ (where $k \leq n$).

If $\theta^0, \theta^1, \theta^2, \theta^3$ is an oriented basis of 1-forms, then this operator is defined by

$$\begin{aligned} *(\theta^{i1} \wedge \theta^{i2} \wedge \theta^{ik}) &= \\ &= \frac{\sqrt{-g}}{(n-k)!} \varepsilon_{j1\dots jn} g^{j1i1} \dots g^{jik} \theta^{jk+1} \wedge \dots \wedge \theta^{jn}. \end{aligned} \quad (16)$$

With this preparation, the Einstein action simply reads

$$*R = R\eta. \quad (17)$$

Varying this action with respect to $\delta\theta^{\beta}$ of the orthonormal tetrad fields, eventually leads to the field equations under the differential form

$$-\frac{1}{2} \eta_{\beta\gamma\delta} \wedge \Omega^{\gamma\delta} = \kappa *T_{\beta}, \quad (18)$$

where T_{α} is related to the energy-momentum tensor $T_{\alpha\beta}$ by $T_{\alpha} = T_{\alpha\beta} \theta^{\beta}$ and include all other contributions.

In the same manner, one has for the Einstein tensor $G_{\alpha} = G_{\alpha\beta} \theta^{\beta}$. For all detailed derivations refer to [3].

2.2 The energy-momentum tensor

In the field equations (18), we insert $\eta^{\alpha\beta\gamma} = \eta^{\alpha\beta\gamma\delta} \theta_{\delta}$. Then, we use the second structure equation under the following form

$$\Omega_{\beta\gamma} = d\Gamma_{\beta\gamma} - \Gamma_{\mu\beta} \wedge \Gamma_{\gamma}^{\mu}, \quad (19)$$

$$-\frac{1}{2} \eta^{\alpha\beta\gamma\delta} \theta_{\delta} \wedge (d\Gamma_{\beta\gamma} - \Gamma_{\mu\beta} \wedge \Gamma_{\gamma}^{\mu}) = \kappa *T_{\alpha}, \quad (20)$$

leading to

$$-\frac{1}{2} \eta^{\alpha\beta\gamma\delta} d(\Gamma_{\beta\gamma} \wedge \theta_{\delta}) = \kappa (*T_{\alpha} + *t_{\alpha}), \quad (21)$$

where [4]

$$*t^{\alpha} = -\frac{1}{2\kappa} \eta^{\alpha\beta\gamma\delta} (\Gamma_{\mu\beta} \wedge \Gamma_{\gamma}^{\mu} \wedge \theta_{\delta} - \Gamma_{\beta\gamma} \wedge \Gamma_{\mu\delta} \wedge \eta^{\mu}). \quad (22)$$

We see that $*t^{\alpha}$ is unaffected by the exterior product terms in the bracket, therefore $t_{\alpha\beta}$ is symmetric.

In that case, we identify $*t^{\alpha}$ with the Landau-Lifshitz 3-form $*t_{L-L}^{\alpha\beta}$ which yields the corresponding pseudo-tensor $t_{L-L}^{\alpha\beta}$ [5, eq.101.7]

$$\begin{aligned} (-g) t_{L-L}^{\alpha\nu} &= \frac{1}{2\kappa} \left\{ \#g_{,\lambda}^{\alpha\nu} \#g_{,\mu}^{\lambda\mu} - \#g_{,\lambda}^{\alpha\lambda} \#g_{,\mu}^{\nu\mu} + \right. \\ &+ \frac{1}{2} g^{\alpha\nu} g_{\lambda\mu} \#g_{,\rho}^{\lambda\theta} \#g_{,\theta}^{\rho\mu} - (g^{\alpha\lambda} g_{\mu\theta} \#g_{,\rho}^{\nu\theta} \#g_{,\lambda}^{\mu\rho} + \\ &+ g^{\nu\lambda} g_{\mu\theta} \#g_{,\rho}^{\alpha\theta} \#g_{,\lambda}^{\mu\rho}) + g_{\mu\lambda} g^{\theta\rho} \#g_{,\theta}^{\alpha\lambda} \#g_{,\rho}^{\nu\mu} + \\ &\left. + \frac{1}{8} (2g^{\alpha\lambda} g^{\nu\mu} - g^{\alpha\nu} g^{\lambda\mu}) (2g_{\theta\rho} g_{\delta\tau} - g_{\rho\delta} g_{\theta\tau}) \#g_{,\lambda}^{\theta\tau} \#g_{,\mu}^{\rho\delta} \right\}, \end{aligned} \quad (23)$$

where

$$\#g^{\alpha\nu} = \sqrt{-g} g^{\alpha\nu}. \quad (24)$$

3 The vacuum energy

3.1 The gravitational field tensor

In General Relativity, it is well known, that the Einstein tensor $G_{\alpha\beta}$ is intrinsically conserved, while the massive tensor $T_{\alpha\beta}$ is not. This is because the gravitational field is not included in $T_{\alpha\beta}$. If so, then one obtains the conservation law

$$\partial_{\beta} \sqrt{-g} (T^{\alpha\beta} + t^{\alpha\beta}) = 0. \quad (25)$$

The tensor $t_{\alpha\beta}$ describes the gravitational field, derived from the Einstein-Dirac pseudo-tensor density [6, p.61]

$$\sqrt{-g} t_{\alpha}^{\beta} = \frac{1}{2\kappa} \left\{ \left(\partial_{\alpha} \#g^{\sigma\tau} \right) \partial \mathcal{L}_E - \delta_{\alpha}^{\beta} \mathcal{L}_E \right\}. \quad (26)$$

However, the Einstein field equations are yet unbalanced since they do not exhibit a full real tensor as a source.

To remedy this problem, we showed that a slightly variable cosmological term Λ -term induces a stress energy tensor of vacuum which restores a true gravitational tensor on the r.h.s. of the equation (6) as it should be [7, 8].

This real vacuum tensor was given by

$$(t_{\alpha\beta})_{\text{vac}} = -\frac{1}{2\kappa} \Lambda g_{\alpha\beta}, \quad (27)$$

where the term Λ was found to be [9]

$$\Lambda = \nabla_\alpha K^\alpha = \theta^2, \quad (28)$$

where K^α is a 4-vector, and

$$\theta = X^\alpha_{;\alpha} \quad (29)$$

is the space-time volume scalar expansion characterizing the vacuum stress-energy tensor $(t_{\alpha\beta})_{\text{vac}}$. X^α is a congruence of non-intersecting unit time lines: $X^\alpha X_\alpha = 1$

$$X^\alpha_{;\alpha} = h^{\alpha\beta} \theta_{\alpha\beta}, \quad (30)$$

where $\theta_{\alpha\beta}$ stands for the expansion tensor, and $h_{\alpha\beta} = g_{\alpha\beta} - X_\alpha X_\beta$ is the projection tensor. Due to the form of (28), the lagrangian (1) differs only from a divergence and varying its action generates the same Einstein equations.

The real tensor $t^{\alpha\beta}_{\text{vac}}$ corresponding to the vacuum stress energy tensor can be added to $t^{\alpha\beta}$ without affecting the Einstein tensor inferred from the variational principle. So the final (real) gravitational tensor density is given by

$$\sqrt{-g} (t^\beta_\alpha)_G = \frac{1}{2\kappa} \left\{ \frac{(\partial_\alpha g^{\sigma\tau})}{(\partial_\beta g^{\sigma\tau})} \frac{\partial \mathcal{L}_E}{\partial \theta} - \delta^\beta_\alpha (\mathcal{L}_E - \sqrt{-g} \Lambda) \right\}. \quad (31)$$

The real tensor $(t^\beta_\alpha)_G$ is afterwards conveniently symmetrized through the Belinfante procedure [10].

With this definition the field equations can be finally written

$$R^{\alpha\beta} - \frac{1}{2} g^{\alpha\beta} R = \kappa (T^{\alpha\beta} + t^{\alpha\beta}_G). \quad (32)$$

Sufficiently far from this matter we always have

$$R^{\alpha\beta} - \frac{1}{2} g^{\alpha\beta} R = \kappa t^{\alpha\beta}_{\text{vac}}. \quad (33)$$

Inspection shows that each energy-momentum tensor is conserved.

3.2 The vacuum stress-energy 3-form

Here we adopt the Landau-Lifshitz symmetric pseudo-3-form $*t^\alpha_{L-L}$ instead of the Einstein-Dirac pseudo-density. We then determine a vacuum energy 3-form designed to render the r.h.s. of (21) fully real according to the previous derivation.

To this end, we first regard the variable cosmological term Λ as inducing a given space-time curvature. This is legitimized by the fact that the real tensor $(t_{\alpha\beta})_{\text{vac}}$ is *a priori* persistent throughout the vacuum.

Since Λ is a scalar, let us then set the resulting curvature 2-form as

$$\Omega = \frac{1}{2} R^\delta_{\sigma\delta\tau} \theta^\sigma \wedge \theta^\tau. \quad (34)$$

By analogy with the classical formalism (4) we then apply the quantity $g^{\gamma\delta} \Omega$ to the field equations (18) as follows

$$\left. \begin{aligned} -\frac{1}{2} \eta_{\alpha\mu\nu} \wedge (\Omega^{\mu\nu} + g^{\mu\nu} \Omega) &= \kappa *T_\alpha \\ -\frac{1}{2} \eta^\mu_{\alpha\nu} \wedge (\Omega^\nu_\mu + \delta^\nu_\mu \Omega) &= \kappa *T_\alpha \end{aligned} \right\}. \quad (35)$$

Using $\Omega^\nu_\mu = \frac{1}{2} R^\nu_{\beta\gamma\delta} \theta^\beta \wedge \theta^\gamma$, these equations can be written in the form

$$-\frac{1}{4} \eta^\mu_{\alpha\nu} \wedge \theta^\sigma \wedge \theta^\tau (R^\nu_{\mu\sigma\tau} + \delta^\nu_\mu R^\delta_{\sigma\delta\tau}) = \kappa T_{\alpha\beta} \eta^\beta. \quad (36)$$

To $R^\nu_{\mu\sigma\tau}$ is now added a new 4th rank curvature tensor which is noted

$$2\Lambda^\nu_{\mu\sigma\tau} = -\delta^\nu_\mu R^\delta_{\sigma\delta\tau}. \quad (37)$$

To make it apparent, we first use the following relations

$$\eta^\alpha \equiv * \theta^\alpha \quad (38)$$

$$\eta_\alpha = \frac{1}{3!} (\eta_{\alpha\beta\gamma\delta} \theta^\beta \wedge \theta^\gamma \wedge \theta^\delta) = \frac{1}{3!} \theta^\beta \wedge \eta_{\alpha\beta}. \quad (39)$$

Then, we apply the following identities

$$\theta^\beta \wedge \eta_\alpha = \delta^\beta_\alpha \eta,$$

$$\theta^\gamma \wedge \eta_{\alpha\beta} = \delta^\gamma_\beta \eta_\alpha - \delta^\gamma_\alpha \eta_\beta,$$

$$\theta^\delta \wedge \eta_{\alpha\beta\gamma} = \delta^\delta_\gamma \eta_{\alpha\beta} + \delta^\delta_\beta \eta_{\gamma\alpha} + \delta^\delta_\alpha \eta_{\beta\gamma},$$

$$\theta^\varepsilon \wedge \eta_{\alpha\beta\gamma\delta} = \delta^\varepsilon_\delta \eta_{\alpha\beta\gamma} - \delta^\varepsilon_\gamma \eta_{\delta\alpha\beta} + \delta^\varepsilon_\beta \eta_{\gamma\delta\alpha} - \delta^\varepsilon_\alpha \eta_{\beta\gamma\delta}.$$

With this preparation, (36) reads

$$\begin{aligned} & -\frac{1}{4} (R^{\mu\nu}_{\sigma\tau} - 2\Lambda^{\mu\nu}_{\sigma\tau}) [\delta^\tau_\nu (\delta^\sigma_\mu \eta_\alpha - \delta^\sigma_\nu \eta_\mu) + \\ & + \delta^\tau_\mu (\delta^\sigma_\nu \eta_\alpha - \delta^\sigma_\mu \eta_\nu) + \delta^\tau_\alpha (\delta^\sigma_\nu \eta_\mu - \delta^\sigma_\mu \eta_\nu)] = \\ & = -\frac{1}{2} (R^{\mu\nu}_{\mu\nu} - 2\Lambda^{\mu\nu}_{\mu\nu}) \eta_\alpha + (R^{\mu\nu}_{\alpha\nu} - 2\Lambda^{\mu\nu}_{\alpha\nu}) \eta_\nu = \\ & = (R^{\beta\nu}_{\alpha\nu} - 2\Lambda^{\beta\nu}_{\alpha\nu}) \eta_\beta - \frac{1}{2} \delta^\beta_\alpha (R^{\mu\nu}_{\mu\nu} - 2\Lambda^{\mu\nu}_{\mu\nu}) \eta_\beta. \end{aligned} \quad (40)$$

As a contributing curvature tensor, $2\Lambda^{\beta\nu}_{\alpha\nu}$ must be included in $R^{\beta\nu}_{\alpha\nu}$ so that we eventually retrieve the classical field equations with a cosmological term

$$\left(R^\beta_\alpha - \frac{1}{2} \delta^\beta_\alpha R + \delta^\beta_\alpha \Lambda \right) \eta_\beta = \kappa T^\beta_\alpha \eta_\beta. \quad (41)$$

Taking account of $\Omega_{\beta\gamma} = d\Gamma_{\beta\gamma} - \Gamma_{\mu\beta} \wedge \Gamma^\mu_\gamma$, we revert to the field equations (22) which are also expressed as

$$-\frac{1}{2} \eta^{\alpha\beta\gamma\delta} \theta_\delta \wedge (d\Gamma_{\beta\gamma} - \Gamma_{\mu\beta} \wedge \Gamma^\mu_\gamma) = \kappa *T^\alpha. \quad (42)$$

Adding the extra-curvature yields

$$-\frac{1}{2} \eta^{\alpha\beta\gamma\delta} \theta_\delta \wedge [(d\Gamma_{\beta\gamma} - \Gamma_{\mu\beta} \wedge \Gamma^\mu_\gamma) + g_{\beta\gamma} \Omega] = \kappa *T^\alpha. \quad (43)$$

that is according to (21)

$$-\frac{1}{2} \eta^{\alpha\beta\gamma\delta} \left[d(\Gamma_{\beta\gamma} \wedge \theta_\delta) + \theta_\delta \wedge g_{\beta\gamma} \Omega \right] = \kappa \left({}^*T^\alpha + {}^*t_{L-L}^\alpha \right). \quad (44)$$

Therefore

$$\begin{aligned} -\frac{1}{2} \eta^{\alpha\beta\gamma\delta} d(\Gamma_{\beta\gamma} \wedge \theta_\delta) &= \\ &= \kappa \left[{}^*T^\alpha + {}^*t_{L-L}^\alpha + \frac{1}{2\kappa} \eta^{\alpha\beta\gamma\delta} (\theta_\delta \wedge g_{\beta\gamma} \Omega) \right], \\ -\frac{1}{2} \eta^{\alpha\beta\gamma\delta} \delta(\Gamma_{\beta\gamma} \wedge \theta_\delta) &= \\ &= \kappa \left[{}^*T^\alpha + {}^*t_{L-L}^\alpha - \frac{1}{4\kappa} \eta^{\alpha\beta\gamma\delta} (\theta_\delta \wedge g_{\beta\gamma} R_{\lambda\sigma\tau}^\lambda \theta^\sigma \wedge \theta^\tau) \right]. \end{aligned}$$

In the expression $-\frac{1}{4\kappa} \eta^{\alpha\beta\gamma\delta} \theta_\delta \wedge g_{\beta\gamma} R_{\lambda\sigma\tau}^\lambda \theta^\sigma \wedge \theta^\tau$, we make the substitution

$$-g_{\beta\gamma} R_{\lambda\sigma\tau}^\lambda = 2\Lambda_{\beta\gamma\sigma\tau}. \quad (45)$$

We eventually find the *vacuum stress-energy momentum 3-form*

$${}^*t_{\text{vac}}^\alpha = \frac{1}{2\kappa} \eta^{\alpha\beta\gamma\delta} \theta_\delta \wedge \Lambda_{\beta\gamma\sigma\tau} \theta^\sigma \wedge \theta^\tau. \quad (46)$$

Therefore the global gravitational field is described by the (real) 3-form

$$\begin{aligned} {}^*t_G^\alpha &= -\frac{1}{2\kappa} \eta^{\alpha\beta\gamma\delta} \left[(\Gamma_{\mu\beta} \wedge \Gamma_\gamma^\mu \wedge \theta_\delta - \Gamma_{\beta\gamma} \wedge \Gamma_{\mu\delta} \wedge \theta^\mu) - \right. \\ &\quad \left. - \theta_\delta \wedge \Lambda_{\beta\gamma\sigma\tau} \theta^\sigma \wedge \theta^\tau \right]. \quad (47) \end{aligned}$$

3.3 The complete Einstein equations

The field equations are

$$-\frac{1}{2} \eta^{\alpha\beta\gamma\delta} d(\Gamma_{\beta\gamma} \wedge \theta_\delta) = \kappa ({}^*T^\alpha + {}^*t_G^\alpha). \quad (48)$$

As per (33) far from matter, we always have

$$-\frac{1}{2} \eta^{\alpha\beta\gamma\delta} d(\Gamma_{\beta\gamma} \wedge \theta_\delta) = \kappa {}^*t_{\text{vac}}^\alpha. \quad (49)$$

Now, let us multiply equation (48) with $\sqrt{-g}$, then taking into account $\eta_{\alpha\beta\gamma\delta} = -\frac{1}{2\sqrt{-g}} \varepsilon_{\alpha\beta\gamma\delta}$, we find a new form for the field equations

$$-d(\sqrt{-g} \eta^{\alpha\beta\gamma\delta} \Gamma_{\beta\gamma} \wedge \theta_\delta) = 2\kappa \sqrt{-g} ({}^*T^\alpha + {}^*t_G^\alpha) \quad (50)$$

or

$$-d(\sqrt{-g} \Gamma^{\beta\gamma} \wedge \eta_{\beta\gamma}^\alpha) = 2\kappa \sqrt{-g} ({}^*T^\alpha + {}^*t_G^\alpha). \quad (51)$$

From these equations follows immediately the differential conservation law

$$d[\sqrt{-g} ({}^*T^\alpha + {}^*t_G^\alpha)] = 0. \quad (52)$$

If we integrate equation (51) over a 3-dimensional space-like region D_3 , then we obtain

$$P^\alpha = -\frac{1}{2\kappa} \int \sqrt{-g} \Gamma^{\beta\gamma} \wedge \eta_{\beta\gamma}^\alpha, \quad (53)$$

which is the total 4-momentum of the isolated system. Inspection shows that P^α is gauge invariant in the following sense

$$\theta(x) \rightarrow A(x) \theta(x), \quad (54)$$

$$\Gamma(x) \rightarrow A(x) \Gamma(x) A^{-1}(x) - dA(x) A^{-1}(x), \quad (55)$$

where $A(x)$ is a local transformation matrix (A_β^α).

General Relativity is invariant with respect to such transformations and is thus a non-abelian gauge theory.

3.4 The early cosmological expansion evolution

The singularity of our universe is generally set at 10^{-43} seconds corresponding to the Planck era.

At this epoch, the size of our universe is predicted to be 10^{-35} meters with an energy of 10^{19} GeV and a temperature amounting to 10^{32} K. We postulate that the cosmological term was present and constant in the early stage of the singularity possessing a huge value. As time was the very first parameter to appear, the cosmological constant Λ would be associated to a large “pre” 3-form time component ${}^*t_{\text{vac}}^0$ with no further explicit structure. At 10^{-35} seconds, strong force and electro-weak force decoupled and at 10^{-12} seconds, the electro-weak force splits into weak and electromagnetic forces. Over this period of time, the cosmological term drastically decreases and becomes slightly variable. These processes cause the Universe’s expansion to accelerate and ${}^*t_{\text{vac}}^0$ would deploy according to equation (46)

$${}^*t_{\text{vac}}^\alpha = \frac{1}{2\kappa} \eta^{\alpha\beta\gamma\delta} \theta_\delta \wedge \Lambda_{\beta\gamma\sigma\tau} \theta^\sigma \wedge \theta^\tau. \quad (56)$$

Such a hypothesis would lend support to the inflation scenario recently suggested by the astronomer Claude Poher. His theory is based on the detection of massless particles moving at the speed of light which are assumed to propagate throughout the entire vacuum [11, 12]. According to Poher, these particles act as a gravitational isotropic flux and each one bears an individual energy measured at $E_u = 8.5 \times 10^{-21}$ Joules [13–15]. Without invoking a quantum aspect, the corpuscular nature of this flux might well appear as a piecewise structure of the vacuum field we have inferred in the above.

Conclusion

If one relaxes our demand on the cosmological term constancy, it is possible to define a real homogeneous vacuum stress-energy tensor which is by essence a pervasive field. In our picture, the gravitational field of a matter appears as an excited state of this field. Far from its matter source, the gravitational field pseudo-tensor asymptotically decreases down

to the level of the vacuum energy-momentum tensor leaving the field equations with a non-zero right hand side. In here, we have shown that starting with the Landau-Lifshitz 3-form, it is also possible to infer a real 3-form representing the vacuum energy-momentum to restore a real r.h.s. of the field equations. The vacuum energy field hypothesis is rewarding in terms of several physical advantages:

- The ill-defined gravitational pseudo-tensor remains here a true tensor restoring the consistency in the field equations with a massive source;
- The inferred global energy-momentum tensor always satisfies the conservation law as well as the vacuum tensor alone;
- Because of the nature of this vacuum tensor there is no need to introducing any other arbitrary ingredients or modification of the general theory of relativity. Despite its smallness, a cosmological term seems to be badly needed to ascertain some major astrophysical observations which are all related to the FLRW expanding model of universe.

The Lambda-CDM model, which uses the FLRW metric, currently measures the cosmological constant to be on the order of 10^{-52} m^{-2} . However, there is no reason “à priori” to consider this term as a constant everywhere which would constitute a strong physical evidence for the vacuum field to exist in General Relativity.

Submitted on May 31, 2024

References

1. Marquet P. Lichnerowicz’ theory of spinors in General Relativity. The Zelmanov approach. *The Abraham Zelmanov Journal*, 2012, v. 5, 117–133.
2. Kramer D., Stephani H., Hertl E., MacCallum M. Exact Solutions of Einstein’s Field Equations. Cambridge University Press, 1979.
3. Marquet P. Twin universes: a new approach confirmed by General Relativity. *Progress in Physics*, 2019, v. 15, no. 2, 64–67.
4. Marquet P. Twin universes confirmed by General Relativity. *Progress in Physics*, 2022, v. 18, no.1, 89–94.
5. Landau L., Lifshitz E. The Classical Theory of Fields. Addison-Wesley, Reading, 1962.
6. Dirac P.A.M. General Theory of Relativity. Princeton University Press, 2nd edition, 1975.
7. Marquet P. The gravitational field: a new approach. *Progress in Physics*, 2013, v.9, no.3, 62–66.
8. Marquet P. Vacuum background field in General Relativity. *Progress in Physics*, 2016, v. 12, no. 4, 314–316.
9. Marquet P. Some Insights on the Nature of the Vacuum Background Field in General Relativity. *Progress in Physics*, 2016, v. 12, no. 4, 366–367.
10. Rosenfeld L. Sur le tenseur d’impulsion-énergie. *Acad. Roy. de Belgique (Mémoires de la Classe des Sciences)*, 1940, t. 18, 1–30.
11. Poher C. European Patent Publication WO 2007/093 699 A2, PCT FR 2007/000249 (February 14, 2006); <https://www.epo.org/searching-for-patents.html>
12. Poher C., Poher D. Physical phenomena observed during strong electric discharges into layered Y123 superconducting devices at 77K. *Applied Physics Research*, 2011, v. 3, no. 2, 51–66.
13. Poher C., Modanese G. Enhanced induction into distant coils by YBCO and silicon-graphite electrodes under large current pulses. *Physics Essays*, 2017, v. 30, no. 4, 435–441.
14. Poher C., Poher D. Gravity and matter quantum behavior from accelerations during electric discharges into graphite-based super conductor. *Applied Physics Research*, 2020, v. 12, no. 3, 48–79.
15. Poher C., Poher D. Quantum model of inertia-predictions-confirmations, consequences for gravitation into galaxies and CDM cosmology models. *Applied Physics Research*, 2020, v. 12, no. 4, 8–62.

Gödel Time Travel: New Highlights

Patrick Marquet

Calais, France. E-mail: patrick.marquet6@wanadoo.fr

The history of fascinating idea of time travel can be traced back to Kurt Gödel who found a solution of Einstein's field equations that contains closed time-like curves (CTCs). Those make it theoretically feasible to go on journey into one's own past. In what follows, we establish a realistic way to provide the required conditions to achieve this time displacement. After having given Gödel's model a physical meaning, we assign an object to move along a closed time-like curve using the warp drive technique. Provided the object bears circulating charges interacting with a surrounding electro-magnetic field, it is possible to extract a negative energy necessary to sustain the warp drive without resorting to the hypothetical "exotic matter". In addition, this field/charge interaction has the virtue to drastically reduce the amount of required negative energy. Lastly, the entropy of the system is shown to be negative during the time journey into the past.

Notations

Space-time indices are: $\mu, \nu = 0, 1, 2, 3$.

Spatial indices are: $a, b = 1, 2, 3$.

The space signature is -2 (unless otherwise specified).

Newton's constant is G .

1 The generalized Gödel metric

The classical Gödel line element is generically given by the interval [1]

$$ds^2 = a^2 \left(dx_0^2 - dx_1^2 + dx_2^2 \frac{1}{2} e^{2x_1} - dx_3^2 + 2 e^{x_1} dx_0 dx_2 \right), \quad (1)$$

or equivalently

$$ds^2 = a^2 \left[-dx_1^2 - dx_3^2 - dx_2^2 \frac{1}{2} e^{2x_1} + (e^{x_1} dx_2 + dx_0)^2 \right] \quad (2)$$

expliciting x_0

$$ds^2 = a^2 \left[c^2 dt^2 + \frac{1}{2} e^{2x} dy^2 - 2 e^x c dt dy - dx^2 - dz^2 \right], \quad (2bis)$$

where $a > 0$.

In the cylindrical coordinates (t, r, ϕ) with the transformations

$$e^x = \cosh 2r + \cosh \phi \sinh 2r,$$

$$ye^x = \sqrt{2} \sinh \phi \sinh 2r,$$

$$\tan \frac{1}{2} \left[\phi + \left(ct - \frac{2t'}{2\sqrt{2}} \right) \right] = e^{-2r} \tan \frac{\phi}{2},$$

the metric reads

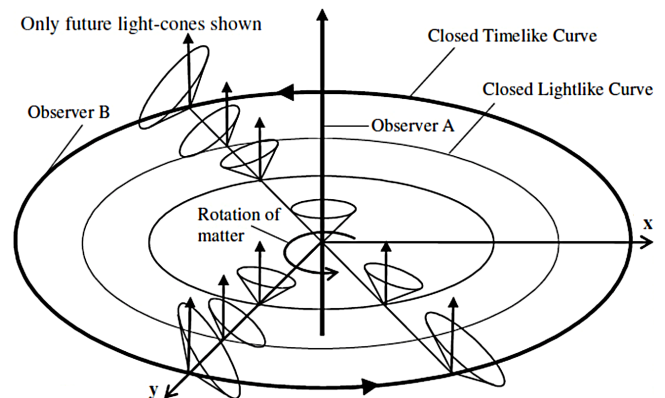
$$ds^2 = 4a^2 \left[(dt')^2 - dr^2 + (\sinh^4 r - \sinh^2 r) d\phi^2 + 2\sqrt{2} \sinh^2 r d\phi dt' \right] \quad (3)$$

(the inessential coordinate z is here suppressed).

In its original formulation, the Gödel universe describes a set of masses (such as galaxies, stars and planets) rotating about arbitrary axes.

The metric (3) exhibits a rotational symmetry about the axis $r = 0$ since we clearly see that the components of the metric tensor do not depend on ϕ .

For $r \geq 0$, we have $0 \leq \phi \leq 2\pi$. If a curve r_G is defined by $\sinh r = 1$ that is $r_G = \log(1 + \sqrt{2})$, then for any curve $r > r_G$ we have $\sinh^4 r - \sinh^2 r > 0$. Such a curve which materializes in the "plane" $t = \text{const}$ is a closed time-like curve (CTC). The radius r_G referred to as the Gödel radius, induces a light-like curve or closed null curve where the light cones are tangential to the plane of constant t . With increasing $r > r_G$, the light cones continue to keel over and their opening angles widen until their future parts reach the negative numerical values of t .



As a consequence a spacecraft can move in such way that its chronological order with the positive cosmic time is reversed.

In order to make his metric compatible solution to Einstein's field equations, Gödel is led to introduce the cosmo-

logical constant Λ as

$$G_{\mu\beta} = \frac{8\pi G}{c^4} \rho c^2 u_\mu u_\beta + \Lambda g_{\mu\beta}. \quad (4)$$

To achieve this compatibility he then further sets

$$a^{-2} = \frac{8\pi G}{c^2} \rho, \\ \Lambda = -\frac{1}{2} R = -\frac{1}{2a^2} = -\frac{4\pi G}{c^2} \rho.$$

Finetuning the hypothetical cosmological constant with the (mean) density of the universe and the Ricci scalar R , appears as a rather dubious physical argument.

In our publication [2], we assumed that a is slightly space-time variable and we set

$$a^2 = e^2. \quad (5)$$

As a result, the Gödel metric tensor components are conformal to the real Gödel metric tensor $g_{\mu\nu}$

$$(g_{\mu\nu})' = e^{2U} g_{\mu\nu}, \quad (g^{\mu\nu})' = e^{-2U} g^{\mu\nu}.$$

The exact Gödel metric reads now

$$ds^2 = e^{2U} \left[c^2 dt^2 + \frac{1}{2} e^{2x} dy^2 - 2e^x c dt dy - dx^2 - dz^2 \right] \quad (6)$$

or

$$ds^2 = 4e^{2U} \left[(dt')^2 - dr^2 + (\sinh^4 r - \sinh^2 r) d\phi^2 + 2\sqrt{2} \sinh^2 r d\phi dt' \right]. \quad (7)$$

This implies that this metric is a straightforward solution of the field equations describing a peculiar perfect fluid [3–5]

$$G_{\mu\beta} = \frac{8\pi G}{c^4} \left[(\rho c^2 + P) u_\mu u_\beta - P g_{\mu\beta} \right]. \quad (8)$$

The model is now likened to a fluid in rotation with mass density ρ and pressure P with an equation of state $\rho = f(P)$.

The positive scalar U is shown to be

$$U(x^\mu) = \int \frac{dP}{\rho c^2 + P}. \quad (9)$$

From (7) one formally infers that the flow lines of matter of the fluid follow conformal geodesics given by

$$s' = \int e^U ds. \quad (10)$$

The 4-vector $K_\nu = \partial_\nu U$ is regarded as the 4-acceleration of the flow lines [6]. The hallmark of the theory is the substitution (5). With this new definition, the Gödel space-time is no longer the representation of a cosmological model but it is

relegated to the rank of an ordinary metric where its physical properties could allow for a possible replication.

Rotation of the model and closed curves now depend on the fluid characteristics.

To this effect consider the metric

$$ds^2 = c^2 (dt'')^2 - \frac{(dr'')^2}{1 + (r''/2e^U)^2} - r'' \left[1 - (r''/2e^U)^2 \right] d\phi^2 + 2(r'')^2 \frac{c}{\sqrt{2}e^U} d\phi dt''. \quad (11)$$

As easily verified it is equivalent to the metric (7) if we set [7]

$$r'' = 2e^U \sinh r, \quad t'' = \frac{2e^U t'}{c}. \quad (12)$$

In this new representation, we see that when $r'' = 2e^U$, the coefficient in front of $d\phi^2$ vanishes. If we choose the cosmic time t'' describing the evolution of our universe as the rotation-axis, then $r''_G = 2e^U$ constitutes the Gödel radius for which the time lines close up and are tangential to the light cones (null curves). These curves are contained in the plane $t'' = \text{const.}$ in the same way as detailed above. Inspection shows that the fluid rotates with the angular velocity

$$\omega = \frac{c}{\sqrt{2}e^U}. \quad (13)$$

Through the equation of state $\rho = f(P)$, the Gödel radius will be set by tuning the pressure parameter P of the considered fluid.

Referring to the work initiated in [8], we complete hereinafter our last publication [9] in which a spacecraft moves along a Gödel trajectory by using a warp drive propulsion. The required negative energy will be now given a physical meaning.

2 A short review on Alcubierre's theory

2.1 The ADM formalism

Arnowitt, Deser and Misner (ADM) suggested to construct a space-time foliation of hypersurfaces parametrized by an arbitrarily chosen time coordinate value x^0 [10]. This foliation is characterised by a proper time $d\tau$ between two nearby hypersurfaces

$$x^0 = \text{const}, \quad \text{and} \quad x^0 + dx^0 = \text{const}, \quad (14)$$

where $cd\tau$ is proportionnal to dx^0

$$cd\tau = N(x^a, x^0) dx^0, \quad (15)$$

and in the ADM terminology, N is called the *lapse function*.

Let us evaluate the 3-vector whose spatial coordinates x^a are lying in the hypersurface $x^0 = \text{const}$, and the vector is normal to the hypersurface on the second hypersurface $x^0 + dx^0 = \text{const}$, where those coordinates become

$$N^a dx^0,$$

and the vector N^a is called the *shift vector*.

From these definitions follows the derivation of the 3-tensor

$$K_{ab} = (2N)^{-1} (-N_{a;b} - N_{b;a} + \partial_0 g_{ab}), \quad (16)$$

It represents the “extrinsic curvature”, and as such describes the manner in which the hypersurface $x^0 = \text{const}$ is embedded in the surrounding space-time.

With this brief preparation we are now able to tackle our topic.

2.2 Alcubierre’s function

In 1994, M. Alcubierre showed that a superluminal velocity can be achieved without violating the laws of Relativity. He considered a perturbed space-time region likened to bubble (“warp drive”) which could transport a spacecraft in a surfing mode inside the bubble, the proper time $d\tau$ is the coordinate time element dt measured by an external observer called “Eulerian”.

The motion is only achieved by the space wave, so that the occupants of the spacecraft are at rest and would not suffer any acceleration nor time dilation in the displacement [11]. This process requires a front contraction of the space while subject to a rear expansion. The spacecraft center distance located in the bubble

$$r_s(t) = \sqrt{(x - x_s(t))^2 + y^2 + z^2} \quad (17)$$

varies until R_e , which is the external radius of the bubble.

With respect to the distant observer the apparent velocity of the spacecraft is

$$v_s(t) = \frac{dx_s(t)}{dt}, \quad (18)$$

where $x_s(t)$ is the coordinate of the bubble’s trajectory along the x -direction.

Alcubierre then defined the step function $f(r_s, t)$

$$f(r_s, t) = \frac{\tanh[\sigma(r_s + R_e)] - \tanh[\sigma(r_s - R_e)]}{2 \tanh(\sigma R_e)}, \quad (19)$$

where $R_e > 0$ is the external radius of the bubble, and σ is a “bump” parameter used to tune the wall thickness of the bubble. The larger the parameter σ , the greater the contained energy density; for its shell thickness decreases. Moreover, the absolute increase of σ means a faster approach of the condition

$$\left. \begin{aligned} \lim_{\sigma \rightarrow \infty} f(r_s, t) &= 1 \quad \text{for } r_s \in [-R_e, R_e] \\ \text{and is 0 everywhere else} \end{aligned} \right\}. \quad (20)$$

The Alcubierre metric is

$$(ds^2)_{\text{AL}} = -c^2 dt^2 + [dx - v_s f(r_s, t) c dt]^2 + dy^2 + dz^2. \quad (21)$$

Inspection shows that

$$K_{ab} = -u_{a;b}, \quad (22)$$

which is sometimes called the second fundamental form of the 3-space.

Within this formalism, the expansion scalar becomes

$$\theta = \partial_1 N^1 = -\text{tr } K_{ab} \quad (23)$$

that with (20) is

$$\theta = v_s \frac{df}{dr_s} \frac{x_s}{r_s}. \quad (24)$$

Let us now write the Alcubierre metric in the following equivalent form

$$(ds^2)_{\text{AL}} = -\left[(1 - v_s^2 f^2(r_s, t)) c^2 dt^2 - 2 v_s f c dt dx + dx^2 + dy^2 + dz^2\right]. \quad (25)$$

Taking account of (20) one finally find the energy density

$$(T^{00})_{\text{AL}} = -\frac{c^4}{32\pi G} v_s^2 \left(\frac{df}{dr_s}\right)^2 \frac{y^2 + z^2}{r_s^2}. \quad (26)$$

This expression is unfortunately negative as measured by the Eulerian observer and therefore it violates the weak energy conditions (WEC) [12]. Notwithstanding this violation, one is nevertheless forced to introduce a way to obtain a negative energy density. This possibility is examined below.

2.3 Nature of the negative energy

We consider a spacecraft having a shell whose thickness is $R_e - R_i$, where R_e is the external radius, while R_i is the inner radius. R_e coincides with the Alcubierre bubble which thus constitutes the whole spacecraft contour.

Consider now a charge μ circulating within the shell thus giving rise of a 4-current density

$$j^\alpha = \mu u^\alpha. \quad (27)$$

This current is coupled to a co-moving electromagnetic field characterized with the 4-potential A^α which yields the interacting energy-momentum tensor

$$(T^{\alpha\beta})_{\text{elec}} = \frac{1}{4\pi} \left(\frac{1}{4} g^{\alpha\beta} F_{\gamma\delta} F^{\gamma\delta} + F^{\alpha\sigma} F_\sigma^\beta \right) + g^{\alpha\beta} j_\nu A^\nu - j^\alpha A^\beta. \quad (28)$$

The extracted energy density is

$$(T^{00})_{\text{elec}} = \frac{1}{4\pi} \left(\frac{1}{4} F_{\gamma\delta} F^{\gamma\delta} + F^{0\nu} F_\nu^0 \right) + j_\nu A^\nu - j^0 A^0. \quad (29)$$

Since we chose an orthonormal basis, we have

$$(T^{00})_{\text{elec}} = \frac{1}{8\pi} (\mathbf{E}^2 + \mathbf{B}^2) \frac{1}{4\pi} \Delta(\Phi \mathbf{E}), \quad (30)$$

where \mathbf{E} and \mathbf{B} are respectively the electric and magnetic field strengths derived from the Maxwell tensor

$$F_{\gamma\delta} = \partial_\gamma A_\delta - \partial_\delta A_\gamma. \quad (31)$$

We assume that the field potential $A^\alpha(\Phi, \mathbf{A})$ is given in the Lorentz gauge.

The charge density is derived from

$$\Delta E = 4\pi\mu, \quad (32)$$

which is just the time component of the 4-current density inferred from Maxwell's equations

$$\nabla_\alpha F^{\alpha\beta} = \frac{4\pi}{c} j^\beta. \quad (33)$$

Therefore negative energy density may be shown explicitly by the interaction tensor

$$(T^{00})_{\text{electint}} = \frac{1}{4\pi} \mathbf{E} \Delta \Phi + \mu \Phi, \quad (34)$$

$$(T^{00})_{\text{elecint}} = \frac{1}{4\pi} \left(-\Delta \Phi - \frac{1}{c} \partial_t \mathbf{A} \right) \Delta \Phi + \mu \Phi \quad (35)$$

since $\mathbf{E} = -\Delta \Phi - \frac{1}{c} \partial_t \mathbf{A}$.

In (35) the first term in the brackets is always negative. As to the last term, it is made negative when the time varying charge density μ and the scalar potential Φ are 180° out of phase (method reached by the use of phasors).

We now suppose that the positive free radiative energy density

$$(T^{00})_{\text{elecra}} = \frac{1}{8\pi} (\mathbf{E}^2 + \mathbf{B}^2)$$

is confined within the spacecraft, i.e., right to the inner side of the shell wall. The interacting tensor $(T^{00})_{\text{elecint}}$ is set so as to exhibit its energy density part on the *external side* of the shell. This is made consistent since the charges are circulating *inside* the surrounding shell of the spacecraft.

So we see that negative energy production can be achieved with such a configuration. The higher the charge density and the higher the scalar potential, then the most effective negative energy density.

The local field equations read

$$G_{\mu\beta} = \frac{8\pi G}{c^4} [(\rho c^2 + P)u_\mu u_\beta - P g_{\mu\beta} + (T_{\mu\beta})_{\text{elec}}]. \quad (36)$$

Remains now the energy density level $(T^{00})_{\text{elecint}}$ which is anticipated to be very huge. There is however a possible drastic reduction which adequately exploits the contribution of the electromagnetic field interacting with the charges.

2.4 Reducing the required negative energy

The spacecraft bubble is externally charged surrounded by a comoving electromagnetic field. As such it follows a *finslerian geodesic* [13] provided the ratio $\frac{\mu}{\rho}$ remains constant along the trajectory

$$(ds)_{\text{shell}} = ds + \frac{\mu}{\rho} A_\alpha dx^\alpha, \quad ds = \sqrt{\eta_{\alpha\beta} dx^\alpha dx^\beta}. \quad (37)$$

Neglecting the non-quadratic terms the metric reads

$$(ds^2)_{\text{shell}} = ds^2 + \left(\frac{\mu}{\rho} A_\alpha dx^\alpha \right)^2. \quad (38)$$

The interacting charge of the spacecraft must now be included in the metric (25).

Because we are considering only the energy density of the spacecraft-bubble as a whole, the spatial components of $\frac{\mu}{\rho} A_\alpha dx^\alpha$ in (38) can be neglected and the interaction term reduces to its time component

$$\frac{\mu}{\rho} A_0 dx^0 = \frac{\Phi\mu}{\rho} c dt. \quad (39)$$

The metric (37) becomes now

$$ds^2 = - \left(1 + \frac{\Phi\mu}{\rho} \right)^2 c^2 dt^2 + dz^2 + dx^2 + dy^2. \quad (40)$$

Notice that the time component of the metric tensor

$$g_{00} = - \left(1 + \frac{\Phi\mu}{\rho} \right)^2 \quad (41)$$

can be expressed by the following formula

$$M = - (1 + N), \quad (42)$$

where the lapse function is defined as

$$N = \Phi \frac{\mu}{\rho}. \quad (43)$$

The Alcubierre metric (25) reads now

$$ds^2 = - [M^2 - v_s^2 f^2(r_s)] c^2 dt^2 - 2v_s f(r_s) c dt dx + dz^2 + dx^2 + dy^2. \quad (44)$$

The interaction term should be only function of r_s , R_e , σ , and of the thickness $(R_e - R_i)$, but not depending on the velocity v_s .

Here, our analysis is not too dissimilar to the approach detailed in [14, 15].

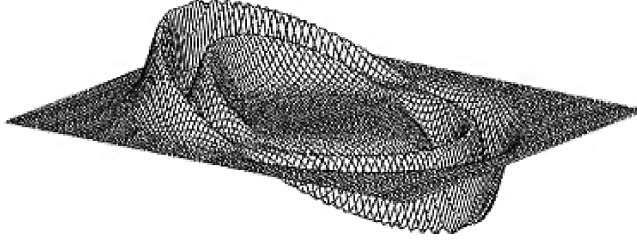
Finally, the negative energy density requirement is

$$\frac{c^4}{8G} v_s^2 \left(\frac{df}{dr_s} \right)^2 \frac{y^2 + z^2}{r_s^2} = \left(\Delta \Phi + \frac{1}{c} \partial_t \mathbf{A} \right) \Delta \Phi + \mu \Phi. \quad (45)$$

The splitting shell/inner part of the spacecraft frame, is really the hallmark of the theory here it implies that the proper time τ of the inner part of the spacecraft is not affected by the term N .

The spacecraft-bubble follows the trajectory $x_s(t)$. Therefore For $R \leq R_e$, the bubble is assumed to be ruled by the new Alcubierre metric (44) expressed with the signature -2

$$ds^2 = (M^2 - v_s^2 f^2) c^2 dt^2 - 2v_s f(r_s) c dt dx - dz^2 - dx^2 - dy^2. \quad (46)$$



A 2D representation of the warped region according to (44). Propagation is from left (expansion) to right (contraction). The groove corresponds to the shell thickness determined by the function N .

This space-time is thus regarded as *globally hyperbolic* and the bubble will never know whether it moves along a CTC. As a result, the bubble is seen by a specific observer (see below) as being transported forward along the x -direction *tangential* to a CTC beyond the Gödel radius r_G .

We may now write down the *Gödel-Alcubierre metric*

$$ds^2 = e^{2U(1-f)} \left\{ \left[\left(1 + \frac{\Phi\mu}{\rho} \right)^2 - v_s^2 f^2 \right] c^2 dt^2 - \left[f - \frac{1}{2} (1-f) e^{2x} \right] dy^2 - 2[v_s f + (1-f) e^x] c dt dy - dx^2 - dz^2 \right\}. \quad (47)$$

In the absence of charge, beyond the distance R_e , we have $R > R_e \rightarrow \infty$ and $f = 0$ outside of the spacecraft-bubble and we retrieve Gödel's original modified metric (6).

3 Entropy along a Gödel trajectory

3.1 Relativistic thermodynamics

Consider a fluid that consists of n particles in motion within a given region. The primary variables are:

— The particle current

$$I^\mu = n u^\mu; \quad (48)$$

— The energy-momentum $T^{\mu\nu}$;

— The entropy flux S^μ ,

where, obviously, $T^{\mu\nu}$ and I^μ are conserved

$$T_{;\nu}^{\mu\nu} = 0 \quad I_{;\mu}^\mu = 0.$$

In a relativistic situation, the second law of thermodynamics requires

$$S_{;\mu}^\mu \geq 0. \quad (49)$$

For equilibrium states we have

$$S^\mu = n s u^\mu, \quad (50)$$

where s is the entropy per particle.

Denoting Q as the chemical potential and T the heat quantity (temperature) of the medium, the Euler relation reads

$$n s = \frac{\rho + P}{T} - \frac{Q n}{T}, \quad (51)$$

where ρ and P are respectively the density and pressure of the medium. We also have the Gibbs fundamental thermodynamic equation

$$T ds = ds \left(\frac{\rho}{n} \right) + P d \left(\frac{1}{n} \right) \quad (52)$$

or

$$T n ds = d\rho - \frac{\rho + P}{n} + dn. \quad (53)$$

From (51), we get

$$S^\mu = - \frac{Q I^\mu}{T} + \frac{(\rho + P) u^\mu}{T}. \quad (54)$$

Since in the rest system, the matter energy flux must vanish, we have

$$u_\lambda T^{\lambda\mu} = \rho u^\mu \quad (55)$$

and thus, we find the following expression for the entropy vector in equilibrium

$$S^\mu = - \frac{Q I^\mu}{T} + \frac{u_\lambda T^{\lambda\mu}}{T} + \frac{P u^\mu}{T}. \quad (56)$$

3.2 Applying to the time travel trajectory

Let us consider a spacecraft moving along a Gödel trajectory. We obviously neglect the chemical potential of the spacecraft's bodyframe as well as the pressure and the entropy vector reduces to

$$S^\mu = \frac{u_\lambda T^{\lambda\mu}}{T}. \quad (57)$$

This vector must be measured by the Eulerian observer which travels along the trajectory tangential to u^μ , where he "sees"

$$\frac{dt}{d\tau} = M^{-1}. \quad (58)$$

With this definition, it is easy to show that its velocity components are

$$(u^\mu)_E = [cM^{-1}, v_s f cM^{-1}, 0, 0] \quad (59)$$

$$(u_\mu)_E = [cM, 0, 0, 0]. \quad (59\text{bis})$$

We are interested in the entropy scalar part

$$(S^0)_E = \frac{(u_0)_E (T^{00})_{AL}}{T} \quad (60)$$

with

$$(T^{00})_{AL} = - \frac{c^4}{32\pi G} \frac{v_s^2 (y^2 + z^2)}{M^4 r_s^2} \left(\frac{df}{dr_s} \right)^2, \quad (61)$$

$$(u_0)_E = cM. \quad (62)$$

We clearly see that the entropy $(S^0)_E$ of the system is negative. Hence, the entropy S^0 attached to the spacecraft is seen negative with respect to the Eulerian observer which thus measures a “negentropy”. While travelling to the past, the occupants of the spacecraft experience a positive entropy, i.e., they are ageing in their own proper time.

Conclusions

In the novel “The time machine” (1895) by H. G. Wells, an english scientist constructs a machine which allows him to travel back and forth in time.

Closed time-like curves were discovered in the 1920’s, but it is really in 1988 that time travel possibility was seriously considered by physicists in the stunning article [16]. The Gödel solution was mainly regarded as a mathematical curiosity and thus it was almost forgotten. We have succeeded in reviving his work by using some transformations which give Gödel’s mathematical derivation a full physical significance. In this view, the major contribution of J. Natário’s work [17, 18] introduces now a complementary perspective.

So far, Gödel’s model only depicts a travel into the past. What about the journey home? If advanced civilizations harness the time travel technology, they must be able to return to their own present, meaning a reversed time orientation. In the light of the aforementioned derivations we conclude that they should take another path. A possibility arises by considering our recent publication [19]. In this article, we recalled that the current Einstein’s field equations are inferred from the second Bianchi’s identity which is verified by the Riemann tensor. The latter tensor can be particularized to the *Landau-Lifchitz superpotential* [20], which is shown to yield two opposite field equations (not necessarily symmetrical) coupled with a common index.

Identifying the time coordinate chosen as the cosmic time-axis, to this common index, the solution of the second field equation would then display a reversed time orientation. In this case an advanced civilization could adequately exploit this circumstance to return to its epoch.

Much remains to be worked out on the subject, but we trust that Gödel’s legacy will continue to stimulate my fundamental researches in this field.

Submitted on May 31, 2024

References

1. Gödel K. An example of a new type of cosmological solutions of Einstein’s field equations of gravitation. *Review of Modern Physics*, 1949, v. 21, no. 3, 447–450.
2. Marquet P. The exact Gödel solution. *Progress in Physics*, 2021, v. 17, no. 2, 133–138.
3. Eisenhart L.P. Space-time continua of perfect fluids in General Relativity. *Trans. Amer. Math. Soc.*, 1924, v. 26, 205–220.
4. Synge J.L. Relativistic hydrodynamics. *Proc. Lond. Math. Soc.*, 1937, v. 43, 376–416.
5. Lichnerowicz A. Les Théories Relativistes de la Gravitation et de l’Electromagnétisme. Masson et Cie, Paris, 1955.
6. Hawking S.W., Ellis G.F.R. The Large Scale Structure of Space time. Cambridge University Press, 1987.
7. Kajari E., Walser R., Schleich P., Delgado A. Sagnac effect of Gödel’s universe. arXiv: 0404032 (2004).
8. Tippet B.J., Tsang D. Traversable achronal retrograde domain in space-time. arXiv: 1310.7985 (2013).
9. Marquet P. Gödel time travel with warp drive propulsion. *Progress in Physics*, 2022, v. 18, no.1, 82–88.
10. Arnowitt R., Deser S., Misner C. Dynamical structure and definition of energy in General Relativity. *Physical Review*, 1959, v. 116, no. 5, 1322–1330.
11. Alcubierre M. The warp drive: hyper fast travel within General Relativity. *Classical and Quantum Gravity*, 1994, v. 11, L73–L77.
12. Marquet P. The generalized warp drive concept in the EGR theory. *The Abraham Zelmanov Journal*, 2009, v. 2, 261–287.
13. Marquet P. Geodesics and Finslerian equations in the EGR theory. *The Abraham Zelmanov Journal*, 2010, v. 3, 90–100.
14. Loup F., Waite D., Held R., Halerewicz E.Jr., Stabno M., Kuntzman M., Sims R. A causally connected superluminal Warp Drive spacetime. arXiv: 020.2021 (2002).
15. Loup F., Waite D., Halerewicz E.Jr. Reduced total energy requirements for a modified Alcubierre warp drive spacetime. arXiv: 010.70975 (2001).
16. Morris M.S., Thorne K.S., Yurtsever U. Wormholes, time machine and the weak energy condition. *Phys. Rev. Let.*, 1988, v. 61, no. 13, 1446–1449.
17. Natário J. Optimal time travel in the Gödel universe. arXiv: 1105.619 (2011).
18. Natario J. Warp Drive with zero expansion. arXiv: 01.10086 (2002).
19. Marquet P. Twin universes confirmed by General Relativity. *Progress in Physics*, 2022, v. 18, no. 1, 89–94.
20. Landau L., Lifshitz E. The Classical Theory of Fields. Addison-Wesley, Reading, 1962.

Inference of Plausible Spatial Sizes of GRB Systems Using Newly Proposed FDSL-Model for GRB Time Delays

Godson Fortune Abbey¹, Joseph Simfukwe¹, Prosperity Christopher Simpemba¹, Saul Paul Phiri¹, Alok Srivastava¹
and Golden Gadzirayi Nyambuya^{1,2}

¹Copperbelt University, School of Mathematics and Natural Sciences, Department of Physics, P. O. Box 21692, Jambo Drive Riverside, Kitwe, Republic of Zambia. E-mail: godsonabbey88@gmail.com, josephsimfukwe2013@gmail.com

²National University of Science & Technology, Faculty of Applied Sciences, Department of Applied Physics, P. O. Box AC 939, Ascot, Bulawayo, Republic of Zimbabwe. E-mail: physicist.ggn@gmail.com

We have used regression analysis to establish a time correction mechanism for four GRBs (030329, 980425, 000418, and 021004) employed from literature on the basis of a frequency-dependent speed of light (FDSL) model which we developed entirely from Maxwell's electromagnetic equations in conjunction with plasma and dispersion effects. In our first instalment (Paper 1), on the assumption that these GRBs all leave the source at the same time we obtained good positive correlations and hence justified the reliability of our fitting model. In this paper, however, on the assumption that each photon leaves the GRB source at different times, we modify the previous model to obtain a more fitting model. Furthermore, the modification led to the unification of the four GRBs into a homogenous albeit perfect correlation leading to the determination of the frequency equivalent of the ISM ($\nu_* = 1.507 \pm 0.0009$ Hz) and hence, the spatial sizes (ΔD) of the internal and external shocks wherein we obtain for the four GRBs $\Delta D = 838.90, 39.00, 7804.00$ and 19188.00 for GRBs 030329, 980425, 000418, and 021004 respectively. If the results provided herein are deemed acceptable or reasonable — *one can on this basis* — say that the relationship we have established from our analysis for the four GRBs supports two GRB models, “the framework of the fireball model” and “the multiple shock wave model” of GRBs production and their afterglow. Additionally, the implications are evident in the variations of relativistic outflows within the jets offering valuable insights into the acceleration mechanisms and interactions between the jet and its surrounding medium.

1 Introduction

One of the most puzzling phenomena in modern astrophysics is perhaps γ -ray bursts (GRBs). These brief flashes of non-thermal γ -ray energy which occur about once a day have consistently defied the *laws of physics* in their explanation. GRBs are highly concentrated high-energy explosions from distant objects deep within space. These explosions create a relativistic blastwave which inevitably collides with the circumburst medium resulting in internal and external shocks [1]. The photons emanating from these shocks possess enormous energies typically on the order of 10^{42} – 10^{47} J [2, 3], and arrive at Earth as cosmic snipers that are uniformly distributed on the sky [4]. Due to these extreme energies, the prompt emission observed in these GRBs before now was believed to have been generated by a relativistic jet from their central engine [5–7]. Similarly, an afterglow is likely produced by external shocks from the interaction between the jet material and the circumburst medium [3].

Despite decades of research, the precise mechanisms driving GRBs and the characteristics of their progenitors remain a subject of intense investigation. One crucial aspect of understanding GRBs lies in estimating the spatial size of the shock waves they generate, as it provides invaluable insights

into their physics and progenitor environments. Recent advancements in time-delay models, e.g. [8–11], have offered a promising avenue to infer the spatial scales of GRBs phenomena. These delays, resulting from the differential arrival times of photons emitted from different parts of the shock region encode valuable information about the size and structure of the emitting source. By exploiting the temporal behaviour of GRB emissions across different frequencies and utilizing theoretical models of light propagation and interaction with the surrounding medium, we can be able to constrain the spatial dimensions of GRB shockwaves.

However, such methods face limitations in resolving the intrinsic size of the shock region, often convoluted by the surrounding environment and instrumental effects. An alternative approach gaining traction involves exploiting the time delay phenomena observed in photons of different frequencies from GRB shocks as they propagate via the Interstellar Medium (ISM). This paper aims to provide an independent method formulated from relativistic mechanics in estimating the spatial size of GRB shocks using one of such time-delay models [8]. We will explore the theoretical foundations underpinning this model, the observational data utilized [12], and the constraints derived from such analyses. Additionally, we will discuss the implications of these spatial estimates on

our understanding of GRB physics, progenitor systems, and their broader astrophysical implications. In the end, we aim to provide insights into the spatial characteristics of GRB shocks and their implications for understanding the physics of these extraordinary cosmic events.

Penultimately, we shall give a synopsis of the remainder of the present article. To begin, in §2 we take a critical look at the GRB time delay shock models to understand the role these shocks play in the generation of photons of different frequencies as they travel through the ISM. §3 gives a brief overview of the fireball model with special emphasis on how the internal and external shock mechanism gives strong support for our ideas on the non-simultaneous release of the photon pairs. §4 discusses our proposed FSDL time delay model and how it all fits into our current instalment. In §5, we give a *step-by-step* process of the current time rectification methodology we adopted, the fitting procedure used to obtain ν_* and the constraints imposed on our parameters. §6, §7 and §8, present our results, the justification of our rectification mechanism and the general discussion accompanying our results. Thereafter, we conclude with §9.

Lastly, we perhaps must hasten and say that, throughout this paper, we assume a flat *Standard Λ CDM-Cosmology Model* where we take [13]: $H_0 = 67.40 \pm 0.50 \text{ km} \times \text{s}^{-1} \times \text{Mpc}^{-1}$, $\Omega_\Lambda = 0.685 \pm 0.007$, and $\Omega_m = 0.315$ and that, for all our calculations of the luminosity distances (D_L) to the different GRBs and their host galaxies, we shall use Wright's [14] online cosmology calculator.*

2 GRB Time Delay Models

Several studies provide valuable insights into the time delay mechanism of GRB shocks. e.g. [15] introduced an improved model-independent method based on time-delay measurements of GRBs at different energy bands. This method allows for probing the energy-dependent velocity due to modified dispersion relations for photons. Additionally, [16] discussed estimating the number of emitting electrons in GRBs based on fitted parameters and assuming specific emission radii predicted by shock models within the outflow. Moreover, [17] demonstrated how delayed and long-lasting afterglow emissions in certain GRBs could be interpreted through a synchrotron forward-shock model. This interpretation was supported by the analysis of radio, optical, and X-ray light curves. Many other authors have also studied time delay models in probing GRB to mention but a few [18]

This paper aims to provide an independent method formulated from relativistic mechanics in estimating the spatial size of GRB shocks using one of such time-delay models [8]. We will explore the theoretical foundations underpinning this model, the observational data utilized [12], and the constraints derived from such analyses. Additionally, we will discuss the implications of these spatial estimates on our

understanding of GRB physics, progenitor systems, and their broader astrophysical implications. In the end, we aim to provide insights into the spatial characteristics of GRB shocks and their implications for understanding the physics of these extraordinary cosmic events. To begin, we will first take a critical look at the GRB fireball model with specific reference to the internal and external shock models to understand the role these shocks play in the generation of photons of different frequencies as they travel through the ISM.

3 Fireball Model

As is well known, a highly effective framework for interpreting observations of GRBs has been made available in the form of the fireball model [19–22]. The fireball model is commonly employed to explain the mechanism that produces the radiation we detect from most GRBs. The most widely accepted, and almost certain explanation for GRB production according to the fireball model is that when there is an ejection of extremely high energetic jets due to the merger of two neutron stars (NS-NS) [23], or a neutron star and a black hole (NS-BH) [4, 23] and a supernova [24] explosion as depicted in Fig. 1, the enormous release of energy gives rise to a Poynting-flux-dominated Magneto-hydrodynamics (MHD) wind with a luminosity of approximately $10^{50} \text{ erg} \times \text{s}^{-1}$ [25] within the ISM confined to the jet cone. These MHD winds generate the GRBs when the kinetic energy of these ultra-relativistic particles, or potentially the electromagnetic energy of the Poynting flux, is converted to radiation [21, 26].

The GRB fireball model is essential for understanding the nature and implications of GRB shocks. In a bid to demystify the radiation mechanism, [27, 28] compared the fireball-shock and millisecond-magnetar models by fitting them to X-ray data of specific GRBs, emphasizing the importance of different shock models in explaining GRB phenomena. Similarly, [29] used a “boosted fireball” model to replicate the hydrodynamics of GRB outflows, highlighting the necessity for comprehensive models to decode the complexities of GRBs. In the same light, [30] provides a comprehensive review of γ -ray bursts and related transients, discussing theoretical models for prompt and afterglow emissions, including the standard fireball model with internal and external shocks. Their study highlights the role of synchrotron radiation from relativistic electrons accelerated in the shocks, emphasizing the importance of magnetic fields in these processes, and the internal and external shock mechanisms for γ -ray burst emission.

Additionally, [31] discussed utilizing GRB emissions as a test-bed for modified gravity theories, demonstrating how GRBs can offer insights into fundamental physics beyond standard models [32–35] and many more have also explored how gravitational wave observations can enhance our understanding of the intrinsic properties of the shock waves from GRBs, showcasing the interdisciplinary nature of studying

*<https://www.astro.ucla.edu/~wright/CosmoCalc.html>

these phenomena. To describe both the initial burst of γ -rays and the lengthy afterglow, the fireball model employs two separate shock wave models — namely, the *internal and external shock wave models* [36, 37].

3.1 Internal Shock

As depicted in Fig. 1, internal shocks are responsible for the high energy of γ -ray particles. Moments after the incident, shock waves (fronts) with a Lorentz factor (Γ) close to 100 are emitted from the inner engine at relativistic speeds leading to multiple shock waves, each travelling at a different relativistic speeds. These shock fronts result in energetic γ -ray emissions which are principally caused by thermal magnetic reconnection activities and relativistic processes. In this process, baryonic mass will be added to the emission, thus helping to convert some radiation energy into relativistic kinetic energy, which in turn increases the γ -ray burst flux. As illustrated in Fig. 1, a significant portion of the initial energy released by the freshly generated BH is transformed straight into photons in a pure radiation fireball [37, 38].

3.2 External Shock

On the other hand, external shocks are predominantly thermal emissions produced as the energy transferred from the shock waves is deposited into the interstellar medium (ISM). The spilt substance can then be trapped in the shock front and release radiation as the shock travels in the outward direction. The resulting broadband synchrotron radiation evolves as the external shock propagates outward into the surrounding medium, depending on various fundamental characteristics of the explosion, the specifics of the shock evolution, and the density profile of the medium into which it expands [26, 40]. When shocks from this external surrounding circumburst matter delay this flow of electrons, the afterglow appears with varying frequencies ranging from X-ray to optical wavelengths. It is generally assumed that most of the GRBs we detect are triggered by internal shocks, while the slow afterglow emanates from the external shocks [41].

It is on this theoretical explanation of this fireball model that we anchor our modified time delay emission model, wherein we now have the radio photon pairs not simultaneously leaving the GRB event as has been assumed in our previous papers [8]. We aim to show that under the above-stated new assumption of non-simultaneous emission of the radio photon pair, the time delay experienced by these photons may very well be a result of the series of shock waves generated by the internal and external production mechanism as is assumed in the fireball model. This may also lead us to understand the shock dynamics and/or the spatial sizes of the shocks.

4 Our Proposed FSDL Model

Here, we adopt a standard fireball scenario for the GRBs afterglow, where a relativistic shock with (Γ) expands into the

circumburst medium (CBM). The afterglow flux arises from the radiation (synchrotron and possibly also inverse Compton) emitted by relativistic electrons accelerated from the internal to the external shocks. To describe the spatial size of these jets, we account for the effects of the conductance of the medium through which these radiations pass en route to the detector and model the shock dynamics using our FDSL-model.

The formulation we came up with was simple and elaborate which is: In [8], without any exogenous or exotic ideas being brought in, the following dispersion relation was derived directly from Maxwell's four fundamental equations of Electrodynamics

$$\omega^2 - c_0^2 k^2 = -4\omega_*\omega, \quad (1)$$

where $\omega_* = 2\pi\nu_* = \mu c^2 \sigma / 4$, $\omega = 2\pi\nu$, with ν being the frequency of the Photon and k its wave-number. Given that the group velocity v_g of a wave is given by $v_g = \partial\omega/\partial k$, thus differentiating Eq. (1) throughout with respect to k and rearranging, it follows that

$$v_g = \frac{c_0^2}{\omega/k} \frac{1}{2\omega_*/\omega} = \frac{c_0^2}{v_p} \frac{1}{1 + 2\omega_*/\omega} = \frac{c_0^2}{v_p} \frac{1}{1 + 2v_*/v}, \quad (2)$$

where $v_p = \omega/k$, is the phase velocity. In a vacuum, we have that $v_g = v_p = c_0$. This assumption (of $v_g = v_p$) was extended to the scenario of a non-vacuum medium and so doing (i.e., maintaining this condition $v_g \neq v_p$, in the non-vacuum medium), one obtains

$$\frac{v_g}{c_0} = \frac{1}{\sqrt{1 + \frac{2v_*}{v}}}. \quad (3)$$

From Eq. (3), it follows that if D is the distance between the Earth and the GRB, and v_l and v_h are the group velocities for the lower and higher frequency Photons, then - to first order approximation we have that $c_0/v_g \simeq 1 + v_*/v$, which in turns implies that for two photons with varying velocities, the time delay Δt is such that

$$\Delta t = \frac{D}{v_l} - \frac{D}{v_h} = \frac{Dv_*}{c} \left(\frac{1}{v_l} - \frac{1}{v_h} \right). \quad (4)$$

It is clear that if the laid down theory has any correspondence with physical and natural reality, then, a plot of $\Delta t \propto (v_l^{-1} - v_h^{-1})$ for the same source (i.e., same D) should accordingly yield a straight-line graph with a slope equal to Dv_*/c_0 . Eq. (4) implies that the time delay will be given by

$$\Delta t = \frac{Dv_*}{C} \left(\frac{1}{v_l} - \frac{1}{v_h} \right). \quad (5)$$

The relation in Eq. (5) was applied to the following GRBs GRB 030329, GRB 980425, GRB 000418 and GRB 021004

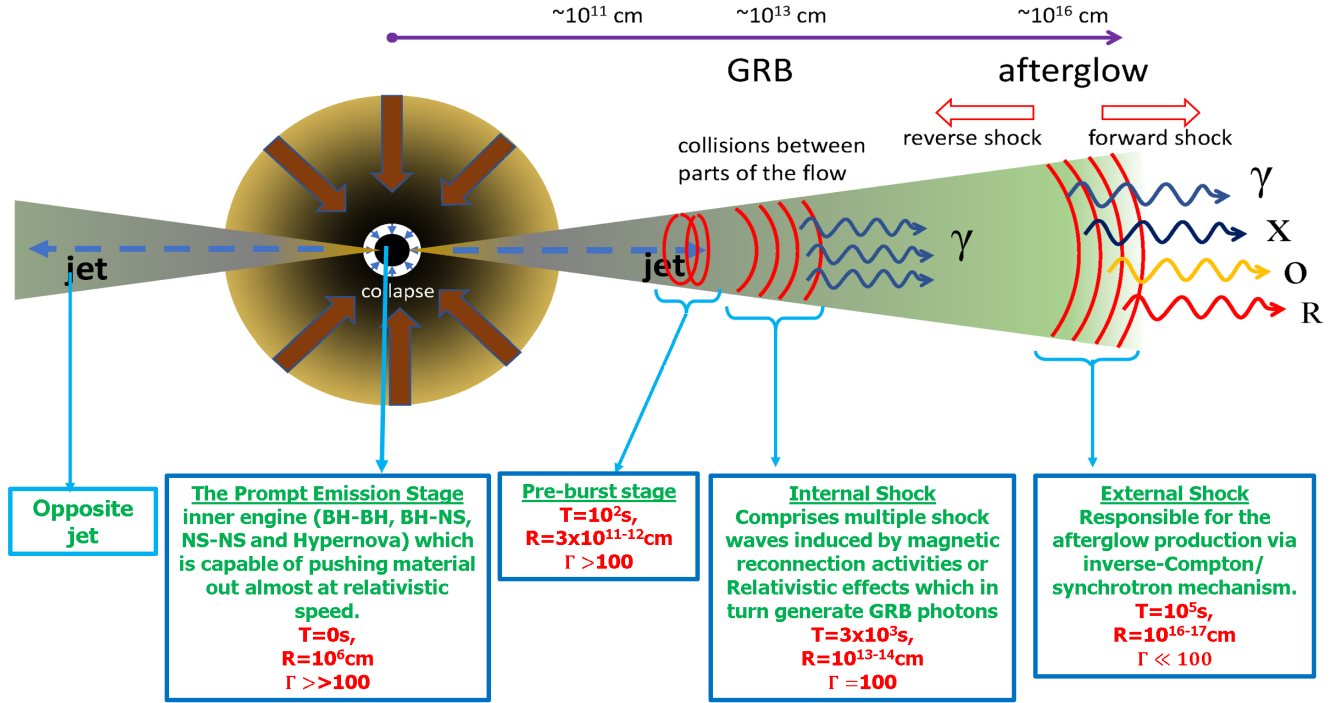


Fig. 1: A Modified cartoon depiction showing schematics description of and the basic mechanism of the GRB fireball model [39], <https://www.swift.ac.uk/about/grb.php>.

obtained from [12] and the result was a strong linear correlation between Δt and Δv^{-1} .

The obtained linear correlation confirms the theory on which Eq. (5) has been derived. Furthermore, in [8], as a major step, Eq. (5) assumes that the pair of GRB photons leave the event simultaneously. The above-stated assumption leads to a biased fit wherein the intercept of the graph of Δt vs Δv^{-1} was made to pass through the point of origin (0, 0) for there to be a zero y-intercept (see Fig. 2). Despite them giving a good correlation, the four graphs also yield slopes which were used to estimate the conductance of the ISM through which these GRB travel (see [8]).

In this current instalment, we develop a model that does not assume a simultaneous release of these pairs of photons. Rather preemptively, we must say that — this new assumption of a non-simultaneous — *albeit systematic* — emission of these photon pairs allows us to obtain a much more convincing and stronger correlation in the time delay. That is to say, this new correlation allows us to build a unified model of the four GRBs in our present sample wherein, we obtain two major results, mainly

1. A constant v_* called the frequency equivalence of the interstellar medium (ISM)'s conductance which allows us to estimate every other parameter involved with the four GRBs in question;
2. The spatial sizes of the internal and external shocks of our four GRB samples.

One significant step involved in our modified FSDL model is the estimation of the time correction parameter t_c . In this modified model, we believe that a pair of events coming from the same shock front will lie on the same slope on a Δt vs Δv^{-1} graph. In the case of our four GRB samples, the GRBs will be delayed by a fraction of the difference between the spatial sizes obtained from our calculation. Furthermore, in line with this assumption, the earlier photon leaves now while the latter leaves a time, t later. We can show that under the above-stated assumption, Eq. (5) will be modified to be

$$\Delta t = \frac{Dv_*}{c_0} \left(\frac{1}{v_l} - \frac{1}{v_h} \right) + t_c, \quad (6)$$

where t_c is a two-fold correction factor we introduced to rectify the time delay in the photon arrival times. Additionally, t_c is the y-intercept of this unbiased* linear regression model. This t_c will turn out to be the time difference between the emission of the photon pair from the internal and external shocks. This time difference is depicted in Figures 5 to 8 as the internal and external shock. We will briefly present our justification for our Non-simultaneous emission model.

4.1 Data Sampling and Description

As pointed out in Paper 1 [8], our data sample is wholly drawn from [12], wherein [12] draw their data from 304 GRB sam-

*By "unbiased plot", we mean a plot that does not force the linear graph to pass through the (0, 0)-point of origin as has been done on Paper 1.

ples compelled from 1997 to 2011 by [42]. From [12], eight of these GRB samples were used by [8] to investigate correlations in γ -ray burst time delays between pairs of radio photons as Paper 1 of a series of research geared towards investigating the cause of time delay in the arrival time of photons of different frequencies emanating from γ -ray burst.

In the said Paper 1 [8], in ascending order, the eight distinct GRBs we selected were 980425, 991208 000418, 000926, 021004, 030329, 031203 and 060218 making a total sample size of 52. Amongst these eight GRB samples, four of them GRB 980425, 000418, 021004 and 030329 when applied to our FDSL model gave good positive linear correlations as expected, which in turn provides a sound basis for our work and reliability of our model. The remaining four samples GRB 991208, 000926, 031203 and 060218 showed a weak correlation, so we didn't include them in our first instalment. In this present instalment, our aim was to put up a working model first with the 4 GRBs that gave a good positive correlation. To avoid constraints, we will differ the remaining weak correlated GRB samples to a later instalment where we can systematically test our model on all the data set in [12]. Additionally, we can now apply this model to recent data.

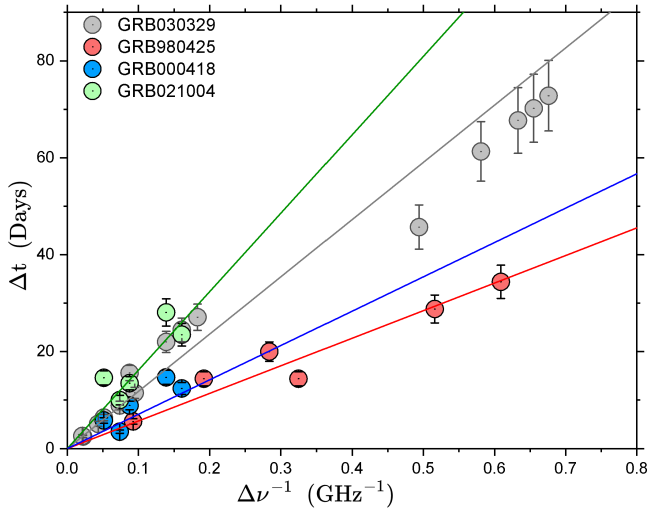


Fig. 2: Graph for Events GRB 030329, 980425, 000418, and 021004. The BLF were made to all passes through the origin.

5 Non-Simultaneous Photon Emission Model

Here we present a brief overview of our modified model as stated in the introductory section — the assumption that the low (ν_l) and high (ν_h) frequency photons are released simultaneously is to be done away with because it is very much possible that the low (or perhaps the high) frequency photon is released first, with the high (low) frequency photon is released a time t_c later (or *vice-versa*). In this event, the photon travel times t_l and t_h of the low and high frequency photons,

respectively — will be related as follows

$$t_l = \frac{D}{v_l} + t_c, \quad (7a)$$

$$t_h = \frac{D}{v_h}, \quad (7b)$$

where, likewise v_l and v_h are the speed of the low and high-frequency photons, respectively. From the foregoing, it follows from Eq. (7), that

$$\Delta t = t_l - t_h = \frac{D}{v_l} - \frac{D}{v_h} + t_c. \quad (8)$$

As given in [8], if we are to substitute into Eq. (8), the following

$$\frac{1}{v_l} = \frac{1}{c_0} \left(1 + \frac{\nu_*}{\nu_l} \right), \quad (9a)$$

$$\frac{1}{v_h} = \frac{1}{c_0} \left(1 + \frac{\nu_*}{\nu_h} \right), \quad (9b)$$

then, one will be led to Eq. (5). In this way — as promised, we have justified Eq. (6).

It is important to note that if t_c is a random variable — *the meaning of which is that this time is not the same for each photon pair* — it would give rise to a clearly visible scatter in the data points along some imagined average straight line. If t_c is uniform for all the data points — imply some welcome define and systematic origin, then, the resulting data points — *if plotted in an unbiased manner* — they would lie on a straight line that does not pass through the (0, 0)-point of origin as is the case with the data point of the GRBs in our sample. In the next subsection, we will briefly describe how we obtained the ν_* from our t_c .

5.1 Fitting Procedures

As promised above, we here describe, in §5.1.1 & 5.1.1, the fitting procedures employed to arrive at a value for the time delay correction t_c and the value of the frequency equivalent of the ISM's conductance (ν_*).

5.1.1 Time Delay Correction (t_c)

To obtain t_c , the following procedures were carried out

1. First, we isolated the different subgroups of the individual GRBs as shown in Fig. 2. That is to say, we noted that for each GRB source, there exist two distinct subgroups — were for:
 - (a) GRB 030329, as can be seen in Fig. 5, we have ($a, b, c, d, e, f, l, m, n, o$) and (g, h, i, j) data points forming the two subgroups with GRB 0302329k being an outlier data point;

- (b) GRB 980425, as can be seen in Fig. 6, we have (a, c, d) and (b, e, f) forming the two distinct subgroups;
 - (c) GRB 000418 of Fig. 7, have (a, d) and (b, c, e) forming the two distinct subgroups;
 - (d) Finally, GRB 021004, in Fig. 8 have (a, b, d) and (c, e) forming the two distinct subgroups;
2. Upon a meticulous observation of Fig. 5 to 8, one can see that the data points for the four GRBs were grouped in two; events group 1 representing the internal shocks and event group 2 representing the external shocks. The idea behind this grouping is to enable us to see the data points that are aligned so we can correct for the time delay (Fig. 7);
 3. When the time delay (t_c) is corrected, one can see that each group's data points have been aligned into an almost straight line. Fig. 3 shows the same four GRBs in Figures 5 to 8 after t_c correction. The scattered and group events have been aligned almost perfectly to a straight line indicating a nearly perfect linear correlation amongst the four samples respectively.

5.1.2 Calculation of the Conductance (ν_*) of the ISM

At this point, we must say that, if our model is correct or has any meaningful correspondence with physical and natural reality, then ν_* can be obtained thus

1. First — we note that the slope of the time delay corrected graphs of Fig. 3 is proportional to the distances to the respective GRBs, i.e.

$$S = \frac{D\nu_*}{c_0}. \quad (10)$$

From this Eq. (10), it is clear that if the distance to the GRB is known, the value of ν_* can be computed. Further, if cosmological space is homogeneous, then ν_* must have a constant value in any given cosmological direction that one chooses. Assuming a homogeneous space as is the case in the Λ CDM-model [43], it follows that $S \propto D$, the meaning of which is that if the distance (D_{\dagger}) to just one GRB is known, then, the distance (D_k) to the rest of the GRBs can be inferred from this Eq. (10).

That is to say: let S_{\dagger} be the slope on the graph of the GRB whose distance D_{\dagger} is known and if S_k is the slope on the graph of the GRB whose distance D_k is unknown, then, we can deduce this distance D_k from the GRB whose slope S_{\dagger} and distance D_{\dagger} are known, i.e.,

$$D_k = \left(\frac{S_{\dagger}}{S_k} \right) D_{\dagger}. \quad (11)$$

From Eq. (10), it is abundantly clear that — *in-order to deduce ν_** — one needs not know the actual distance to the GRB whose distance D_{\dagger} is known, but a relative distance — e.g., $D_{\dagger} \equiv 1$, can be assigned, so that the relative distance $D_{\text{rel}}(k)$, to the k^{th} GRB on our list can be computed, i.e.,

$$D_{\text{rel}}(k) = \frac{S_{\dagger}}{S_k}. \quad (12)$$

From (11) and (12), it follows that

$$D_k = D_{\text{rel}}(k) D_{\dagger}. \quad (13)$$

It must be noted that $D_{\text{rel}}(k)$ is a dimensionless quantity while D_{\dagger} has the dimensions of length;

2. Inserting D_k as given in Eq. (13) into Eq. (10), where Δt has been corrected for the non-simultaneous time delay, we will have

$$\frac{\Delta t}{D_{\text{rel}}} = \frac{D_{\dagger}\nu_*}{c_0} \left(\frac{1}{v_l} - \frac{1}{v_h} \right). \quad (14)$$

What Eq. (14) implies is that if all our assumptions are correct or have a meaningful correspondence with physical and natural reality, then, a plot of $\Delta t/D_{\text{rel}}$ vs $\Delta\nu^{-1}$ should yield a straight line graph. the result of the assumption is evident in (3);

3. In the present, for our standard GRB with distance D_{\dagger} and slope S_{\dagger} , we took the GRB with the smallest redshift, namely GRB 980425, which has a redshift $z = 0.009$. The justification for doing this is spelt out in §7;
4. On careful observation of Fig. 4b one can see that the scatter in the plots has all been fully corrected into an almost perfectly straight line graph. A *t-test* was carried out on the combined plot to test for statistical significance. The result was not only consistent but also significant at a 95% confidence level. The complete regression fittings and other regression parameters are shown in Table 1 and 3;
5. Therefore, From the foregoing, we have that $D_{\dagger} = 40.00$ Mpc, and $S_{\dagger} = 70.00 \pm 2.00$ GHz \times Days. Substituting these numerical values into 10 and converting to standard units we calculated ν_* to be 1.507 ± 0.0009 as the frequency equivalence of the conductance of the ISM. Following we now estimate the spatial sizes of the internal and external shocks as presented in §6.

6 Result and Analysis

According to the Fireball model depicted in Fig. 1, a GRB will have two shock fronts, the internal and external. The events emanating from these shock fronts will have a large gradient on the Δt vs $\Delta\nu^{-1}$ graph. Given that in the present GRB time delay model, the distance (D) of the group events

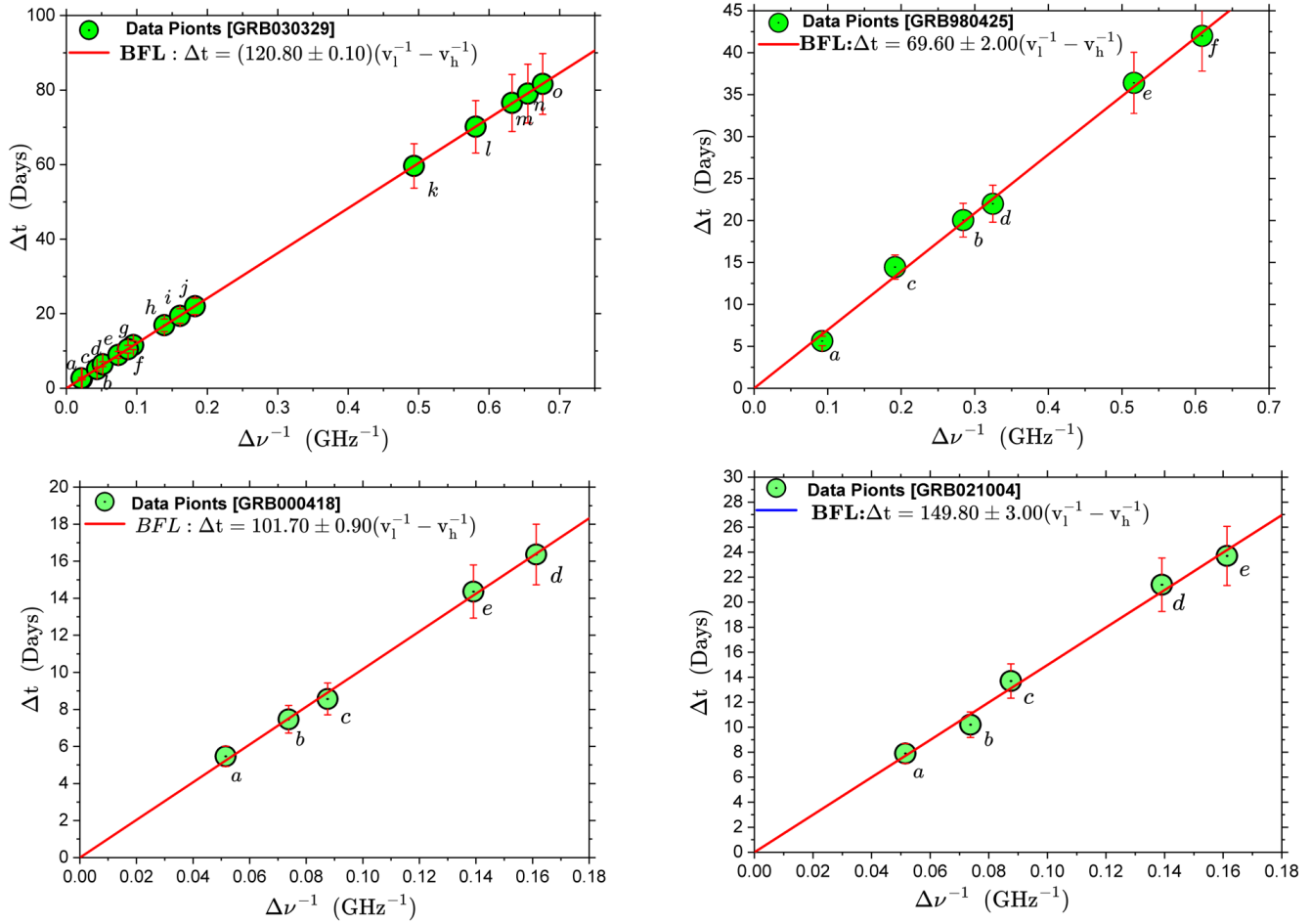


Fig. 3: Graph of GRB 030329, 980425, 000418, and 021004 events after t_C correction.

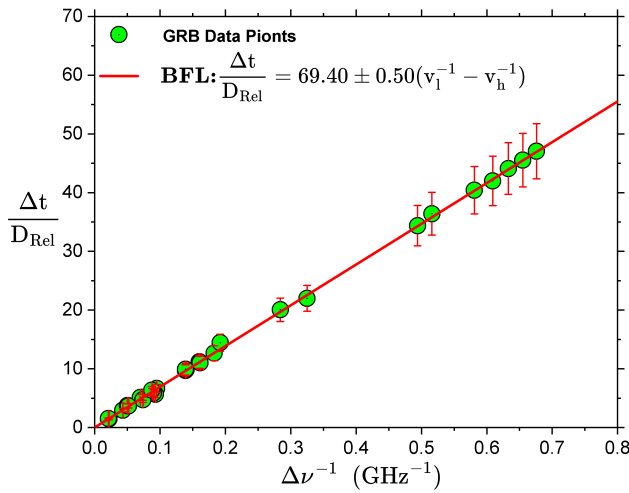


Fig. 4: Relative distance Plot. The combined scatter plots for GRB 030329, GRB 980425, GRB 000418 and GRB 021004 after relative distance correction respectively. Regression fitting for this plot passes through the (0,0)-point of origin unbiased showing that the t_c has been eliminated naturally via our correction procedure

emanating from the same shock front is such that $D = c_0 S / \nu_*$. It follows from the foregoing that event group (1) must therefore be emanating from the internal shock while event group (2) are coming from the external shock. If both events have slopes S_1 and S_2 , from the bare facts at hand, the spatial size, ΔD , between these two shocks is such that

$$\Delta D = \left(\frac{c_0 \Delta S}{\nu_*} \right) \quad (15)$$

where $\Delta S = S_2 - S_1$, $\Delta D = D_2 - D_1$ and $\nu_* = 1.507 \pm 0.009$ Hz (see [8]). Under the above premise, we now present the results of the spatial sizes of the four GRBs in question.

6.1 Estimating the Spatial Size

Following the procedures laid down so far, the spatial size (ΔD) can be estimated from the plot of Δt vs $\Delta \nu^{-1}$ as shown in Fig. 5 to 8 while keeping ν_* as a constant. Fig. 5 to 8 shows a scattered plot of GRB 030329, GRB 980425, GRB 000418 and GRB 021004, with two fittings representing both the internal shocks (red line with yellow data points) and external shock (blue line with red data points). Regression analysis and fittings in accordance with the FDSL model yield the following result.

6.1.1 GRB 030329

GRB 030329 have a set of two events, namely — events ($a, b, c, d, e, f, l, m, n, o$) and (g, h, i, j) as shown in Fig. 5, each with slopes $S_1 = 105.90 \pm 0.60$, and $S_2 = 120.80 \pm 2.00$ respectively. Substituting these values into Eq. 15 after converting to SI units with $\nu_* = 1.507 \pm 0.009$ Hz, we obtain the spatial

size $\Delta D = 8.00 \pm 1.00$ Mpc. What this implies is that the spatial size between the jets is occurring at megaparsec scales. However, from the fireball model, this value seems to be very large compared to what has been obtained [49–51]. The significance is that the time delay is a result of the distance the Photons travel from the internal to the external shocks due to the reduction in their velocity as they travel via the ISM, thus making our fitting model more significant. It is also important to note that such distinct results greatly improve our understanding of GRBs if these results are to be corroborated with more data points.

6.1.2 GRB 980425

GRB 980425 have two events, namely — (a, c, d) and (b, e, f) forming the two distinct subgroups. as shown in Fig. 6, each with slopes $S_1 = 71.00 \pm 4.00$, and $S_2 = 75.00 \pm 8.00$ respectively. we obtain $\Delta D = 2.00 \pm 5.00$ Mpc. This GRB is also of the mega Parsec scale as expected.

6.1.3 GRB 000418

In the case of GRB 000418, we have two events, namely — events (a, d) and (b, c, e) as shown in Fig. 7, each with slopes $S_1 = 101.70 \pm 0.00$, and $S_2 = 102.40 \pm 7.00$ respectively. Substituting these parameters into 15, we obtain $\Delta D = 1.00 \pm 4.00$ Mpc. Similarly, the spatial size of this GRB is also of the mega Parsec scale as expected.

6.1.4 GRB 021004

Regression fittings for both the internal and external shocks for GRB 021004 are shown in Fig. 8. with $S_1 = 150.00 \pm 20.00$ and $S_2 = 154.00 \pm 0.00$ respectively, we obtain the spatial size to be $\Delta D = 13.00 \pm 4.00$ Mpc.

7 Interim Discussion

For the distances to the GRBs, we can use the Λ CDM-redshift distance estimates. Our reservation with this is that distances deduced using high redshift (i.e., $z > 0.009$) may not be accurate. For example, over the years, there has been a raging debate on this [52, 53]. This debate has somehow subsided with most astrophysicists and cosmologists accepting the Λ CDM-redshift distance estimates [54]. If any, there has not been any controversy with low redshifts and using these for distance determinations via Hubble's law [55, 56].

Rather fortuitously, we have in our four sample GRB the source GRB 980425 with a low redshift of $z = 0.0090$. This redshift is small enough so much that, one can easily apply the usual *Hubble law** to determine the distance to this

*On 26 October 2018, through an electronic vote conducted among all members of the International Astronomical Union (IAU), the resolution to recommend renaming the *Hubble law* as the *Hubble-Lemaître law* was accepted. This resolution was proposed in order to pay tribute to both —

Table 1: Result Table. In column 2 the number (1) is the internal shock and (2) is the external shock

Events	Shocks	Slopes for Shocks (S_1, S_2) (GHz \times Days)	Slope ΔS ($S_2 - S_1$) (GHz \times Days)	y -Intercept (t_c) (t_{c1}, t_{c2}) (Days)	R^2
GRB 030329	(1)	105.90 ± 0.60	15.00 ± 2.00	$+0.70 \pm 0.20$	0.9997
	(2)	120.80 ± 2.00		$+5.00 \pm 0.20$	0.9997
GRB 980425	(1)	71.00 ± 4.00	4.00 ± 9.00	-9.00 ± 2.00	0.9975
	(2)	75.00 ± 8.00		-1.00 ± 2.00	0.9884
GRB 000418	(1)	102.00 ± 7.00	1.00 ± 7.00	-4.00 ± 0.00	1.0000
	(2)	102.00 ± 0.00		$+0.30 \pm 0.70$	0.9949
GRB 021004	(1)	150.00 ± 20.00	10.00 ± 20.00	-0.30 ± 2.00	0.9889
	(2)	154.00 ± 0.00		$+7.00 \pm 0.00$	1.0000

Table 2: Summary Table. Columns (1)-(4) lists (1) Source name, (2) Cosmological redshift of the host galaxies [44–48], (3) Distance to the GRB as obtained from Wright’s cosmological calculator (4) the Spatial Size of the GRB shocks. The last row of the table presents the error-weighted average of the frequency equivalence of the conductance of the ISM, which we find to be $\nu_* = 1.507 \pm 0.009$ Hz.

Source	Host Galaxy Redshift	Distance (\mathcal{D}_L) (Mpc)	Spatial size (ΔD) (Mpc)
GRB 030329	0.1683 ± 0.0001	838.9000	8.0000 ± 1.0000
GRB 980425	0.0087 ± 0.0000	39.0000	2.0000 ± 5.0000
GRB 000418	1.1181 ± 0.0001	7804.0000	1.0000 ± 4.0000
GRB 021004	2.3304 ± 0.0005	19188.0000	13.0000 ± 3.0000

source without the need e.g. for Wright’s [14] online cosmology calculator. If we can have confidence in the distance to this GRB as determined by Hubble’s law, it means we can safely estimate the the ISM conductance σ . Taking $\mathcal{H}_0 = 67.4 \text{ km} \times \text{s}^{-1} \times \text{Mpc}^{-1}$ [57], we obtain that the source GRB 980425 is at a distance of approximately, $\mathcal{D} = 40 \text{ Mpc}$. Given that for this GRB, we have $\mathcal{D}\nu_*/c_0 = (6.00 \pm 2.00) \times 10^{15}$, it follows from all this — that, we will have that $\sigma = (1.0800 \pm 0.0400) \times 10^{-11} \Omega^{-1} \times \text{m}^{-1}$. If what we have obtained is to be taken seriously, not only are these results consistent, but they also show a great possibility of querying the standard distance method adopted over the years for GRBs using redshift and cosmological methods.

8 General Discussion

The results we have obtained so far not only justify the authenticity of our model but also support the fireball model

Georges Henri Joseph Édouard Lemaître (1894–1966), and, Edwin Powell Hubble (1889–1953), for their fundamental contributions to the development of the modern expanding cosmology model.

for the internal and external shock mechanism. Similar work has been done to understudy the mechanism of the internal and external shocks e.g. [33, 58–63]. One such major work by [64] delves into the width of γ -ray burst spectra as a measure to understand the emission processes in highly relativistic jets. Although the study highlights the differences in spectra widths, one can infer from this that such width may be a result of the large distances travelled by the photons indicating a large fraction across the jets. Similarly, [58] in a recent study investigated the long-term evolution of relativistic collisionless shocks in electron-positron plasma using 2D particle-in-cell simulations. Their results reveal the generation of intermittent magnetic structures by the shock, with magnetic coherence scales increasing over time as the photons travel along the jet cone. Their findings further suggest implications for γ -ray burst afterglow models, particularly in understanding the interplay between internal prompt emission and external shock mechanisms that power the afterglows in these astrophysical phenomena. Our findings and results also underscores the ongoing debate surrounding the

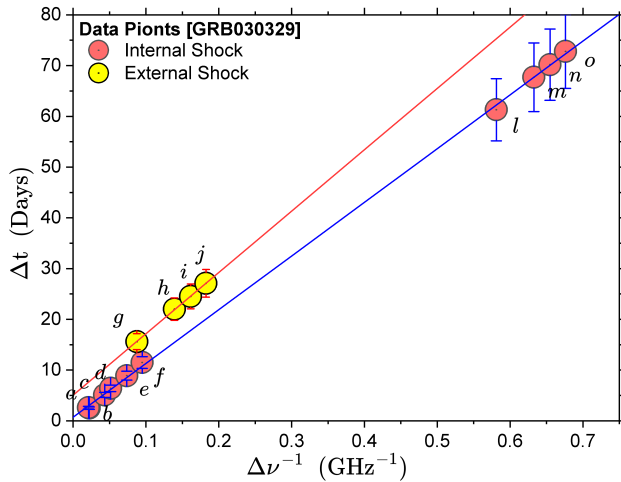


Fig. 5: Graph for Events GRB 030329 ($a, b, c, d, e, f, l, m, n, o$) and (g, h, i, j). The BLF yields slopes of $S_1 = (105.90 \pm 0.60)x + (0.70 \pm 0.20) @ R^2 = 0.9997$ and $S_2 = (120.80 \pm 2.00)x + (5.00 \pm 0.20) @ R^2 = 0.9997$.

internal and external shock mechanisms responsible for GRB emission which we believe is a step forward in the right direction.

For the internal shocks, one approach is to consider the variability timescale of the burst, which is related to the spatial size of the emitting region. On the other hand, the external shocks, are formed when the GRB outflow interacts with the surrounding medium, leading to a slower, and more prolonged emission phase.

This slowing down of the photons we believe is due to the vast difference between the internal and external shock which our model is accounting for. [65] has already shown that the radius of the external shocks can be estimated based on the deceleration timescale, which depends on the density of the surrounding medium. His findings agree with our rarefied plasma model as the interactions of the photons and the plasma medium through which these photons travel can significantly affect their propagation.

Additionally, as far back as the mid and late 1990's (see e.g. [21, 66]), it has been shown that the “fireball model” often used in GRB studies suggests that the internal shocks occur within the relativistic outflow produced during the GRB event. [67] further highlighted the transition from a stratified stellar wind to a homogeneous interstellar medium (ISM) and concluded that favourable parameters could lead to the detection of GRBs at hundreds of GeVs, emphasizing the importance of considering both internal and external shock mechanisms in understanding GRB emission dynamics. In both cases (internal and external shock mechanisms), detailed modelling and analysis of observational data, such as light curves and spectra, are necessary to constrain the parameters and obtain accurate estimates of the shock radii and possibly

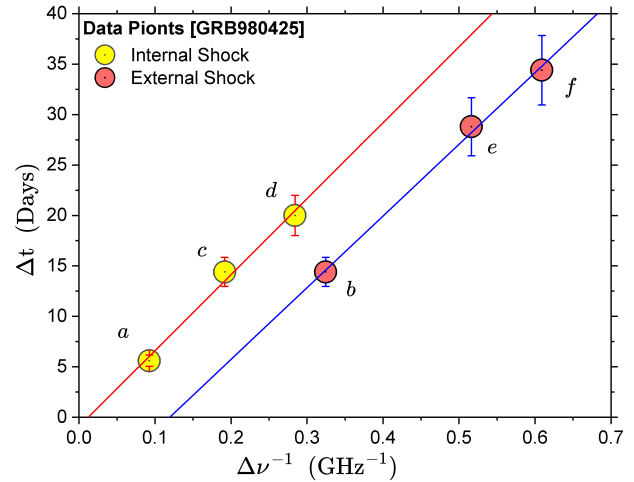


Fig. 6: Graph for Events GRB 980425 (a, c, d) and (b, e, f). The BLF yields slopes of $S_1 = (71.00 \pm 4.00)x + (9.00 \pm 2.00) @ R^2 = 0.9975$ and $S_2 = (75.00 \pm 8.00)x + (1.00 \pm 2.00) @ R^2 = 0.9884$.

the spatial sizes.

This is the next phase of this work as we work to gather more data to carry out further analysis. What our model presents so far is in support of the fireball model but on a much larger scale. It is our hope that as we fine-tune this model and incorporate more data in subsequent work, we can be able to come close to what has been established and possibly improve on the existing knowledge of these extreme astrophysical phenomena.

It is paramount we bring this to the reader for better clarity that the spatial size of the internal and external shocks plays a significant role in determining how the photons and plasma interact and propagate through the ISM. Now, with regard to the interaction mechanism between the Photon and the plasma in the present model, one will rightly ask: *Since the Photon and the plasma are here interacting, what is different between this proposed interaction mechanism and the Plasma Effect?* To that, we have the following to say. The Compton wavelength of Photon — or more so, its radius — is much smaller than the wavelength of radio waves. From an intuitive physical standpoint, it is possible to imagine an Electron being engulfed by the Photon in such a manner that the Electron can be pictured to be moving inside the \vec{E} and \vec{B} -fields of the Photon. Succinctly stated, the Electron is absorbed by the Photon in much the same manner as the Photon is absorbed by the Electron in such phenomenon as the *Photoelectric effect* [68], i.e., this simple but elaborate explanation will lead to our next instalment “can a photon absorb an electron”.

It is our hope that our FSDL time delay model if properly fine-tuned with the right dataset will demystify the interaction mechanism between the photons and the plasma as they travel via the ISM.

Table 3: Combined Data Table [12]. Columns (1)-(8) list the (1) Initial/low frequency of the burst, (2) Final/high frequency of the burst (3) Initial time of the burst (4) Final time of the burst (5) Difference in the frequency (6) Values obtain from the two-fold correction (7) Relative distance obtained from the slopes of the four GRBs (8) Final values obtained from the relative distance correction

GRB Event Label	ν_1 (GHz)	ν_2 (GHz)	t_1 (Days)	t_2 (Days)	$\Delta\nu^{-1}$ (GHz ⁻¹)	Δt_c (Days)	D_{rel}	$\Delta t_c / D_{rel}$ (Days)
GRB030329a	15.00	22.50	8.40	10.90	0.022	2.56	1.7360 ± 0.0030	2.00 ± 0.10
GRB030329b	22.50	43.00	5.80	8.40	0.021	2.64	1.7360 ± 0.0030	2.00 ± 0.20
GRB030329c	15.00	43.00	5.80	10.90	0.043	5.14	1.7360 ± 0.0030	3.00 ± 0.30
GRB030329d	8.46	15.00	10.90	17.30	0.052	6.44	1.7360 ± 0.0030	4.00 ± 0.40
GRB030329e	8.46	22.50	8.40	17.30	0.074	8.94	1.7360 ± 0.0030	5.00 ± 0.50
GRB030329f	8.46	43.00	5.80	17.30	0.095	11.54	1.7360 ± 0.0030	7.00 ± 0.70
GRB030329g	4.86	8.46	17.30	32.90	0.088	10.49	1.7360 ± 0.0030	6.00 ± 0.60
GRB030329h	4.86	15.00	10.90	32.90	0.139	16.89	1.7360 ± 0.0030	10.00 ± 1.00
GRB030329i	4.86	22.50	8.40	32.90	0.161	19.39	1.7360 ± 0.0030	11.00 ± 1.00
GRB030329j	4.86	43.00	5.80	32.90	0.183	21.99	1.7360 ± 0.0030	13.00 ± 1.00
GRB030329k	1.43	4.86	32.90	78.60	0.494	59.65	1.7360 ± 0.0030	34.00 ± 3.00
GRB030329l	1.43	8.46	17.30	78.60	0.581	70.15	1.7360 ± 0.0030	40.00 ± 4.00
GRB030329m	1.43	15.00	10.90	78.60	0.633	76.55	1.7360 ± 0.0030	44.00 ± 4.00
GRB030329n	1.43	22.50	8.40	78.60	0.655	79.05	1.7360 ± 0.0030	46.00 ± 5.00
GRB030329o	1.43	43.00	5.80	78.60	0.676	81.65	1.7360 ± 0.0030	47.00 ± 5.00
GRB980425a	4.80	8.64	12.70	18.30	0.093	5.65	1.0000 ± 0.0000	6.00 ± 0.60
GRB980425c	2.50	4.80	18.30	32.70	0.192	14.45	1.0000 ± 0.0000	14.00 ± 1.00
GRB980425d	2.50	8.64	12.70	32.70	0.284	20.05	1.0000 ± 0.0000	20.00 ± 2.00
GRB980425b	1.38	2.50	32.70	47.10	0.325	21.60	1.0000 ± 0.0000	22.00 ± 2.00
GRB980425e	1.38	4.80	18.30	47.10	0.516	36.40	1.0000 ± 0.0000	36.00 ± 4.00
GRB980425f	1.38	8.64	12.70	47.10	0.609	42.00	1.0000 ± 0.0000	42.00 ± 4.00
GRB000418e	4.86	15.00	12.30	27.00	0.140	14.36	1.4600 ± 0.0100	10.00 ± 1.00
GRB000418b	8.46	15.00	12.30	18.10	0.050	5.46	1.4600 ± 0.0100	4.00 ± 0.40
GRB000418c	4.86	8.46	18.10	27.00	0.090	8.56	1.4600 ± 0.0100	6.00 ± 0.60
GRB000418d	4.86	22.50	14.60	27.00	0.160	16.37	1.4600 ± 0.0100	11.00 ± 1.00
GRB000418a	8.46	22.50	14.60	18.10	0.070	7.47	1.4600 ± 0.0100	5.00 ± 0.50
GRB021004a	8.46	22.50	8.70	18.70	0.074	10.2	2.1500 ± 0.0300	5.00 ± 0.50
GRB021004b	4.86	8.46	18.70	32.20	0.088	13.7	2.1500 ± 0.0300	6.00 ± 0.60
GRB021004d	4.86	22.50	8.70	32.20	0.161	23.7	2.1500 ± 0.0300	11.00 ± 1.00
GRB021004c	8.46	15.00	4.10	18.70	0.052	7.89	2.1500 ± 0.0300	4.00 ± 0.40
GRB021004e	4.86	15.00	4.10	32.20	0.139	21.39	2.1500 ± 0.0300	10.00 ± 1.00

9 Conclusion

We have used regression analysis to establish a time correction mechanism for four GRBs (030329, 980425, 000418, and 021004) employed from [12] on the basis of a frequency-dependent speed of light model (FDSL model) which we developed entirely from Maxwell's electromagnetic equations in conjunction with plasma and dispersion effects. In line with this model, on the assumption that these GRBs all leave the source at the same time, we have shown in our previous paper [8] that these four GRBs gave good positive correlations and hence reliable for testing our model. In this paper, however, on the assumption that each individual photon leaves the GRB source at different times, we modify the previous model to obtain a more fitting model. Additionally, the

correction led to the unification of the four GRB into a homogenous albeit perfect correlation which led to the determination of the frequency equivalent of the ISM (ν_*) and hence, the spatial sizes of the internal and external shocks.

If the results provided herein are deemed acceptable or reasonable — *one can on this basis* — make the following tentative conclusion regarding the implication of the spatial sizes of GRB internal and external shocks using our FSDL time delay model:

1. The relationship we have established from our analysis for the four GRBs, clearly supports two GRB models “the framework of the fireball model” and “the multiple shock wave model” of GRBs production and their afterglow.
2. From our regression analysis that here, we can infer that not only is our model reliable and consistent but was used to

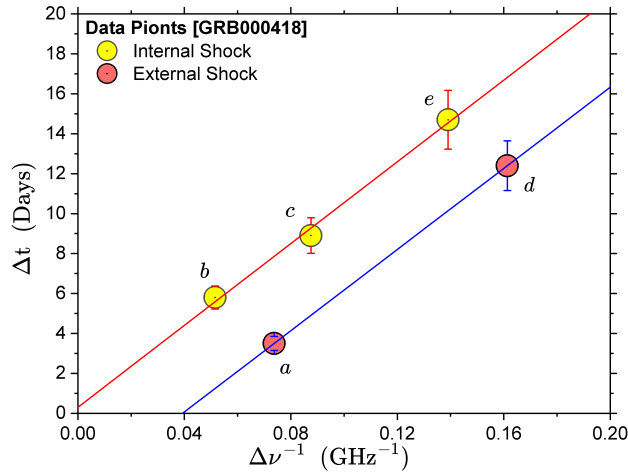


Fig. 7: Graph for Events GRB 000418 (b, c, e) and (a, d). The BLF yields slopes of $S_1 = (102.00 \pm 7.00)x + (4.00 \pm 0.00)$ @ $R^2 = 1.0000$ and $S_2 = (102.00 \pm 0.00)x - (0.30 \pm 0.70)$ @ $R^2 = 0.9949$.

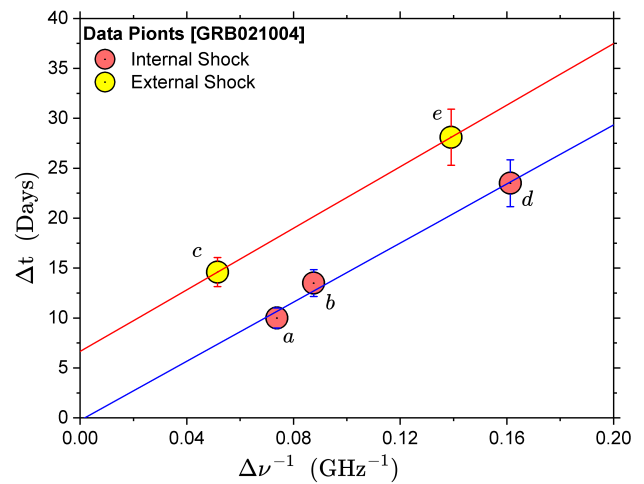


Fig. 8: Graph for Events GRB 021004 (b, c, e) and (a, d). The BLF yields slopes of $S_1 = (150.00 \pm 20.00)x + (0.30 \pm 2.00)$ @ $R^2 = 9.889$ and $S_2 = (154 \pm 0.00)x - (7.00 \pm 0.00)$ @ $R^2 = 1.0000$.

estimate the spatial sizes between the internal and external shocks.

- From our FSDL time delay models and the fitting procedures we employ, we are able to say unequivocally that the internal shocks arise from variations in the relativistic outflows within the jet itself, which offer valuable insights into the acceleration mechanisms and particle interactions occurring within the jet. On the other hand, the external shocks, result from the interaction between the jet and its surrounding medium, which shed light on the environmental conditions and the impact of the jet on its surroundings. This we are able to deduce due to the nature of the differential time in the arrival time of the photons and the vast distances obtained in the spatial sizes between the internal and external shocks.

Furthermore, the determination of the spatial size of γ -ray jets for both internal and external shocks is a crucial endeavour in understanding the dynamics and emission processes of astrophysical jets. We believe that through meticulous observations, corroboration of more data sets and sophisticated modelling techniques for e.g. intense spectral analysis of the radiations from these shocks, 3D modelling of the particle dynamics emanating from the shocks, and magnetohydrodynamic (MHD) effects, we can be able to unravel the complexities of these high-energetic phenomena.

Acknowledgements

We hereby acknowledge the financial support rendered by the Education, Audio and Culture Executive Agency of the European Commission through the Pan-African Planetary and Space Science Network under funding agreement number 6242.24-PANAF-12020-1-BW-PANAF-MOBAF. Also, we would like to acknowledge the invaluable support from our workstations — The Copperbelt University (Republic of

Zambia) and the National University of Science and Technology (Republic of Zimbabwe) for the support rendered in making this work possible.

Submitted on June 17, 2024

References

- Joshi J.C., Chand V., and Razzaque S. Synchrotron and synchrotron selfcompton emission components in GRBs detected at very high energies. *Proceedings of the 16th Marcel Grossmann Meeting*, 5–10 July 2021, World Scientific, 2023, 3009–3016.
- Piro L., De Pasquale M., Soffitta P., et al. Probing the environment in gamma-ray bursts: the case of an x-ray precursor, afterglow late onset, and wind versus constant density profile in GRB 011121 and GRB 011211. *The Astrophysical Journal*, 2005, v.623, no.1, 314–324.
- Ze-Cheng Zou, Bin-Bin Zhang, Yong-Feng Huang, and Xiao-Hong Zhao. Gamma-ray burst in a binary system. *The Astrophysical Journal*, 2021, v.921, id2, 1–7.
- Janiuk A. Many faces of accretion in gamma ray bursts. arXiv: 2112.14086, 2021.
- Bromberg O., Nakar E., and Piran T. Are low-luminosity gamma-ray bursts generated by relativistic jets? *The Astrophysical Journal Letters*, 2011, v.739, no.2, L55, 1–12.
- Konigl A. Relativistic jets as X-ray and gamma-ray sources. *The Astrophysical Journal*, 1981, v.243, 700–709.
- Kumar P., Zhang B. The physics of gamma-ray bursts & relativistic jets. *Physics Reports*, 2015, v.561, no.12, 1–109.
- Nyambuya G.G., Marusenga S., Abbey G.F., Simpemba P., Simfukwe J. Correlation in gamma-ray burst time delays between pairs of radio photons. *International Journal of Astronomy and Astrophysics*, 2023, v.13, 195–216.
- Hao J.M., Yuan Y.F. Progenitor delay-time distribution of short gamma-ray bursts: Constraints from observations. *Astronomy & Astrophysics*, 2013, v.558, A22.
- Mao Shude. Gravitational lensing, time delay, and gamma-ray bursts. *The Astrophysical Journal*, 1992, v.389, no.2, L41–L44.

11. Zhang B., Zhang B. Gamma-ray burst prompt emission light curves and power density spectra in the ICMART model. *The Astrophysical Journal*, 2014, v.782, no.2, id92, 1–11.
12. Zhang B., Chai Y.T., Zou Y.C., Wu X.F. Constraining the mass of the photon with gamma-ray bursts. *Journal of High Energy Astrophysics*, 2016, v.11–12, 20–28.
13. Ade P.A., Aghanim N., Alves M.I., et al. Planck 2013 results. I. Overview of products and scientific results. *Astronomy & Astrophysics*, 2014, v.571, A1, 1–66.
14. Wright E.L. A cosmology calculator for the world wide web. *Publications of the Astronomical Society of the Pacific*, 2006 v.118, no.850, 1711–1715.
15. Pan Y., Qi J., Cao S., Liu T., Liu Y., Geng S., Lian Y., Zhu Z.H. Model-independent constraints on Lorentz invariance violation: implication from updated Gamma-ray burst observations. *The Astrophysical Journal*, 2020 v.890, no.2, id169, 1–7.
16. Burgess J.M., Bégué D., Greiner J., Giannios D., Bacelj A., Berlato F. Gamma-ray bursts as cool synchrotron sources. *Nature Astronomy*, 2020 v.4, no.2, 174–179.
17. Fraija N., De Colle F., Veres P., Dichiaro S., Duran R.B., A.C. Caligula do E.S. Pedreira, Galvan-Gamez A., Kamenetskaia B.B. Description of atypical bursts seen slightly off-axis. *The Astrophysical Journal*, 2020, v.896, no.1, id25, 1–22.
18. Alexander K.D., Laskar T., Berger E., Johnson M.D., Williams P.K., Dichiaro S., Fong W.F., Gomboc A., Kobayashi S., Margutti R., Mundell C.G. An unexpectedly small emission region size inferred from strong high-frequency diffractive scintillation in GRB 161219B. *The Astrophysical Journal*, 2019, v.870, no.2, id67, 1–12.
19. Taylor G.B., Frail D.A., Berger E., Kulkarni S.R. The angular size and proper motion of the afterglow of GRB 030329. *The Astrophysical Journal*, 2004 v.609, no.1, L1, 1–3.
20. Eichler D., Levinson A. A compact fireball model of gamma-ray bursts. *The Astrophysical Journal*, 2000, v.529, no.1, 146–150.
21. Piran T. Gamma-ray bursts and the fireball model. *Physics Reports*, 1999, v.314, no.6, 575–667.
22. Fox D.B., Mészáros P. GRB fireball physics: prompt and early emission. *New Journal of Physics*, 2006, v.8, 199–223.
23. Cioffi R. Short gamma-ray burst central engines. *International Journal of Modern Physics D*, 2018, v.27, no.13, 1842004.
24. Levan A.J., Tanvir N.R., Starling R.L., Wiersema K., Page K.L., Perley D.A., Schulze S., Wynn G.A., Chornock R., Hjorth J., Cenko S.B. A new population of ultra-long duration gamma-ray bursts. *The Astrophysical Journal*, 2014, v.781, no.1, A13, 1–13.
25. Thompson C. A model of gamma-ray bursts. *Monthly Notices of the Royal Astronomical Society*, 1994, v.270, no.3, 480–498.
26. Mészáros P. The fireball shock model of gamma ray bursts. *AIP Conference Proceedings 2000, Jun 23*, v.522, no.1, 213–225.
27. Sarin N., Lasky P.D., Ashton G. X-ray afterglows of short gamma-ray bursts: Magnetar or Fireball? *The Astrophysical Journal*, 2019, v.872, no.1, id114, 1–6.
28. Kopač D., Mundell C.G., Japelj J., Arnold D.M., Steele I.A., Guidorzi C., Dichiaro S., Kobayashi S., Gomboc A., Harrison R.M., Lamb G.P. Limits on optical polarization during the prompt phase of GRB 140430A. *The Astrophysical Journal*, 2015, v.813, no.1, id1, 1–14.
29. McDowell A., MacFadyen A. Revisiting the parameter space of binary neutron star merger event GW170817. *The Astrophysical Journal*, 2023, v.945, no.2, id135, 1–8.
30. Willingale R., Mészáros P. Gamma-ray bursts and fast transients: multi-wavelength observations and multi-messenger signals. *Space Science Reviews*, 2017, v.207, 63–86.
31. Capozziello S., Lambiase G. The emission of Gamma Ray Bursts as a test-bed for modified gravity. *Physics Letters B*, 2015, v.750, 344–347.
32. Wang Y., Jiang L.Y., Ren J. GRB 201104A: A “repetitive” short gamma-ray burst? *The Astrophysical Journal*, 2022, v.935, no.2, id179, 1–10.
33. Fraija N., Veres P. The origin of the optical flashes: The case study of GRB 080319B and GRB 130427A. *The Astrophysical Journal*, 2018, v.859, no.1, id70, 1–9.
34. Fan X., Messenger C., Heng I.S. Probing intrinsic properties of short gamma-ray bursts with gravitational waves. *Physical Review Letters*, 2017, v.119, no.18, 181102.
35. Abbott B.P., Abbott R., Abbott T.D., et al. Gravitational waves and gamma-rays from a binary neutron star merger: GW170817 and GRB 170817A. *The Astrophysical Journal Letters*, 2017, v.848, no.2, L13, 1–7.
36. Pe’Er A. Physics of Gamma-Ray Bursts Prompt Emission. *Advances in Astronomy*, 2015, no.1, 907321.
37. Piran T. The physics of gamma-ray bursts. *Reviews of Modern Physics*, 2004 v.76, no.4, 1143–1210.
38. Yu Y.W., Gao H., Wang F.Y., Zhang B.B. Gamma-Ray Bursts. *Handbook of X-ray and Gamma-ray Astrophysics*, Springer Nature Reference Book, Singapore, 2022, 34 pages.
39. Dado S., Dar A., De Rújula A. Critical Tests of Leading Gamma Ray Burst Theories. *Universe*, 2022, v.8, no.7, 350–395.
40. Yost S.A., Harrison F.A., Sari R., Frail D.A. A study of the afterglows of four gamma-ray bursts: constraining the explosion and fireball model. *The Astrophysical Journal*, 2003, v.597, no.1, 459–473.
41. Oates S.R., Page M.J., Schady P., et al. A statistical study of gamma-ray burst afterglows measured by the Swift Ultraviolet Optical Telescope. *Monthly Notices of the Royal Astronomical Society*, 2009, 395, no.1, 490–503.
42. Chandra P., Frail D.A. A radio-selected sample of gamma-ray burst afterglows. *The Astrophysical Journal*, 2012, v.746, no.2, id156, 1–28.
43. Fay S. Λ CDM periodic cosmology. *Monthly Notices of the Royal Astronomical Society*, 2020, v.494, no.2, 2183–2190.
44. Stanek K.Z., Matheson T., Garnavich P.M., et al. Spectroscopic discovery of the supernova 2003dh associated with GRB 030329. *The Astrophysical Journal*, 2003, v.591, no.1, L17, 1–3.
45. Hurley K., Sommer M., Atteia J.L., Boer M., Cline T., Cotin F., Henoux J.C., Kane S., Lowes P., Niel M. The solar X-ray/cosmic gamma-ray burst experiment aboard ULYSSES. *Astronomy and Astrophysics Supplement Series*, 1992, v.92, no.2, 401–410.
46. Bloom J.S., Berger E., Kulkarni S.R., Djorgovski S.G., Frail D.A. The redshift determination of GRB 990506 and GRB 000418 with the Echelle Spectrograph Imager on Keck. *The Astronomical Journal*, 2003, v.125, no.3, 999–1005.
47. Klose S., Stecklum B., Masetti N., et al. The very red afterglow of GRB 000418: Further evidence for dust extinction in a gamma-ray burst host galaxy. *The Astrophysical Journal*, 2000, v.545, no.1, 271–276.
48. Waxman E. The nature of GRB 980425 and the search for off-axis gamma-ray burst signatures in nearby Type Ib/c supernova emission. *The Astrophysical Journal*, 2004, v.602, no.2, 886–891.
49. Aad G., Abajyan T., Abbott B., Abdallah J., Khalek S.A., Abdelalim A.A., Aben R., Abi B., Abolins M., Abouzaid O.S., Abramowicz H. Observation of a new particle in the search for the Standard Model Higgs boson with the ATLAS detector at the LHC. *Physics Letters B*, 2012, v.716, no.1, 1–29.
50. Zhang B. A possible connection between fast radio bursts and gamma-ray bursts. *The Astrophysical Journal Letters*, 2013, v.780, no.2, L21, 1–4.
51. Jackson N. The hubble constant. *Living Reviews in Relativity*, 2015, v.18, v.1, 1–52.

52. Parker B.R. The Vindication of the Big Bang: Breakthroughs and Barriers. Springer Verlag, 2013.
53. Lian Y., Cao S., Biesiada M., Chen Y., Zhang Y., Guo W. Probing modified gravity theories with multiple measurements of high-redshift quasars. *Monthly Notices of the Royal Astronomical Society*, 2021, v.505, no.2, 2111–2123.
54. Salpeter E.E., Hoffman Jr G.L. The galaxy luminosity function and the redshift-distance controversy (a review). *Proceedings of the National Academy of Sciences*, 1986, v.83, no.10, 3056–3063.
55. Hubble E. A relation between distance and radial velocity among extragalactic nebulae. *Proceedings of the National Academy of Sciences*, 1929, v.15, no.3, 168–173.
56. Davis T. An expanding controversy. *Science*, 2019 v.365, no.6458, 1076–1077.
57. Aghanim N., Akrami Y., Ashdown M., et al. Planck 2018 results-VI. Cosmological parameters. *Astronomy & Astrophysics*, 2020, v.641, A6, 1–67.
58. Grošelj D., Sironi L., Spitkovsky A. Long-term evolution of relativistic unmagnetized collisionless shocks. *The Astrophysical Journal Letters*, 2024, v.963, no.2, L44, 1–8.
59. Kathirgamaraju A., Duran R.B., Giannios D. GRB off-axis afterglows and the emission from the accompanying supernovae. *Monthly Notices of the Royal Astronomical Society*, 2016, v.461, no.2, 1568–1575.
60. Bégué D., Burgess J.M. The anatomy of a long gamma-ray burst: a simple classification scheme for the emission mechanism(s). *The Astrophysical Journal*, 2016, v.820, no.1, id68, 1–6.
61. Sarin N., Hamburg R., Burns E., Ashton G., Lasky P.D., Lamb G.P. Low-efficiency long gamma-ray bursts: a case study with AT2020blt. *Monthly Notices of the Royal Astronomical Society*, 2022, v.512, no.1, 1391–1399.
62. Arimoto M., Asano K., Ohno M., Veres P., Axelsson M., Bissaldi E., Tachibana Y., Kawai N. High-energy non-thermal and thermal emission from GRB 141207A detected by Fermi. *The Astrophysical Journal*, 2016, v.833, no.2, id139, 1–13.
63. Zhang B.T., Murase K., Ioka K., Song D., Yuan C., Mészáros P. External inverse-Compton and proton synchrotron emission from the reverse shock as the origin of VHE gamma rays from the hyper-bright GRB 221009A. *The Astrophysical Journal Letters*, 2023, v.947, no.1, L14, 1–7.
64. Axelsson M., Borgonovo L. The width of gamma-ray burst spectra. *Monthly Notices of the Royal Astronomical Society*, 2015, v.447, no.4, 3150–3154.
65. Re'em S., Piran T. Hydrodynamic timescales and temporal structure of gamma-ray bursts. *The Astrophysical Journal*, 1995, v.455, no.2, L143–L146.
66. Rees M.J., Mészáros P. Unsteady outflow models for cosmological gamma-ray bursts. arXiv: astro-ph/9404038, 1994.
67. Fraija N., Duran R.B., Dichiara S., Beniamini P. Synchrotron self-Compton as a likely mechanism of photons beyond the synchrotron limit in GRB 190114C. *The Astrophysical Journal*, 2019, v.883, no.2, id162, 1–13.
68. Lenard P. Ueber die lichtelektrische Wirkung. *Annalen der Physik*, 1902, Bd.313, No.5, 149–198.

Graph Theory Entropy Values for Lepton and Quark Discrete Symmetry Quantum States and Their Decay Channels

Franklin Potter

Sciencegems, 8642 Marvale Drive, Huntington Beach, CA, United States. E-mail: frank11hb@yahoo.com

We assume that each lepton family and each quark family represents its own unique discrete symmetry modular group, one which is also a binary subgroup of SU(2). Equivalently, we have a different regular 3-D polyhedral group for each lepton family and a different regular 4-D polytope group for each quark family. Being discrete symmetry subgroups representing 3-D and 4-D geometric objects that are known also as complete graphs, they each possess a different graph theory entropy based upon the number of connected paired vertices. We examine the various decay channels of the leptons and the quarks that obey all the conservation laws as well as the special theory of relativity to look for a violation of a fundamental graph theory entropy inequality constraint. Such a violation and its experimental verification would confirm the importance of graph theory entropy in particle physics.

1 Introduction

The identification of the symmetry group or groups for the lepton families and for the quark families of the Standard Model (SM) has been an interesting challenge for decades. In recent years there has been an emphasis on the discrete symmetry modular groups [1] such as $\Gamma_3 = A_4$, $\Gamma_4 = S_4$, $\Gamma_5 = A_5$, as well as their double groups Γ'_3 , Γ'_4 , and Γ'_5 , where the A_4 , S_4 , and A_5 refer to equivalent permutation groups. These discrete symmetry modular groups not only connect directly to a top-down approach using superstring concepts (see e.g. [2, 3] for recent reviews) but also represent the discrete symmetries of the regular polyhedrons in R^3 . However, no discrete symmetry group or set of discrete symmetry groups has been accepted yet, even though neutrino mass values are predicted, because the true mass values for the neutrinos are not known for direct comparison [4].

In a series of articles and conference presentations since 1987 we have proposed [5–7] that each lepton family represents a unique discrete symmetry binary subgroup of the continuous group SU(2), or equivalently, of the quaternion group Q and the modular group. That is, they represent the only finite quaternion subgroups that enclose a 3-D volume. Specifically, the electron family (ν_e, e^-) represents $2T = (3,3,2) = \Gamma'_3$, the muon family (ν_μ, μ^-) represents $2O = (3,4,2) = \Gamma'_4$, and the tau family (ν_τ, τ^-) represents $2I = (3,5,2) = \Gamma'_5$, where the first and second group notations are also the familiar geometrical names for the 3-D regular polyhedron groups, i.e. the Platonic solids in R^3 . As subgroups of SU(2), there is an upper and lower quantum state in each family.

We proposed also [5, 6] that quark families represent the related discrete symmetry groups for the 4-D regular polytopes that enclose a volume, (3,3,3) for the (u, d) family, (3,3,4) for the (c, s) family, (3,4,3) for the (t, b) family, and (3,3,5) for the predicted 4th quark family, i.e. a top/bottom family (t' , b') or (T, B). Of course, the predicted 4th quark



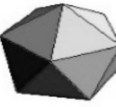


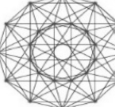
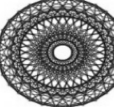
family (T, B) has not been discovered yet, but its existence might resolve several problems within the SM and would increase the value of the Jarlskog constant for the baryon asymmetry of the Universe (BAU) by a factor of about 10^{13} [8].

How do we know that the lepton families and the quark families represent these particular discrete symmetry groups? By imposing the conservation of total lepton family number as the rationale for lepton family mixing and the conservation of total baryon number as the rationale for quark family mixing, we derived the lepton mixing matrix and the quark mixing matrix from first principles without any free parameters [6]. That is, with these discrete symmetry groups, by having a linear superposition of their quaternion group generators for the lepton families and separately for the quark families, we could mimic the continuous symmetry group SU(2) for each and therefore meet the continuous symmetry requirement of Noether's theorem [9] for a conservation law.

All 9 predicted elements of the lepton 3x3 Pontecorvo-Maki-Nakagawa-Sakata (PMNS) mixing matrix match the experimentally determined value ranges, while 8 of 9 elements in the quark 3x3 Cabibbo-Kobayashi-Maskawa (CKM) agree with experimentally determined value ranges, with only the V_{ub} element disagreeing. Of course, with 4 quark families predicted, one has a 4x4 quark mixing matrix CKM4, and we predict reasonable values for the 4th column and the 4th row. Our values also agree with recent concerns that the first row of the normal 3x3 CKM matrix does not sum to unity (for a review see [10, 11]).

However, this mismatch of family numbers, 4 to 3, might raise concerns for triangle anomaly cancellations, which normally cancel with 3 lepton families matching 3 quark families 1-to-1. But we have the cancellation because the lepton families and quark families separately form linear superpositions to each collectively mimic SU(2), so the anomaly cancellation still occurs via quark SU(2) negative contribution against lepton SU(2) positive contribution.

Table 1: Fermion Group and Graph Entropy Assignments

Family	ν_e, e^-	ν_μ, μ^-	ν_τ, τ^-	u, d	c, s	t, b	T, B
Group	(332)	(342)	(352)	(333)	(334)	(343)	(335)
Graph							
n	4	6	12	5	8	24	120
H	2.0	2.585	3.585	2.322	3.0	4.585	6.907

In addition to providing the rationale for the lepton family mixing and for the quark family mixing, we predicted [7] a normal neutrino mass hierarchy (NH) to the neutrino mass values with $m_1 = 0.3$ meV, $m_2 = 8.9$ meV, and $m_3 = 50.7$ meV, reasonable mass values just within the proposed cosmological constraint limit of 60 meV [12]. We await further experiments that will determine the actual neutrino mass values in the near future.

In the following, we utilize the mathematical graph theory property that each discrete symmetry group represents a 3-D or 4-D complete graph and that graph theory identifies an entropy for each complete graph that is determined by its number of vertices, or nodes. This graph theory entropy is not the entropy normally considered in the decay of particles but is an additional entropy to be considered.

Why do we investigate graph theory entropy for these lepton family and quark family discrete symmetries? Because if space happens to be discrete at the Planck scale of about 10^{-35} meters, then this graph entropy could be important. The hope is that we might encounter a graph theory entropy forbidden decay that is allowed by all the known conservation laws and the special theory of relativity (STR). This constraint placed by these graph entropy values for the decays of the leptons and the quarks could either provide further support for the possible existence of a 4th quark family or possibly eliminate a 4th quark family. Therefore, an investigation into the properties and predictions of graph theory entropy seems justified.

2 Graph entropy

Each lepton family and each quark family is represented by a complete undirected graph as illustrated in Table 1, meaning that every pair of distinct vertices is connected by a unique edge [13]. A complete graph G with n vertices has a graph theory entropy

$$H(G) = \log_2 n, \quad (1)$$

and given two complete graphs G_1 and G_2 their union entropy

$$H(G_1 \cup G_2) \leq H(G_1) + H(G_2). \quad (2)$$

Therefore the two resulting graphs must have at least the entropy of the original graph. So when a lepton or a quark decays, the total graph entropy of the particle products of the

decay must be at least equal to the graph entropy of the decaying particle or else the decay cannot occur.

As an example, consider the weak interaction decay of the muon μ^- first to the W^- plus the muon neutrino, and then the W decays:

$$\mu^- \rightarrow W^- + \nu_\mu \rightarrow e^- + \bar{\nu}_e + \nu_\mu. \quad (3)$$

In Table 1 are given the entropy values for the lepton families and the quark families. The entropy $H(\mu^-) = 2.585$, and the final products of the decay sum to a total entropy 6.585, so the entropy inequality condition is met,

$$H(e^- + \bar{\nu}_e + \nu_\mu) > H(\mu^-) \quad (4)$$

as expected for this prevalent decay channel for the muon.

Tables 2 and 3 contain the entropy values for spontaneous decay channels for the leptons and for spontaneous semileptonic decay channels for the quarks that obey the conservation laws and the special theory of relativity (STR). I have included decay channels for a predicted 4th quark family (T,B).

The up quark in the 1st quark family has a smaller mass than its down quark partner, so a spontaneous decay channel is not available to the down quark, and therefore no decay channel is shown even though given enough energy in a proton-proton collision, for example, the up quark in a proton can change into a down quark to produce a neutron plus a positron and electron neutrino.

Table 4 provides the entropy values for spontaneous quark decays to a different quark plus a meson. With no evidence for the predicted 4th quark family and for the mass values of the T and B quarks, the last two columns contain entropy values for both reasonable decay channels as well as possibly some forbidden decay channels. The predicted mass values for the B and T quarks are estimated by using a four family Koide formula [14].

Intermediate stages in each decay process involve a weak interaction boson, a W or a Z , which have the extremely short lifetime [4] of about 3×10^{-25} seconds. Alternative quantum states for the W 's and Z can be expressed in terms of the discrete symmetry of the $2I$ group as the direct product $2I \times 2I'$, where $2I'$ is the group $2I$ with one of its quaternion generators modified to provide "reciprocal" operations to ensure that

Table 2: Final Graph Entropy Values for Lepton Decays

Particle	Mass (MeV)	Group	H	Decay Channel Total H	
				$e^- + \bar{\nu}_e + \nu_\mu$	$\mu^- + \bar{\nu}_\mu + \nu_\tau$
e^-	0.511	(332)	2.0		
μ^-	105.66	(342)	2.585	6.585	
τ^-	1776.84	(352)	3.585	7.585	8.755

all 7 families properly experience the weak interaction [15]. Therefore,

$$W^+ = |\nu_\tau\rangle|\tau^+\rangle \quad (5)$$

$$Z^0 = (|\nu_\tau\rangle|\bar{\nu}_\tau\rangle + |\tau^-\rangle|\tau^+\rangle)/\sqrt{2} \quad (6)$$

$$W^- = |\tau^-\rangle|\bar{\nu}_\tau\rangle \quad (7)$$

$$\gamma = (|\nu_\tau\rangle|\bar{\nu}_\tau\rangle - |\tau^-\rangle|\tau^+\rangle)/\sqrt{2}. \quad (8)$$

In each expression for an electroweak (EW) boson there exists the product of two identical complete graphs for the tau family representing the discrete symmetry groups 2I and 2I'. Each group in the product uses the same 12 vertices as the single tau family graph for 2I and therefore this product has the same graph theory entropy value as the tau family entropy $H = 3.585$. The W and Z bosons, having the extremely short lifetimes, immediately decay to the various long-lived final states which have final graph theory entropies that are expected to obey the graph entropy inequality in (2).

3 Discussion

We have applied graph theory entropy to lepton and quark decay channels. We had hoped to encounter some forbidden decays as a result of additional graph theory entropy restrictions for decays that are allowed by the normal conservation laws and STR. That is, we looked for forbidden decays that would violate the final state graph entropy inequality in (2):

$$H(G_1 \cup G_2) \leq H(G_1) + H(G_2)$$

where $G_1 \cup G_2$ represents the initial decaying particle state graph and G_1 and G_2 are the final state particle graphs.

We did find two decays that are in violation of this graph entropy inequality in two separate channels, both of them for 4th quark family T and B semileptonic decays to the (u, d) quark family plus the electron family as shown by the two underlined and bold entries in Table 3. These decays:

$$T^{+2/3} \rightarrow d^{-1/3} + W^+ \rightarrow d^{-1/3} + e^+ + \nu_e \quad (9)$$

$$B^{-1/3} \rightarrow u^{+2/3} + W^- \rightarrow u^{+2/3} + e^- + \bar{\nu}_e \quad (10)$$

satisfy all normal constraints but would be prohibited in graph theory because the initial graph entropy of 6.907 would result in a final graph entropy of 6.322, a violation of the graph entropy inequality rule. No other violations were found in the decay channels.

Unfortunately, we have no evidence that the 4th quark family actually exists, so we cannot check Nature for this violation yet. Therefore, we must wait for the opportunity in the future should the T and B quarks make their existence known.

Acknowledgements

We thank Sciencegems for continued support and for encouragement to investigate various challenges in particle physics.

Received on July 18, 2024

References

1. Feruglio F. Are neutrino masses modular forms? arXiv: hep-ph/1706.08749.
2. Ding G. J. and King S. F. Neutrino Mass and Mixing with Modular Symmetry. arXiv: hep-ph/2311.09282.
3. Kobayashi T. and Tanimoto M. Modular flavor symmetric models. arXiv: hep-ph/2307.03384.
4. Navas S. *et al.* (Particle Data Group) Neutrino Properties. *Phys. Rev. D*, 2024, v. 110, 030001.
5. Potter F. Geometrical Basis for the Standard Model. *Int. J. of Theor. Phys.*, 1994, v. 33, 279–305.
6. Potter F. CKM and PMNS mixing matrices from discrete subgroups of SU(2). *J. Phys: Conf. Ser.*, 2015, v. 631, 012024.
7. Potter F. Fermion Mass Derivations: I. Neutrino Masses via the Linear Superposition of the 2T, 2O, and 2I Discrete Symmetry Subgroups of SU(2). *Prog. in Phys.*, 2023, v. 19 (1), 55–61. Online: <https://progress-in-physics.com/2023/PP-65-06.PDF>
8. Hou W. S. Source of CP Violation for the Baryon Asymmetry of the Universe. *Int. J. of Mod. Phys.*, v. D20, 2011, 1521–1532. arXiv: hep-ph/1101.2161v1.
9. Baez J. Noether's Theorem in a Nutshell. accessed 12 July 2024. <https://math.ucr.edu/home/baez/noether.html>.
10. Kitahara T. Theoretical point of view on Cabibbo angle anomaly. arXiv: hep-ph/2407.00122v1.
11. Alexandrou C. *et al.* Inclusive hadronic decay rate of the τ lepton from lattice QCD: the $\bar{u}s$ flavour channel and the Cabibbo angle. arXiv: hep-ph/2403.05404v2.
12. Noriega H. E. and Aviles A. Unveiling Neutrino Masses: Insights from Robust (e)BOSS Data Analysis and Prospects for DESI and Beyond. arXiv: astro-ph/2407.06117v1.
13. Wikipedia contributors. Graph Entropy. In *Wikipedia, the Free Encyclopedia*. 2024 May 15, retrieved 14:02, July 13, 2024, from <https://w.wiki/Aewq>.
14. Kocik J. The Koide Lepton Mass Formula and the Geometry of Circles. arXiv: physics.gen-ph/1201.2067v1.
15. Potter F. Elimination of Anomalies Reported for $b \rightarrow s\ell\ell$ and $b \rightarrow c\bar{\nu}_\ell$ Semi-Leptonic Decay Ratios $R(K,K^*)$ and $R(D,D^*)$ when the Lepton Families Represent Discrete Symmetry Binary Subgroups 2T, 2O, 2I of SU(2). *Prog. in Phys.*, 2018, v. 14 (4), 185–188. Online: <https://progress-in-physics.com/2018/PP-55-01.PDF>.

Table 3: Final Graph Entropy Values for Quark Semileptonic Decays

Quark	$u^{+2/3}$	$d^{-1/3}$	$c^{+2/3}$	$s^{-1/3}$	$t^{+2/3}$	$b^{-1/3}$	$T^{+2/3}$	$B^{-1/3}$
Mass	2.3 MeV	4.8 MeV	127.5 MeV	95 MeV	173.2 GeV	4.8 GeV	3.4 TeV	95 GeV
Group H	(333) 2.322		(334) 3.0		(343) 4.585		(335) 6.907	
Decay Channel								
$d^{-1/3} + e^+ + \nu_e$			6.322		6.322		<u>6.322</u>	
$u^{+2/3} + e^- + \bar{\nu}_e$		6.322		6.322		6.322		<u>6.322</u>
$s^{-1/3} + e^+ + \nu_e$			7.0		7.0		7.0	
$c^{+2/3} + e^- + \bar{\nu}_e$						7.0		7.0
$b^{-1/3} + e^+ + \nu_e$					8.585		8.585	
$t^{+2/3} + e^- + \bar{\nu}_e$								
$B^{-1/3} + e^+ + \nu_e$					10.907		10.907	
$T^{+2/3} + e^- + \bar{\nu}_e$								
$d^{-1/3} + \mu^+ + \nu_\mu$			7.492		7.492		7.492	
$u^{+2/3} + \mu^- + \bar{\nu}_\mu$						7.492		7.492
$s^{-1/3} + \mu^+ + \nu_\mu$					8.17		8.17	
$c^{+2/3} + \mu^- + \bar{\nu}_\mu$						8.17		8.17
$b^{-1/3} + \mu^+ + \nu_\mu$					9.755		9.755	
$t^{+2/3} + \mu^- + \bar{\nu}_\mu$								
$B^{-1/3} + \mu^+ + \nu_\mu$					12.077		12.077	
$T^{+2/3} + \mu^- + \bar{\nu}_\mu$								
$d^{-1/3} + \tau^+ + \nu_\tau$					9.492		9.492	
$u^{+2/3} + \tau^- + \bar{\nu}_\tau$						9.492		9.492
$s^{-1/3} + \tau^+ + \nu_\tau$					10.17		10.17	
$c^{+2/3} + \tau^- + \bar{\nu}_\tau$						10.17		10.17
$b^{-1/3} + \tau^+ + \nu_\tau$					11.755		11.755	
$t^{+2/3} + \tau^- + \bar{\nu}_\tau$								
$B^{-1/3} + \tau^+ + \nu_\tau$					14.077		14.077	
$T^{+2/3} + \tau^- + \bar{\nu}_\tau$								

Table 4: Final Graph Entropy Values for Quark Decay Channels to Mesons

Quark	u ^{+2/3}	d ^{-1/3}	c ^{+2/3}	s ^{-1/3}	t ^{+2/3}	b ^{-1/3}	T ^{+2/3}	B ^{-1/3}
Mass	2.3 MeV	4.8 MeV	127.5 MeV	95 MeV	173.2 GeV	4.8 GeV	3.4 TeV	95 GeV
Group <i>H</i>	(333) 2.322		(334) 3.0		(343) 4.585		(335) 6.907	
Decay Channel								
u + dū				6.966		6.966		6.966
u + sĉ						8.322		8.322
c + dū						7.644		7.644
c + sĉ						9.0		9.0
d + dū			6.966		6.966		6.966	
d + sĉ			8.322		8.322		8.322	
d + b̄t							11.492	
s + dū					7.644		7.644	
s + sĉ					9.0		9.0	
s + b̄t							12.17	
b + dū					9.229		9.229	
b + sĉ					10.585		10.585	
b + b̄t							13.755	
B + dū							11.551	
B + sĉ							12.907	
B + b̄t							16.077	

Progress in Physics is an American scientific journal on advanced studies in physics, registered with the Library of Congress (DC, USA): ISSN 1555-5534 (print version) and ISSN 1555-5615 (online version). The journal is peer reviewed.

Progress in Physics is an open-access journal, which is published and distributed in accordance with the Budapest Open Initiative. This means that the electronic copies of both full-size version of the journal and the individual papers published therein will always be accessed for reading, download, and copying for any user free of charge.

Electronic version of this journal: <http://progress-in-physics.com>

